

Factors regulating the onset of
epithelial-like polygonal architecture in
the syncytial *Drosophila* embryo

Submitted in partial fulfilment of the requirements
of the degree of

DOCTOR OF PHILOSOPHY

By
Bipasha Dey
20133250



INDIAN INSTITUTE OF SCIENCE EDUCATION AND RESEARCH
PUNE

CERTIFICATE

It is certified that the thesis entitled "**Factors regulating the onset of epithelial-like polygonal architecture in the syncytial *Drosophila* embryo**" submitted by **Ms. Bipasha Dey** represents her original work which was carried out by the candidate at IISER, Pune, under my guidance and supervision during the period from **July 2013 to July 2019**.

The work presented here or any part of it has not been included in any other thesis submitted previously for the award of any degree or diploma from any other University or institution. I further certify that the above statements made by her in regard to her thesis are correct to the best of my knowledge.

Date:

**Dr. Richa Rikhy
(Supervisor)**

DECLARATION

I declare that this written submission represents my idea in my own words and where others' ideas have been included; I have adequately cited and referenced the original sources. I also declare that I have adhered to all principles of academic honesty and integrity and have not misrepresented or fabricated or falsified any idea/data/fact/source in my submission. I understand that violation of the above will be cause for disciplinary action by the Institute and can also evoke penal action from the sources which have, thus, not been properly cited or from whom proper permission has not been taken when needed. The work reported in this thesis is the original work done by me under the guidance of Dr. Richa Rikhy.

Date:

Bipasha Dey
Reg. no. 20133250

Acknowledgements

I see the last six years of my PhD as a collaborative effort that could not have been possible without each person doing their unique bit to create a wonderful whole. Therefore, I would like to thank a whole bunch of people without whom it would not have been possible.

To begin with, I would like to express my deepest gratitude to my PhD advisor, Dr. Richa Rikhy, for giving me the opportunity to work in her lab. The scientific training provided by her is a complete package which not just includes learning to perform experiments, but also critical data analysis, accurate interpretation, scientific writing and presentation skills. Most importantly, she has always given me the freedom to design my own experiments and follow the leads that I was interested in. She has been very understanding throughout, and has given personal attention to foster each student as per need. One particular skill that I could not have learnt without her was to stick to my convictions until clearly proven wrong by an experiment. I am very quick to conclude that a certain experiment won't work, but because of her persistent approach to tease apart the problem, I could learn to think through and not give up until a clear negative result. In addition, I learned to value the information provided by negative results.

Next, I would like to thank IISER, Pune, Biology department, for creating a healthy and democratic scientific environment with the common lab system and giving me the opportunity to be a part of this fun department. Thanks to CSIR for the monthly fellowship that kept us going financially and EMBO and Infosys for funding towards various conferences.

IISER, Pune Imaging facility and the Leica Imaging centre are fantastic facilities without which none of my experiments would have been possible. Special thanks to the imaging facility team Vijay, Santosh, Aditi and Rahul for guiding me from time to time. I would also like to thank The Bloomington stock centre for providing us with a wide variety of stocks and DSHB for cheap and easily available antibodies to perform our experiments.

The Fly stock centre of IISER, Pune is a big help as we had a quick back up for whenever we ended up killing our stocks (by mistake). It was only possible due to the diligence and careful planning of Snehal and Ashwini towards maintaining the

stocks. Thanks to Yashwant for managing the fly media centre and the housekeeping staff for washing our glass wares/ plastic wares and autoclaving. Because of them we had a big chunk of work off our shoulders. Hats off to them!!!

I will be eternally grateful to RR lab members, a bunch of really cool people, for maintaining a friendly yet productive environment in the lab. I could get many useful suggestions from the discussions that took place in the lab meetings because of them. Aparna was the one to come up with the idea of looking at polygon distribution in the syncytial embryo which I got the opportunity to follow when I joined. Her understanding of the system set up a baseline for me to work on. Darshika was this fun senior, with whom you could party as well as run to for advice. Dnyanesh would always ask the maximum questions during lab meets which were very helpful. Sayali, although my senior, was a like a peer I could freely discuss my work with. The young members of the lab, Bhavin, Debasmita and Somya are of the same frequency as our older team and I am sure that they will maintain an equally fun atmosphere in the lab. Friends are an important part of all phases of our lives and I was lucky to find my best pals in the lab itself. Thanks to Sameer for being a big support throughout the ups and downs in my life during my PhD. His bad jokes were sometimes the only respite from a bad day at work! Swati, who is like a younger sister to me, unintentionally, was a marvellous source of entertainment, which is sometimes badly needed during the long hours of lab work. Both of them have not only been there for me as great friends but also as great scientific peers with whom I could have many productive brainstorming sessions.

I would especially like to thank Tirthasree Das, for her contributions in identifying the edge-vertex polarity in the syncytial embryo and also for characterizing the Shg Δ JM phenotype. Her careful observations and quantifications were instrumental in formulating the lateral membrane length hypothesis later. Special thanks to Sayali, Swati, Debasmita and Somya for help in proofreading my thesis.

I would like to thank and dedicate this thesis to my lifelong mentor, Dr. Daisaku Ikeda, whose guidance and encouragement were the stepping stones for progress in these last 6 years. One of his guidances, that was like a ship to navigate through my PhD was “Fierce winds make new flights possible”. This enabled me to turn every deadlock, whether personal or professional, as a starting point for new progress.

Last but not the least, I would really like to thank my family for their unconditional support and understanding throughout my PhD. My parents have always been the biggest pillar of support for me. This thesis is, in particular, dedicated to my late father, who always encouraged me to follow my dreams irrespective of how daunting my reality was; and my mother, whose courageous smile inspired me to never get defeated. Thanks to my dear grandmother for being a pillar of support for my mother and sister after my father. Also thanks to my dear sister for being there with my family while I couldn't, so that I could work at ease and be confident of their well-being even if physically apart.

Table of Contents

CERTIFICATE	i
DECLARATION	ii
Acknowledgements	iii
Table of Contents	1
List of Figures	8
List of Movies	11
List of Tables	12
List of Abbreviations	13
Abstract	16
Synopsis	17
CHAPTER 1	27
Introduction	
1.1 Properties and functions of epithelia	27
1.1.1 Epithelial cell plasma membrane polarity	27
1.1.2 Junctional components of epithelial cells across metazoans.	29
1.1.2.1 Adherens junctions (AJ)	30
1.1.2.2 Tight or Septate junctions (TJ or SJ)	30
1.1.2.3 Desmosomes and Hemidesmosomes	30
1.1.3 Hexagon dominated Polygon architecture of epithelial cells.	30
1.2 Early embryos as a model system for onset of epithelial polarity and polygonal packing	31
1.2.1 Early <i>D. melanogaster</i> embryogenesis as a model system to study the onset of polarity and polygonal packing	35

1.3 Aims and Objectives	36
1.3.1 Characterizing the early syncytial embryo for the emergence of polygonal architecture	36
1.3.2 Identifying molecular factors responsible for the circular to polygonal transition.	37
1.3.3 Characterizing the early syncytial embryo for the presence of epithelial-like polarity.	37
1.3.4 Genetic analysis of the role of polarised protein distribution in regulating hexagon-dominated polygonal architecture	37
CHAPTER 2	38
Material and Methods	
2.1 Fly strains and Genetics	38
2.2 Immunostaining	40
2.3 Antibodies and Reagents	41
2.4 Live Imaging of <i>Drosophila</i> embryos	42
2.5 Microscopy specifications	42
2.6 Fluorescence Recovery after Photobleaching (FRAP)	42
2.7 Quantification and statistical analysis	43
2.7.1 Quantification of relative fluorescent signal	43
2.7.3 Quantification of circularity	43
2.7.4 Polygon analysis	43
2.7.5 Quantification of the furrow length	44
2.7.8 Statistical analysis	44
CHAPTER 3	45
Circular to polygonal transition correlates with lateral membrane length in the syncytial <i>Drosophila</i> embryo.	

3.1 Introduction	45
3.2 Materials and methods	46
3.2.1 Fly stocks	46
3.2.2 Live imaging	46
3.2.3 Analysis	46
3.2.3.1 Quantification for circularity versus length graph	46
3.3 Results	47
3.3.1 A threshold plasma membrane ingression length correlates with the onset of polygonal architecture	47
3.3.2 The onset of polygonality is dependent on threshold irrespective of cell crowding, size and edge lengths.	50
3.4 Discussion and conclusion	51
 CHAPTER 4	 52
Onset of epithelial-like hexagon-dominated polygon distribution in the syncytial <i>Drosophila</i> embryo	
4.1 Introduction	52
4.2 Materials and methods	54
4.2.1 Fly stocks	54
4.2.2 Live imaging	54
4.2.3 Immunostaining	54
4.2.4 Analysis and Quantification	55
4.2.4.1 Polygon analysis	55
4.3 Results	55
4.3.1 Hexagon dominated plasma membrane organization emerges at nuclear cycle 12	55
4.3.2 Both lateral membrane length and crowding influence onset of hexagon-dominance	56

4.3.3 Small embryos show a delay in the onset of hexagon-dominated polygon distribution	58
4.4 Conclusion and discussion	59
CHAPTER 5	61
Onset of epithelial-like plasma membrane polarity in the syncytial <i>Drosophila</i> embryo	
5.1 Introduction	61
5.2 Materials and Methods	63
5.2.1 Fly stocks	63
5.2.2 Live imaging	64
5.2.3 Immunostaining	64
5.2.4 Analysis and quantification	64
5.2.4.1 Quantification of relative fluorescent signal across depth and in planar sections of the plasma membrane	64
5.3 Results	65
5.3.1 XZ Polarity in the syncytial <i>Drosophila</i> embryo	65
5.3.2 XY Polarity in the syncytial <i>Drosophila</i> embryo (Done in collaboration with Tirthasree Das)	66
5.4 Conclusion and Discussion	66
CHAPTER 6	72
Adhesion and contractility balance at the threshold lateral membrane length regulates circular to polygonal transition	
6.1 Introduction	72
6.2 Material and Methods	73
6.2.1 Fly stocks	73
6.2.2 Live imaging	74

6.2.3 Immunostaining	75
6.2.4 Fluorescence Recovery after Photobleaching (FRAP)	75
6.2.5 Laser Ablation	75
6.2.6 Analysis and quantification	76
6.2.6.1 Quantification of the metaphase furrow length	76
6.2.6.2 Quantification of relative fluorescent signal for DE-cad-GFP and Sqh-mCherry across time from interphase to metaphase.	76
6.2.6.3 Estimation of mobile fractions from FRAP experiments	76
6.2.6.4 Quantification of recoil velocities after laser ablation	77
6.3 Results	77
6.3.1 Myosin II levels decrease while DE-cadherin levels increase at the lateral plasma membrane with length above the threshold	77
6.3.2 Myosin II is stabilized more after crossing the threshold whereas DE-cadherin dynamics remain unchanged	78
6.3.3 The lateral furrow plasma membrane with length above the threshold has higher tension	78
6.3.4 DE-cadherin depletion results in decreased lateral furrow length and increased circularity causing a loss of polygonal architecture formation	81
6.3.5 Depleting Myosin II activity leads to polygon architecture formation below the threshold lateral membrane length	83
6.3.6 Increased Myosin II activity shows unbalanced cap contraction, loss of DE-cadherin and abrogation of polygonal architecture	87
6.4 Conclusion and Discussion	88
CHAPTER 7	95
Plasma membrane polarity proteins regulate the onset of hexagon-dominated polygonal architecture	
7.1 Introduction	95
7.2 Material and Methods	96

7.2.1 Fly stocks	96
7.2.2 Live imaging	97
7.2.3 Immunostaining	97
7.2.4 Analysis and quantification	98
7.2.4.1 Quantification of the metaphase furrow length	98
7.2.4.2 Quantification of circularity for different metaphase furrow length mutant embryos	98
7.3 Results	98
7.3.1 Baz affects Pnut recruitment to the plasma membrane and depletion of both result in shorter furrow lengths	99
7.3.2 Baz and Pnut depletion results in delayed hexagon dominance in syncytial cells	100
7.3.3 DE-cad knockdown results in greater disruption in furrow length and loss of hexagon dominance in syncytial cells	103
7.3.4 p120-catenin is more important for regulation of furrow length stabilization as compared to other catenins in the syncytial embryo	103
7.3.5 Loss of contractility in the plasma membrane also results in delay in the onset of hexagon dominance	108
7.3.6 Overexpression of DE-cad with juxtamembrane domain deletion shows severe disruption of F-actin, furrow length and polygonality as compared to DE-cad depletion (Done in collaboration with Tirthasree Das)	108
7.3.7 Arp2/3 and Dia are additionally lost on overexpression of DE-cad with juxtamembrane domain deletion as compared to DE-cad and p120 loss of function	112
7.4 Conclusions and Discussion	114
Chapter 8	119
Thesis summary and future perspectives	

8.1 Circular to polygonal shape transition of epithelial cells correlates with a threshold lateral membrane ingression.	119
8.2 The syncytial <i>Drosophila</i> plasma membrane is polarized in both XZ and XY planes before cellularization.	121
8.3 The conserved hexagon dominated polygonal distribution depends on the length as well as polarity protein composition of the lateral membrane	122
Bibliography	127

List of Figures

Chapter 1

- 1.1 Epithelial cell polarity protein localization in vertebrates and invertebrates
- 1.2 Hexagon dominance is a conserved property of epithelia across metazoans
- 1.3 Early embryos as a model system to study the onset and progression of polarity and polygonal packing.
- 1.4 Early stages (0-3hrs) of *Drosophila* embryogenesis

Chapter 2

- 2.1 Steps involved in quantifying polygon distribution in tissues using packing analyzer.

Chapter 3

- 3.1 Schematic overview of confocal imaging of the syncytial blastoderm in *Drosophila* embryos
- 3.2 Circularity of syncytial cells decreases with increase in furrow lengths
- 3.3 Polygonality is seen above a threshold lateral membrane length irrespective of cell size and crowding

Chapter 4

- 4.1 Hexagon dominated plasma membrane organization emerges at NC12
- 4.2 NC12 does not show hexagon dominance at a furrow length just above the threshold
- 4.3 Comparison between small, large and wildtype embryos.
- 4.4 Small embryos show a delay in the onset of hexagon dominance.

Chapter 5

- 5.1 Asymmetric localization of polarity regulators and septin family proteins in the syncytial embryo.
- 5.2 DE-cad, Baz and Pnut show polarized distribution in the syncytial cells.

5.3 Schematic representing the polarized localization of proteins in XZ and XY planes.

Chapter 6

6.1 DE-cad levels increase while MyoII levels decrease at the plasma membrane in NC13 during furrow extension.

6.2 Myosin II is stabilized on the lateral membrane above the threshold

6.3 Junctional tension is higher at lateral membrane length above the threshold

6.4 DE-cad depletion leads to short furrows, increased circularity and no effect on Zipper levels.

6.5 RhoGEF2 and Rok depletion reduces MyoII activity and changes the lateral membrane threshold for polygonality.

6.6 RhoGEF2 overexpression and MBS depletion leads to retention of MyoII in patches

in metaphase and abrogation of polygonal architecture.

6.7 Actin cap area expansion as an indicator of MyoII based cortical contractility

6.8 Summary model showing the role of DE-cad and MyoII balance in formation of polygonal epithelial architecture

Chapter 7

7.1 Baz and Pnut depletions show decrease in lateral membrane length and delay in

hexagon dominance.

7.2 Characterization of Baz truncation mutants for Pnut localization.

7.3 Baz and Pnut depletion show delay in hexagon dominance while DE-cad depletion

results in loss of hexagon dominance.

7.4 DE-cad depletion results in mislocalization of Baz and Pnut and loose membrane

morphology.

7.5 p120-catenin depletion results in short furrows delay in hexagon-dominance

7.6 α -cat and p120-cat knockdowns show delayed onset of hexagon dominance

7.7 RhoGEF2 and Rok knockdowns show delayed onset of hexagon dominance.

7.8 Overexpression of Shg Δ JM domain results in severely short furrows, F-actin, Baz

and Pnut disorganization and loss of polygonal architecture

7.9 Shg Δ JM embryos show decreased furrow extension and increased circularity

7.10 Actin regulatory proteins are affected in DE-cad mutant embryos

7.11 Schematic showing the importance of DE-cad in lateral membrane formation and hexagonal packing.

Chapter 8

8.1 Summary models

List of Movies

Chapter 3

- 3.1 [tGPH imaging in the syncytial cycles in XY surface and orthogonal planes.](#)
- 3.2 [tGPH in NC13 shows increased polygonality from interphase to metaphase](#)

Chapter 6

- 6.1 [DE-cad-GFP and Sqh-mCherry dynamics across syncytial cycles in XY surface](#)
- 6.2 [shg RNAi expressing embryos have very short furrows and circular membrane](#)
- 6.3 [shg RNAi expressing embryos have short furrows and membrane ruffling.](#)
- 6.4 [shg RNAi expressing embryos have short furrows.](#)
- 6.5 [rhoGEF2 RNAi expressing embryos have short and irregular furrows.](#)
- 6.6 [rok RNAi expressing embryos have short and highly irregular furrows.](#)
- 6.7 [RhoGEF2 overexpression embryos have no furrow ingression and form circular.](#)
- 6.8 [mbs RNAi expressing embryos have no furrow ingression and form circular cells.](#)

Chapter 7

- 7.1 [baz RNAi embryos have a shorter metaphase furrow.](#)
- 7.2 [pnut RNAi embryos have a shorter metaphase furrow.](#)
- 7.3 [p120 RNAi expressing embryos show a shorter metaphase furrow.](#)
- 7.4 [Shg \$\Delta\$ JM expressing embryos show a loss of furrow formation.](#)



List of Tables

Chapter 1

1.1 Comparison of early embryonic polarity across metazoans.

Chapter 2

2.1 Fly strains

2.2 Antibodies and reagents

Chapter 3

3.1 Fly stocks

Chapter 4

4.1 Fly stocks

Chapter 5

5.1 Summary of polarity in the syncytial *Drosophila* embryo

5.2 Fly stocks

Chapter 6

6.1 Fly stocks

Chapter 7

7.1 Fly stocks

7.2 List of DE-cad truncation mutants overexpressed in the syncytial embryo.

List of Abbreviations

ArpC	Actin-Related Proteins complex
aPKC	Atypical protein kinase
ANOVA	Analysis of variance
α -cat	α -catenin
β -cat	β -catenin
Baz	Bazooka
C	Circularity
Crb	Crumbs
Dia	Diaphanous
Dlg	Discs large
DE-cad	<i>Drosophila</i> E-cadherin
ECM	Extra-cellular matrix
FRAP	Fluorescence recovery after photobleaching
FRT	Flippase recognition target sites
GAP	GTPase activating factor
GEF	Guanine nucleotide exchange factor
GFP	Green fluorescent protein
GRP1	General receptor of phosphoinositides 1
GTP	Guanosine-5'-triphosphate
<i>hsflp</i>	Heat shock FLP recombinase

Lgl	Lethal giant larvae
MBS	Myosin binding subunit of Myosin phosphatase
MT	Microtubules
MyoII	Non-muscle myosin II
NC	Nuclear division cycle
P120-cat	p120-catenin
PATJ	PALS1 associated tight junction homologue
PBS	Phosphate buffer saline
PCP	Planar cell polarity
PFA	Paraformaldehyde
Phall	Phalloidin
PH	Pleckstrin homology
PIP2	Phosphatidylinositol 4,5-bisphosphate
PIP3	Phosphatidylinositol 3,4,5-trisphosphate
Pnut	Peanut
ROI	Region of interest
SD	Standard deviation
Sep-1	Septin 1
Sep2	Septin 2
SJ	Septate Junction
Scrib	Scribble
<i>shg</i>	Shotgun

Std	Stardust
tGPH	Transgenic GFP tagged PH domain of GRP1
TJ	Tight junction
Zip	Zipper
ZO	Zona Occludens

Abstract

Epithelial cell shapes in metazoans have a conserved hexagon-dominated polygon distribution. However, the geometric constraints and mechanisms that result in the spherical to polygonal transition remain to be elucidated. Here, we use syncytial *Drosophila* embryos to characterize the temporal onset of polygonal plasma membrane organization. We find that circular to polygonal plasma membrane shape transition occurs when the length of the lateral membrane increases beyond a threshold from interphase to metaphase in each nuclear division cycle. DE-cadherin levels increase while Myosin II levels decrease during the threshold ingression. DE-cadherin depletion leads to decrease in furrow length and increase in circularity. Increased Myosin II activity results in complete loss of lateral membrane extension, thereby, giving rise to spherical plasma membrane architecture. Decreased myosin activity, on the other hand, leads to the transition to polygonal shape at a length below the threshold length. Our study, thus, elucidates the role of a balance between DE-cadherin and Myosin II across the lateral domain length in stable formation of polygonal architecture in syncytial *Drosophila* embryos. It further highlights the importance of fine tuning Myosin II-based contractility for achieving this threshold length.

We also look at the onset of epithelial-like polarity in the syncytial *Drosophila* embryos and find that the onset of epithelial-like polarity occurs at nuclear division cycle 12. This is coincident with the onset of hexagon dominance. Knockdown of polarity proteins, like Bazooka and Peanut, results in delayed onset of this hexagon dominance, while DE-cadherin depletion results in loss of hexagon dominance.

Taken together, we show that the syncytial *Drosophila* embryo shows epithelial-like characteristics in terms of shape distributions and polarity despite lacking a basal domain.

Synopsis

Name of the Student: Bipasha Dey

Registration number: 20133250

Name of Thesis advisor: Dr. Richa Rikhy

Date of Registration: 1st August 2013

Place: Indian Institute of Science Education and Research, Pune

Title: **Factors regulating the onset of epithelial-like polygonal architecture in the syncytial *Drosophila* embryo**

1. Introduction

Epithelial fate is considered to be the default state of a cell, since forming an epithelial cell is the first step taken by blastomeres of an early metazoan embryo. Epithelial cells are also the first polarised cells to be formed during development in metazoans. The most important function of the epithelium is to provide a physical barrier that separates the organism's interior from the external environment. They are particularly suited for this function since they are held together by junctional molecules that help them perform this function. The plasma membrane of an epithelial cell is divided into three domains; the apical domain that faces the external environment (or the lumen in some cases) and has microvilli, the lateral domain that interacts with the neighbouring cells, and the basal domain that attaches to the extracellular matrix (Laprise and Tepass, 2011). Each of these domains is occupied by distinct protein complexes, referred to as the polarity regulators and hence, the cell is polarized along the apico-basal axis. Since these cells assemble into a sheet with their polarity aligned in the same direction, the entire epithelial layer is polarised. In addition to this, there is asymmetric distribution of nutrient and fluid transporters on the plasma membrane that facilitates selective and vectorial exchange of materials with the surroundings (Rodriguez-Boulán and Macara, 2014).

Over the past few decades, a large number of polarity regulators have been identified mainly through studies in *C. elegans*, *D. melanogaster* and mammalian epithelial cell lines. The apical domain contains the Crumbs complex that consists of

the transmembrane protein crumbs (Crb; CRB1 in vertebrates), stardust (Sdt; PALS1 in vertebrates) and PALS1 associated tight junction homologue (PATJ). Another apical protein complex is the PAR complex which consists of Par3 (Bazooka in *D.melanogaster*), atypical protein kinase (aPKC) and its regulator Par6. A RhoGTPase Cdc42 also localizes to the apical end. The basolateral domain contains the scribble complex which consists of Lethal giant larvae (Lgl), Discs large (Dlg) and scribble (Scrib). Par1 also associates with the basolateral end (Laprise and Tepass, 2011).

Cell polarization occurs in response to a polarity cue, the identity of which is currently unclear in most systems. Cell-cell contact, cell-matrix adhesion or even sperm entry (in oocytes) are some of the events implicated in initiating the polarity program in an unpolarized cell, but the complete picture still does not exist. The mechanism of maintenance of polarity, however, is well studied and it is known that most of the proteins retain their localization in the respective domains by mutual antagonism (Rodriguez-Boulant and Macara, 2014).

Another unique property of these polarized epithelial cells is that they pack into an epithelial sheet as an irregular polygonal array with the highest frequency of hexagons. This property of hexagon dominance is observed in all kinds of epithelia and in organisms ranging from *Hydra* to *Xenopus*. What initiates such an organization is not very clear, although various studies point out numerous factors that influence it. For example, in the wing disc epithelium, the planar cell polarity proteins regulate hexagon dominance through junctional remodelling. On the other hand, in proliferating epithelia, differential rates of cell division in the same tissue can influence their shapes (Classen et al., 2005; Gibson et al., 2006). Nonetheless, not much is known about how the transition from circular to polygonal shape occurs. Most studies about polygon distribution approximate the cells as a two dimensional array of cells, while ignoring the third dimension of cell height that houses most of the polarity regulators and adhesion molecules. Studying the contribution of the cell height in the onset of polygonal shape is, therefore, an interesting open question.

Plasma membrane polarity is important in maintaining cell morphology (Bilder and Perrimon, 2000; Hayashi and Carthew, 2004; Letizia et al., 2013). One example is Armadillo loss of function mutant, which forms pear shaped cells during gastrulation because of the loss of adherens junctions. Another example is Crumbs overexpression that results in apical constriction and formation of wedge shaped

cells, in contrast to Crumbs mutants, that have an expanded apical domain and form cuboidal cells (Harris and Peifer, 2004; Letizia et al., 2013). However, how polarity influences the polygon distribution is not well studied. As many reports point out to polarity being important for cell morphology, it will be worth looking into the role of plasma membrane polarity in the polygonal packing of cells.

Early embryos of many species also show some hints of polarity. In fact, the PAR proteins were first identified in *C.elegans* for their role in polarizing the zygote (Chalmers et al., 2005; Herzberg et al., 1991; Laprise and Tepass, 2011; Miller and McClay, 1997; Müller and Hausen, 1995; Nance and Priess, 2002; Nance et al., 2003; Vestweber et al., 1987). Asymmetries in the plasma membrane have been observed in very early stages of development starting from the one-to-two cell stage embryos of various species. Such epithelial-like polarity in the early embryo has also been shown to be important for many processes during embryogenesis, for example adhesion between the blastomeres, progression of gastrulation and asymmetric division (Anderson et al., 2008; Nance and Priess, 2002; Tabler et al., 2010; Vinot et al., 2005). Additionally, the primary epithelia of early embryos show polygonal architecture (Holly et al., 2015; Miller and McClay, 1997; Ohsugi et al., 1997). The advantage of studying polarity in early stages of embryogenesis is the actual presence of the first symmetry breaking event. In contrast to cell culture studies, where epithelial cells are first depolarised to follow the onset of polarity, the early embryo provides a natural system to study the onset as well as progression of polarity. Similarly, polygon shape onset can also be tracked from the very first contact formation at the two cell stage till the formation of the primary epithelium.

Embryogenesis in *Drosophila* begins with 9 nuclear divisions that take place in the interior of the fertilized embryos and approximately take 8 minutes each. After the 9th nuclear division, the nuclei start migrating towards the embryo periphery or cortex, following which they continue with 4 more rounds of nuclear division close to the plasma membrane. The fascinating feature of the early stages in *Drosophila* embryogenesis is that the nuclear division is not accompanied by cytokinesis and hence, many nuclei share the same plasma membrane and cytoplasm, a system called the syncytial blastoderm. Although there are no complete cells, each nucleus is incompletely surrounded by an umbrella shaped plasma membrane region which is in continuity with neighbouring such regions and is referred to as a pseudo-cell. After the 13th nuclear division, which results in approximately 6000 nuclei at the

cortex, cleavage furrows extend and close around each nucleus to form complete epithelial cells in a process called cellularization (Foe and Alberts, 1983).

Onset and progression of polarity during cellularization, when epithelial cells are first formed during development in *Drosophila*, is an intense area of research. However, there are very few reports about the characterization of the syncytial stage for polarity. Even though the syncytial blastoderm has pseudocells, their organization, at least morphologically, resembles epithelial cells. For example, they have the apical microvilli-like structures, and there are contacts between the neighbouring pseudo-cells established via the pseudo cleavage furrows. They also already show polygonal architecture despite lacking a basal domain. Thus, it will be interesting to see if the epithelial-like polarity is also initiated at this stage. At the same time, finding a correlation, if any, between the onset of polarity and polygonal packing can provide us with insights into the regulators of hexagon dominance.

2. Results

2.1 Circular to polygonal transition occurs when the lateral membrane length crosses a threshold

The plasma membrane of syncytial cells is organised into polygons even before complete cell formation in cellularization (Holly et al., 2015; Mavrakis et al., 2009; McCartney et al., 2001; Zhang et al., 1996). To determine the temporal emergence of this polygonal architecture with respect to furrow or lateral membrane length in the syncytial embryo, we imaged living embryos expressing the GFP tagged PH domain of GRP1 (tGPH) which preferentially binds PIP3 in the plasma membrane (Britton et al., 2002). We tracked the change in shape of syncytial cell plasma membrane with respect to furrow length. Syncytial cells in interphase with short furrows (approximately $\leq 4 \mu\text{m}$), had almost circular plasma membrane organization and transformed to a polygonal shape in metaphase with longer furrow lengths (approximately $\geq 10 \mu\text{m}$). Polygonality was seen when the furrows ingressed beyond a threshold length range of 4.75-5.75 μm . The plasma membrane around syncytial cells remained circular in all nuclear division cycles (NCs), when the lateral membrane length was less than the threshold at approximately 4 μm . Only at furrow

length greater than the threshold, at approximately 6.5 μm , the plasma membrane was polygonal in NC11-14. Polygonality in the syncytial *Drosophila* embryo was, therefore, a function of furrow length, independent of syncytial cell number, size or crowding.

2.2 Adhesion and contractility balance regulate the threshold membrane length for circular to polygonal shape transition

Two fundamental forces that drive cell shape changes and, therefore, tissue morphogenesis are actomyosin based contractions and cadherin mediated cell-cell adhesion. These two forces play opposing roles with adhesion facilitating expansion of the contact area between cells while actomyosin contractions working to reduce it (Heisenberg and Bellaïche, 2013; Maître and Heisenberg, 2013). Cellular force generation typically relies on molecular motors like Myosin II which can bind to and reorganize actin filaments in the cell. The cytoskeletal changes within a cell are then transmitted to other cells via cell-cell and cell matrix adhesion molecules like cadherins and integrins. Thus, in order to test molecular players that regulate the threshold, we focused our attention on DE-cadherin (DE-cad) and Myosin II (MyoII). DE-cad levels increased while MyoII levels decreased during the threshold lateral length ingression. Lowering adhesion resulted in increased circularity and disruption of polygonal architecture of the plasma membrane in only a small percentage of embryos. All embryos had significantly short furrow lengths. On the other hand, lowering MyoII activity allowed adhesive forces to take over and form polygons earlier than usual. In other words, the threshold was shifted to a lower length. Conversely, increasing MyoII activity prevented the threshold length from being achieved and resulted in completely circular cells. In addition, DE-cad was lost from the membranes in these embryos thereby giving rise to a scenario where adhesion is lowered and contractility is increased simultaneously. Thus, the threshold length range for circular to polygonal transition is a result of balancing MyoII activity relative to DE-cad on the lateral membrane.

2.3 Syncytial cells have molecular asymmetries in both XY and XZ planes

Epithelial polarity in *Drosophila* embryos is distinctly present at the end of

cellularization when epithelial cells are first formed (Harris and Peifer, 2004). It is known that polarity proteins such as Bazooka, DE-cadherin, PatJ and Dlg are already present on the membrane before cellularization, i.e. in the syncytial cycles, and molecular asymmetries with respect to some of these proteins have been noted (Mavrakakis et al., 2009; Schmidt and Grosshans, 2018; Schmidt et al., 2018). Thus, with these hints, we decided to quantitatively describe these asymmetries in the syncytial cells. We also decided to carefully observe asymmetries, if any, in the XY plane.

In order to characterize the temporal distribution of DE-cad, Baz and Pnut as compared to tGPH, we performed live imaging of embryos expressing DE-cad-GFP (Huang et al., 2009), Baz-GFP (Benton and St Johnston, 2003) and Pnut-mCherry (Guillot and Lecuit, 2013). We found that, Baz and Pnut asymmetrically distributed between edges and vertices, respectively, in NC11. By NC12, Baz and Pnut were collectively enriched in the basolateral furrow region. DE-cad was enriched along the edges in NC13 and was spread throughout the lateral domain from NC11-13. Collectively, these data characterized the onset of molecular asymmetry in the lateral furrow of syncytial *Drosophila* embryos before cellularization. These molecular asymmetries in syncytial cells were in the form of relative enrichments along the lateral furrow length or edges and vertices. This was different from later stages in fully formed epithelial cells where there are distinct domains marked by mutually exclusive localizations of polarity complexes (Bilder and Perrimon, 2000; Bilder et al., 2003; Harris and Peifer, 2004).

2.4 Syncytial cells show onset of hexagon dominance at nuclear cycle 12

The conserved property of hexagon-dominated polygonal packing has also been seen to evolve over developmental stages in some cases. For example, in the wing disc of *D. melanogaster*, there is an increase in the percentage of hexagons from 60% to 80% from larval to pupal stages, although the distribution is hexagon dominated from the very beginning (Classen et al., 2005; Sánchez-Gutiérrez et al., 2013). However, the factors for the onset of this distribution are not clearly understood. So we decided to follow the onset and progression of packing from NC10 in the syncytial embryo, where the nuclei first arrive at the cortex, to NC14, when cellularization begins. We observed that the polygon architecture is first seen

at NC11 metaphase, but here the frequency of pentagons and hexagons are equal. At NC12 metaphase, hexagon dominance is achieved for the first time during development, which is then achieved in each subsequent NC metaphase till cellularization. Thus, hexagon dominance is seen even with syncytial cells that lack a basal domain altogether.

2.5 Optimal adhesion is important for hexagon dominance

Asymmetric distribution of polarity complexes is important for cell shape, tissue integrity and tissue remodelling (Bilder and Perrimon, 2000; Hayashi and Carthew, 2004; Letizia et al., 2013). Besides one report on planar cell polarity mutants showing a decrease in the frequency of hexagons in the wing epithelium, no other report on the analysis of the role of polarity proteins in regulating the polygonal distribution of epithelia exists (Classen et al., 2005). As noted above, the syncytial *Drosophila* embryo shows asymmetric distribution of polarity regulators. Besides the conventional apico-basal polarity, the syncytial cells also show asymmetries in the XY plane, i.e. between edges and vertices. This lead us to believe that these asymmetries may be important in regulating the polygonal distribution of the syncytial cells. Thus, we looked at the effect of Baz, Pnut and DE-cad on polygonal distribution. We found that Baz and Pnut mutants show a delay in the onset of hexagon dominance, whereas DE-cad mutants do not achieve hexagon dominance at all. Hexagon dominance may also be interpreted as increased contacts per cell in the tissue. Thus, it seems that optimal adhesion between syncytial cells favours more contact formation and, hence, favours hexagon dominance.

Taken together, we find that the syncytial plasma membrane has epithelial-like characteristics both in terms of polarity and polygon morphology, even before complete cell formation in cellularization. We show that a minimum lateral membrane length ingression is sufficient for circular to polygonal shape transition of the syncytial cells. Thus, we show minimalistic factors responsible for the onset of polygonal architecture of epithelial cells and the molecular factors regulating them.

3. References

- Anderson, D.C., Gill, J.S., Cinalli, R.M., and Nance, J. (2008). Polarization of the *C. elegans* embryo by RhoGAP-mediated exclusion of PAR-6 from cell contacts. *Science* 320, 1771–1774.
- Benton, R., and St Johnston, D. (2003). *Drosophila* PAR-1 and 14-3-3 inhibit Bazooka/PAR-3 to establish complementary cortical domains in polarized cells. *Cell* 115, 691–704.
- Bilder, D., and Perrimon, N. (2000). Localization of apical epithelial determinants by the basolateral PDZ protein Scribble. *Nature* 403, 676–680.
- Bilder, D., Schober, M., and Perrimon, N. (2003). Integrated activity of PDZ protein complexes regulates epithelial polarity. *Nat. Cell Biol.* 5, 53–58.
- Britton, J.S., Lockwood, W.K., Li, L., Cohen, S.M., and Edgar, B.A. (2002). *Drosophila*'s insulin/PI3-kinase pathway coordinates cellular metabolism with nutritional conditions. *Dev. Cell* 2, 239–249.
- Chalmers, A.D., Pambos, M., Mason, J., Lang, S., Wylie, C., and Papalopulu, N. (2005). aPKC, Crumbs3 and Lgl2 control apicobasal polarity in early vertebrate development. *Development* 132, 977–986.
- Classen, A.-K., Anderson, K.I., Marois, E., and Eaton, S. (2005). Hexagonal packing of *Drosophila* wing epithelial cells by the planar cell polarity pathway. *Dev. Cell* 9, 805–817.
- Foe, V.E., and Alberts, B.M. (1983). Studies of nuclear and cytoplasmic behaviour during the five mitotic cycles that precede gastrulation in *Drosophila* embryogenesis. *J. Cell Sci.* 61, 31–70.
- Gibson, M.C., Patel, A.B., Nagpal, R., and Perrimon, N. (2006). The emergence of geometric order in proliferating metazoan epithelia. *Nature* 442, 1038–1041.
- Guillot, C., and Lecuit, T. (2013). Adhesion disengagement uncouples intrinsic and extrinsic forces to drive cytokinesis in epithelial tissues. *Dev. Cell* 24, 227–241.
- Harris, T.J.C., and Peifer, M. (2004). Adherens junction-dependent and -independent steps in the establishment of epithelial cell polarity in *Drosophila*. *J. Cell Biol.* 167, 135–147.
- Hayashi, T., and Carthew, R.W. (2004). Surface mechanics mediate pattern formation in the developing retina. *Nature* 431, 647–652.
- Heisenberg, C.-P., and Bellaïche, Y. (2013). Forces in Tissue Morphogenesis and Patterning. *Cell* 153, 948–962.
- Herzberg, F., Wildermuth, V., and Wedlich, D. (1991). Expression of XBCad, a novel cadherin, during oogenesis and early development of *Xenopus*. *Mech. Dev.* 35, 33–42.

Holly, R.M., Mavor, L.M., Zuo, Z., and Blankenship, J.T. (2015). A rapid, membrane-dependent pathway directs furrow formation through RalA in the early *Drosophila* embryo. *Development* *142*, 2316–2328.

Huang, J., Zhou, W., Dong, W., Watson, A.M., and Hong, Y. (2009). Directed, efficient, and versatile modifications of the *Drosophila* genome by genomic engineering. *Proc. Natl. Acad. Sci. U. S. A.* *106*, 8284–8289.

Laprise, P., and Tepass, U. (2011). Novel insights into epithelial polarity proteins in *Drosophila*. *Trends Cell Biol.* *21*, 401–408.

Letizia, A., Ricardo, S., Moussian, B., Martín, N., and Llimargas, M. (2013). A functional role of the extracellular domain of Crumbs in cell architecture and apicobasal polarity. *J. Cell Sci.* *126*, 2157–2163.

Maître, J.-L., and Heisenberg, C.-P. (2013). Three functions of cadherins in cell adhesion. *Curr. Biol.* *23*, R626–R633.

Mavrakis, M., Rikhy, R., and Lippincott-Schwartz, J. (2009). Plasma Membrane Polarity and Compartmentalization Are Established before Cellularization in the Fly Embryo. *Dev. Cell* *16*, 93–104.

McCartney, B.M., McEwen, D.G., Grevenkoed, E., Maddox, P., Bejsovec, A., and Peifer, M. (2001). *Drosophila* APC2 and Armadillo participate in tethering mitotic spindles to cortical actin. *Nat. Cell Biol.* *3*, 933–938.

Miller, J.R., and McClay, D.R. (1997). Changes in the pattern of adherens junction-associated beta-catenin accompany morphogenesis in the sea urchin embryo. *Dev. Biol.* *192*, 310–322.

Müller, H.A., and Hausen, P. (1995). Epithelial cell polarity in early *Xenopus* development. *Dev. Dyn.* *202*, 405–420.

Nance, J., and Priess, J.R. (2002). Cell polarity and gastrulation in *C. elegans*. *Development* *129*, 387–397.

Nance, J., Munro, E.M., and Priess, J.R. (2003). *C. elegans* PAR-3 and PAR-6 are required for apicobasal asymmetries associated with cell adhesion and gastrulation. *Development* *130*, 5339–5350.

Ohsugi, M., Larue, L., Schwarz, H., and Kemler, R. (1997). Cell-junctional and cytoskeletal organization in mouse blastocysts lacking E-cadherin. *Dev. Biol.* *185*, 261–271.

Rodriguez-Boulan, E., and Macara, I.G. (2014). Organization and execution of the epithelial polarity programme. *Nat. Rev. Mol. Cell Biol.* *15*, 225–242.

Sánchez-Gutiérrez, D., Sáez, A., Pascual, A., and Escudero, L.M. (2013). Topological progression in proliferating epithelia is driven by a unique variation in polygon distribution. *PLoS One* *8*, e79227.

Schmidt, A., and Grosshans, J. (2018). Dynamics of cortical domains in early

Drosophila development. *J. Cell Sci.* 131.

Schmidt, A., Lv, Z., and Großhans, J. (2018). ELMO and Sponge specify subapical restriction of Canoe and formation of the subapical domain in early Drosophila embryos. *Development* 145.

Tabler, J.M., Yamanaka, H., and Green, J.B.A. (2010). PAR-1 promotes primary neurogenesis and asymmetric cell divisions via control of spindle orientation. *Development* 137, 2501–2505.

Vestweber, D., Gossler, A., Boller, K., and Kemler, R. (1987). Expression and distribution of cell adhesion molecule uvomorulin in mouse preimplantation embryos. *Dev. Biol.* 124, 451–456.

Vinot, S., Le, T., Ohno, S., Pawson, T., Maro, B., and Louvet-Vallée, S. (2005). Asymmetric distribution of PAR proteins in the mouse embryo begins at the 8-cell stage during compaction. *Dev. Biol.* 282, 307–319.

Zhang, C.X., Lee, M.P., Chen, A.D., Brown, S.D., and Hsieh, T. (1996). Isolation and characterization of a Drosophila gene essential for early embryonic development and formation of cortical cleavage furrows. *J. Cell Biol.* 134, 923–934.

CHAPTER 1

Introduction

1.1 Properties and functions of epithelia

Epithelial tissues form the outer covering for organs and structures in the animal body as well as line the lumens of various organs. Epithelial fate is the first fate assumed by the blastomeres of an early metazoan embryo and, therefore, is considered to be the default state of a cell. The most important function of the epithelium is to provide a physical barrier that separates an organism's or organ's interior from the external environment. They are particularly suited for this function since they are held together by a group of junctional molecules that facilitate this function by sealing the gaps between cells. The plasma membrane of an epithelial cell is divided into three domains; the apical domain that faces the external environment (or the lumen in some cases) and has microvilli, the lateral domain that interacts with the neighbouring cells in the cell sheet, and the basal domain that attaches to the extracellular matrix. The following section enlists the various properties of epithelia and the functions that these properties confer to an epithelial tissue (Rodriguez-Boulán and Macara, 2014). In addition, it alludes to the open questions in the field.

1.1.1 Epithelial cell plasma membrane polarity

Asymmetric distribution of various components in a cell is referred to as cell polarity. Epithelial cells are the first polarised cells to be formed during development in metazoans. They are polarized along the apico-basal axis with asymmetric distribution of various proteins, lipids and morphological features on the plasma membrane and in the cytosol (Laprise and Tepass, 2011). As mentioned above, the plasma membrane of an epithelial cell is divided into three domains; apical, lateral and basal, each of which is occupied by a unique set of protein complexes. Such polarized distribution of cellular components in the plasma membrane is referred to as **plasma membrane polarity**.

Over the past few decades a large number of epithelial polarity regulators have been identified mainly through studies in *C. elegans*, *D. melanogaster* and mammalian epithelial cell lines. The apical domain contains the Crumbs complex and the PAR complex. The Crumbs complex consists of the transmembrane protein Crumbs (Crb; CRB1 in vertebrates), Stardust (Sdt; PALS1 in vertebrates) and PALS1 associated tight junction homologue (PATJ). The PAR complex consists of Par3 (Bazooka in *D. melanogaster*), Atypical protein kinase (aPKC) and its regulator, Par6. In addition, a RhoGTPase Cdc42 also localizes to the apical end. The basolateral domain is occupied by the Scribble complex which consists of Lethal giant larvae (Lgl), Discs large (Dlg) and Scribble (Scrib). Par1 also associates with the basolateral end of epithelial cells (Laprise and Tepass, 2011) (Figure 1.1).

Since the epithelial cells assemble with their polarity axes aligned in the same direction in the tissue, the entire epithelial layer is polarized with one side of the sheet facing the exterior/lumen and the other side being attached to a matrix. This also allows the cells to have asymmetric distribution of nutrient and fluid transporters suited to facilitate selective and vectorial exchange of materials with the surroundings (Rodriguez-Boulán and Macara, 2014).

Apart from the organization of the plasma membrane into discrete domains, components of the cytoskeleton and secretory machinery are also organised asymmetrically in these cells. The centrosomes are present sub-apically above the nucleus, while microtubules (MTs) run parallel to the lateral cortex with their minus ends and plus ends pointing towards the apical and basal end, respectively. In *Drosophila* epithelial cells, the MT minus ends remain attached to the sub-apical centrosomes, while in mammalian epithelial cell lines, they remain detached. The Golgi apparatus is clustered around the centrosome in the sub-apical region. This positioning of the Golgi has been implicated in sorting and directing the polarity proteins to the target site in an MT dependent manner (Mays et al., 1994).

Cell polarization occurs in response to a polarity cue, the identity of which is currently unclear in most systems. There are a few studies that implicate events like cell-cell contact, cell-matrix adhesion or sperm entry (in oocytes), in initiating the polarity program in an unpolarized cell. Yet the polarity cue varies from system to system and is mostly context dependent. The mechanism of maintenance of epithelial plasma membrane polarity is, on the other hand, very well studied. Most polarity proteins retain their localization by mutual antagonism. Two proteins play a

key role in this process: Par1 and aPKC. aPKC phosphorylates and excludes any basolateral protein diffusing into the apical side. The phosphorylated proteins then attract PAR5, which releases them from the cell cortex into the cytoplasm, thus excluding them from the apical surface (Rodriguez-Boulán and Macara, 2014). Similarly, Par 1 at the lateral cortex phosphorylates any protein trespassing from the apical side to the lateral side and excludes them from its domain. How the localization of Par1 itself is maintained is not so clear, although aPKC from the apical domain is shown to exclude Par1 in the same way as it excludes other basolateral proteins. aPKC itself is recruited to the apical cortex with the help of the Crumbs complex, while its activity is regulated by Par6.

In conclusion, although a vast body of literature exists about the maintenance of epithelial cell polarity, initiation of polarity is still an active area of investigation.

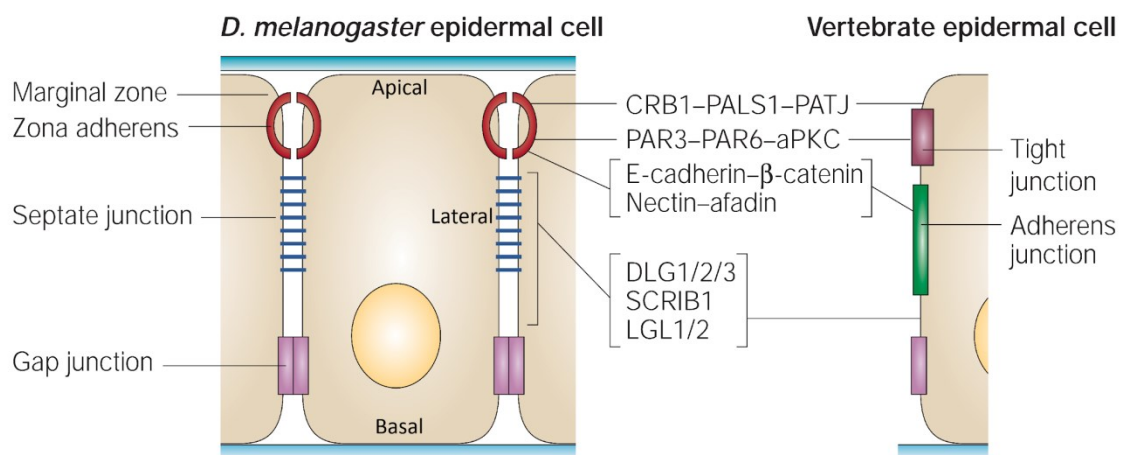


Figure 1.1 Epithelial cell polarity protein localization in vertebrates and invertebrates (Adapted from Macara,2004). This figure shows the domain specific localization of various polarity complexes in both invertebrates (left cell) and vertebrates (right cell shown only partially). The apical domain is occupied by the CRB1-PALS1-PATJ complex and the PAR3-PAR6-aPKC complex. The lateral domain is occupied by the DLG-SCRIB-LGL complex. In addition, there are different types of junctions shown to be present from apical to basal direction of the cell. Adherens junctions with E-cadherin and catenins are at the top, followed by the septate junctions and gap junctions in the invertebrates. On the other hand, tight junctions are at the top, followed by the adherens junction and gap junctions in the vertebrates.

1.1.2 Junctional components of epithelial cells across metazoans.

Junctions are very important components of epithelia that hold the epithelial cells together in a sheet. They impart the property of sealing the gaps between the

cells that allows epithelia to function as physical barriers. There are four types of junctions usually found in epithelia; Adherens junctions, Tight or Septate junctions, Desmosomes and Hemidesmosomes. Each of these is discussed in detail below:

1.1.2.1 Adherens junctions (AJ)

AJ complexes are made up of the transmembrane protein E-Cadherin (E-cad) with α -Catenin (α -cat), β -Catenin (β -cat), and p120-Catenins (p120-cat) linking the cytosolic domain of E-cad to the underlying actin cytoskeleton. Homophilic interactions between the ectodomains of E-cad molecules from neighbouring cells establish cell-cell contacts. Adherens junction based cell-cell contacts are Ca^{2+} -dependent, due to E-Cad.

1.1.2.2 Tight or Septate junctions (TJ or SJ)

TJs are made up of transmembrane proteins called Claudins and Occludins, and are required to form a paracellular barrier in epithelia. TJs are placed above the adherens junctions in vertebrates. On the other hand, invertebrates lack tight junctions and instead have SJs which are placed below the AJs (Figure 1.1). They consist of claudin-like proteins which are also essential for the barrier function of epithelia.

1.1.2.3 Desmosomes and Hemidesmosomes

Desmosomes and hemidesmosomes are structures that link cells to neighbouring cells and the extracellular matrix, respectively. These are also composed of Cadherin-like transmembrane molecules but their cytosolic domains are attached to intermediate filament stress fibers instead of actin. Because of the lack of cytosolic intermediate filaments in invertebrates, desmosomes and hemidesmosomes are absent there (Laprise and Tepass, 2011; Macara, 2004; Tyler, 2003)

Therefore, the junctional components across metazoan epithelia are very well conserved with minor variations in their structures and localization patterns.

1.1.3 Hexagon dominated Polygon architecture of epithelial cells.

Another interesting property of epithelial cells is that they organize themselves into a polygonal array in epithelial tissues. Proliferating epithelia are seen to be forming irregular polygonal arrays, unlike the regular polygonal arrays of honeycombs or soap bubbles. The polygonal arrays are always hexagon dominated while also having a fixed proportion of pentagons and heptagons. This kind of a polygon distribution is seen in epithelia of many species, ranging from *Hydra* to *Xenopus* (Fig. 1.2) (Gibson et al., 2006). Although the functional relevance of such a distribution is not very clear, there are many physical and molecular factors shown to influence it. It is known that perturbations in junctional remodelling, planar cell polarity and cytoskeletal dynamics skew the polygon distribution (Classen et al., 2005; Gibson et al., 2006; Farhadifar et al., 2007; Sugimura and Ishihara, 2013). However, the mechanisms by which the key factors regulate spherical to polygonal shape transition and maintenance in epithelial cells are not understood. In other words, not much is understood about the factors governing the initiation of this conserved distribution.

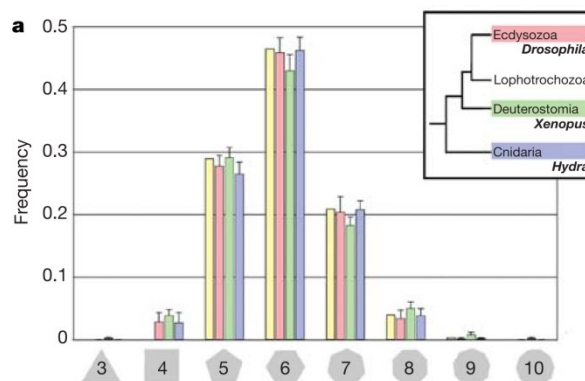


Figure 1.2 Hexagon dominance is a conserved property of epithelia across metazoans. This figure shows a frequency distribution graph of different polygon shapes in epithelia from various organisms, ranging from *Hydra* to *Xenopus*, showing a predominance of hexagonal cells with a fixed proportion of pentagons and heptagons (Gibson et al, 2006).

1.2 Early embryos as a model system for onset of epithelial polarity and polygonal packing

Early metazoan embryos are reported to show hints of epithelial-like polarity. Asymmetries in the plasma membrane have been observed in as early as two cell

stage embryos (Figure 1.3 A). These early asymmetries have been shown to be important for many processes during embryogenesis, for example adhesion between the blastomeres, gastrulation and asymmetric division (Anderson et al., 2008; Nance, 2014; Nance and Priess, 2002; Tabler et al., 2010).

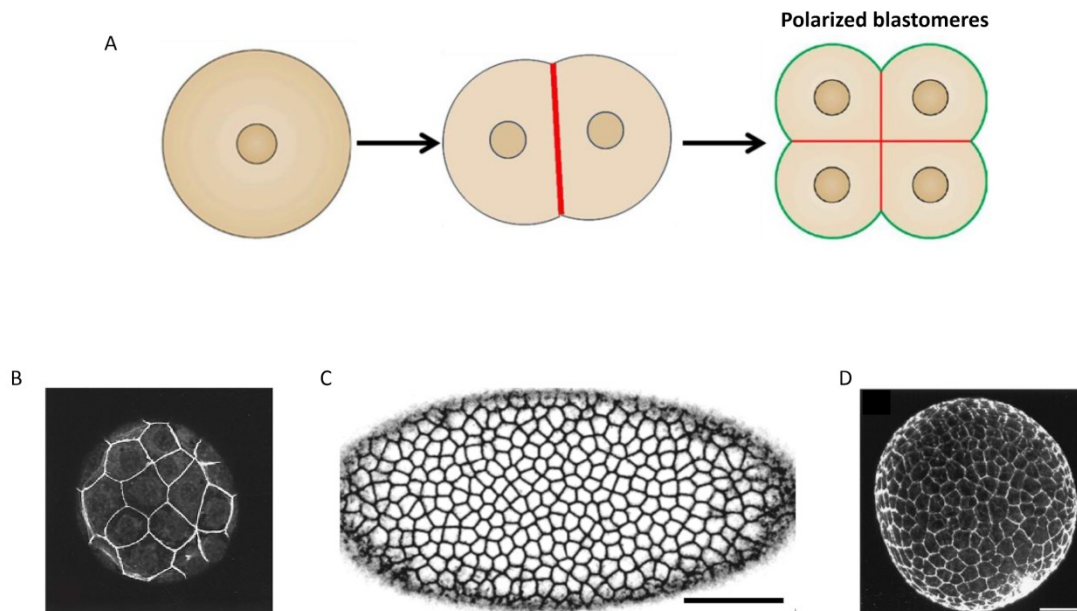


Figure 1.3 Early embryos as a model system to study the onset and progression of polarity and polygonal packing. A general model of onset and progression of polarity during embryogenesis, beginning with an unpolarized zygote and progressing towards polarized blastomeres (A). The different colours represent different set of molecules accumulating at the contacted and contact-free surfaces (Adapted from Nance, 2014). Examples of polygonal architecture in early embryos of mouse (B), *Drosophila* (C) and Sea urchin (D). (Krueger et al., 2018; Miller and McClay, 1997; Ohsugi et al., 1997)

Table 1.1 summarizes the existing evidences of epithelial-like polarity in various early metazoan embryos. Comparing the molecular players of polarity across various organisms, allows us to conclude that polarity regulators and adhesion molecules are very well conserved across metazoans (Table 1.1). In addition, the polarity in early embryos appears to progressively evolve towards the mature epithelial cell polarity. This, together with the presence of the first symmetry breaking event in early embryogenesis, makes it a good model system to study the onset and progression of polarity. In contrast to cell culture studies, where epithelial cells are first depolarised and then the onset of polarity is observed, the early embryo provides a natural system to study the initiation as well as progression of polarity *in vivo*.

Stages of embryogenesis	Animal Model	Protein/Lipid Asymmetries	Junctional Molecules	References
One cell	<i>C.elegans</i>	Anterior: PAR3-PAR6-PKC3 and Cdc42 Posterior: PAR2 and PAR1	NA	(Nance and Priess, 2002)
	Mouse	No		
	<i>Xenopus</i>	No		
	Sea urchins	No		
Two cell	<i>C.elegans</i>	Only in the germline precursor A-P Polarity is maintained	HMR-1	(Nance and Priess, 2002)
	Mouse	No	E-Cadherin	(Vestweber et al., 1987; Vinot et al., 2005)
	<i>Xenopus</i>	Basolateral: β -Integrins, Ecadherin. PAR asymmetries not checked	XB/U-Cadherin Cingulin, ZO-1, Occludin	(Herzberg et al., 1991; Müller and Hausen, 1995)
	Sea urchins	Apical: Integrins, PAR6 and Cdc42 and Gangliosides. No basolateral marker checked	CAD-1	(Alford et al., 2009; Miller and McClay, 1997)
Four cell	<i>C.elegans</i>	Apical: PAR3-PAR6-PKC3, Cdc42 Basolateral: PAR2 and PAR1	HMR-1	(Nance et al., 2003)
	Mouse	No	E-Cadherin	
	<i>Xenopus</i>	Basolateral: β -Integrins, XB/U-cadherin PAR asymmetries not checked	XB/U-Cadherin Cingulin, ZO-1, Occludin	
	Sea urchins	Not known	CAD-1	

Stages of embryogenesis	Animal Model	Protein/Lipid Asymmetries	Junctional Molecules	References
8-32 cell	<i>C.elegans</i>	Apical: PAR3- PAR6-PKC3, Cdc42 Basal: PAR2 and PAR1	HMR-1	(Vinot et al., 2005)
	Mouse	Apical: Par3, par6B and aPKC Basolateral: Par1/EMK1	E-Cadherin	
	<i>Xenopus</i>	Apical: Par6, aPKC, CRB3 Basolateral: Par1 and Lgl2	XB/U-Cadherin Cingulin, ZO-1, Occludin	(Chalmers et al., 2005)
	Sea urchins	Not known	CAD-1	
Epithelial cells	<i>D. melanogaster</i> and Mammalian epithelial cells	Apical: CRB- Sdt-PATJ and Par3/Bazooka- aPKC- Par6 Basolateral: Lgl,Dlg and Scrib	E-Cadherin	(Laprise and Tepass, 2011)

Table 1.1 Comparison of early embryonic polarity across metazoans.

At the same time, architecturally, the primary epithelium in most early embryos shows polygonal organization similar to epithelial tissues. Figure 1.3 B-D shows examples of some embryos with polygonal organization. Although some theoretical and experimental studies exist, which outline factors that influence the hexagon dominated polygonal distribution of epithelial cells, how the onset of this architecture happens is not very well understood. Early embryos provide us with the opportunity to follow the onset and progression of this architecture in real time *in vivo*. In this study, we have used *Drosophila melanogaster* early embryos to study the initiation of polarity and polygonal organization of epithelial cells.

1.2.1 Early *D. melanogaster* embryogenesis as a model system to study the onset of polarity and polygonal packing

Embryogenesis in *Drosophila* begins with 9 nuclear divisions that take place in the interior of the fertilized embryos with duration of approximately 8 minutes each. After the 9th nuclear division, the nuclei start migrating towards the embryo cortex, following which they continue with 4 more rounds of nuclear division close to the plasma membrane. The fascinating feature of early stages of *Drosophila* embryogenesis is that nuclear division is not accompanied by cytokinesis and, hence, many nuclei share a common plasma membrane and cytoplasm, forming a syncytial blastoderm. Although there are no complete cells, each nucleus has a domain of umbrella shaped plasma membrane region on top, which is in continuity with neighbouring such regions and is referred to as a pseudo-cell. Nuclear cycles 10-13 occur at the cortex, having a duration of approximately 8, 10, 15 and 25 minutes, respectively. The plasma membrane ingresses perpendicular to the embryo surface between adjacent nuclei to form a lateral membrane, called a furrow (Figure 1.4) (Foe and Alberts, 1983; Schejter and Wieschaus, 1993; Sullivan and Theurkauf, 1995). This furrow initiates during each cycle at interphase-prophase, reaches a maximum length at metaphase and then retracts during anaphase-telophase (Figure 1.4, (Holly et al., 2015a; Sherlekar and Rikhy, 2016; Silverman-Gavrila et al., 2008a). After the 13th nuclear division, which results in close to 6000 nuclei at the cortex, cleavage furrows extend and close around each nucleus to form complete epithelial cells, in a process called cellularization (Foe and Alberts, 1983).

Thus, the *Drosophila* embryo goes from a single cell to 6000 cells in a span of approximately 1.5-2 hours. These rapid early divisions make it convenient to follow the onset and progression of polarity and polygonal packing in a short span of time. In addition to this, the property of extensive lateral membrane remodelling provides the opportunity to follow the initiation of asymmetry along the apico-basal axis while the pseudo-cell is extending in that dimension. The repeated cycles of formation and disassembly of the lateral membrane can be likened to the formation and breaking of contacts between epithelial cells. Therefore, the impact of the stability of the lateral membrane on the polygonal architecture can also be followed in a natural *in vivo* scenario.

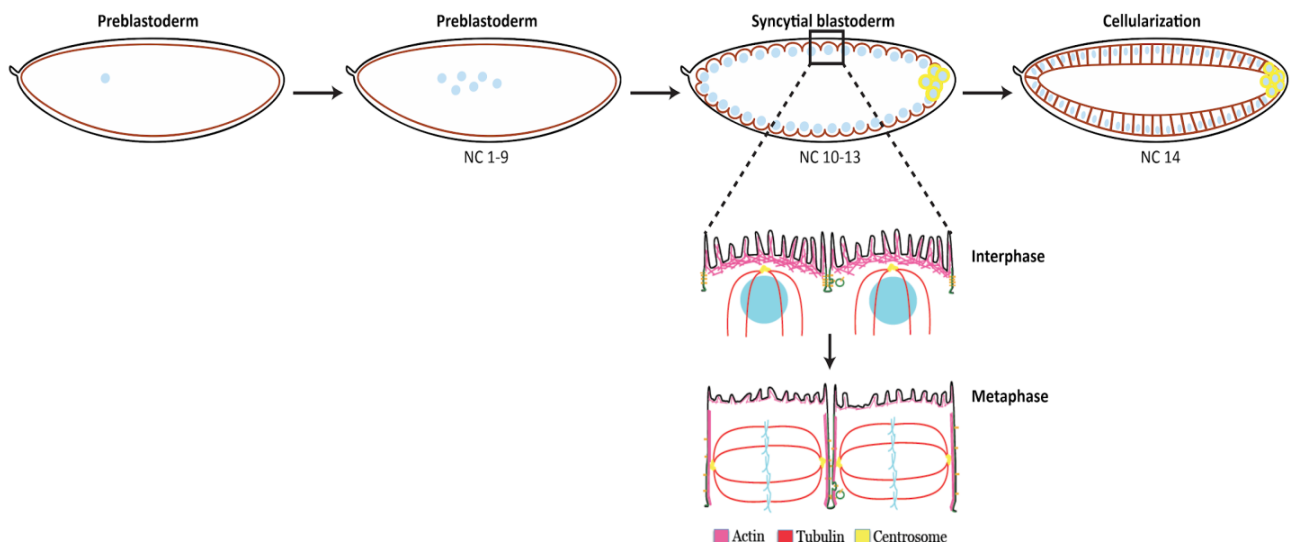


Figure 1.4 Early stages (0-3hrs) of *Drosophila* embryogenesis. The boxed region in the syncytial blastoderm stage is expanded to show the organization of the plasma membrane around the syncytial nuclei in interphase versus metaphase.

1.3 Aims and Objectives

Based on the open questions discussed above and the advantages of using the *Drosophila* early embryos as a model system, we devised the following aims and objectives towards studying the factors regulating the polygonal distribution of epithelial cells:

1.3.1 Characterizing the early syncytial embryo for the emergence of polygonal architecture

- Observing and quantifying the shape transitions from circular to polygonal in the early embryo.
- Identifying the physical or geometrical constraints responsible for the transition from circular to polygonal.
- Quantifying the frequency distribution of polygonal architecture across the syncytial cycles.

1.3.2 Identifying molecular factors responsible for the circular to polygonal transition.

- Checking the effect of perturbations in various classes of proteins responsible for shape change, namely, cytoskeletal regulators, adhesion regulators and polarity proteins.
- Elucidating the mechanism of shape change with genetic analysis and microscopy.

1.3.3 Characterizing the early syncytial embryo for the presence of epithelial-like polarity.

- Checking the expression and distribution of canonical polarity proteins and other proteins with unique asymmetries in the syncytial plasma membrane.
- Quantitative description of the localization and distribution of the polarity regulators present across the syncytial cycles.

1.3.4 Genetic analysis of the role of polarised protein distribution in regulating hexagon-dominated polygonal architecture

- Checking the effect of mutation in one polarity protein on the localization of other polarity proteins.
- Checking the effect of mutation in each polarity protein on the polygonal distribution of the plasma membrane.

CHAPTER 2

Material and Methods

2.1 Fly strains and Genetics

Drosophila melanogaster stocks were raised in regular cornmeal agar at 25 °C or 28 °C. Embryos obtained from Canton S flies or Canton S flies crossed to *maternal* α -*tubulin* Gal4-VP16 (*mat*-Gal4) or *nanos*-Gal4-VP16 (*nos*-Gal4) were used as controls. Maternal driver line *mat67;mat15* carrying *maternal* α 4 *tubulin*-Gal4-VP16, homozygous for chromosome II and III was used for all RNAi and overexpression experiments except for *shg*^j and *mbs*ⁱ for live imaging with tGPH. *shg*^j was crossed to a single chromosomal copy of *nos*-Gal4 and maintained at 18 °C to lower the severity of phenotype and obtain fertilized eggs to perform experiments. F1 flies expressing *shg*^j with *nos*-Gal4 laid embryos that were arrested early in the pre-blastoderm stage of development when the cross was grown at 25 or 29 °C and, hence, the experiments were performed at 18 °C to allow for Gal4 dilution. The lethality of *shg*^j embryos was 100% (n=150) at 25 °C and 29 °C and 70% (n=200) at 18°C after 24 hours. The *shg*^j expressing embryos laid from the cross at 18 °C gave an opportunity to test the effect of loss of DE-cad in the syncytial blastoderm embryo. RhoGEF2-OE embryos had 87% (n=200) lethality at 25 °C after 24 hours. Germline clones of *pnut*^{XP} were made by crossing *ovo*^D FRTG13 males to *hsflp; GlaB/c* females to obtain *hsflp; ovo*^D FRTG13/*GlaB/c* males. These males were then crossed to *pnut*^{XP} FRTG13/*Cyo* females. Larvae, pupae and adults emerging from this cross were heat shocked at 37.5 °C. *hsflp;ovo*^D FRTG13/*pnut*^{XP} FRTG13 adults were then put in a cage to collect embryos depleted of Pnut.

Stock name	Source	ID
<i>D. melanogaster</i> : CantonS	L.S. Shashidhara	N/A
<i>D. melanogaster</i> : tGPH	Bloomington stock center	#8163,RRID:BDSC_8163
<i>D. melanogaster</i> : <i>shg</i> RNAi	Bloomington stock	#38207,RRID:BDS

	center	C_38207
<i>D. melanogaster</i> : <i>rhogef2</i> RNAi	Bloomington stock center	#34643,RRID:BDS C_34643
<i>D. melanogaster</i> : <i>rok</i> RNAi	Tony J. Harris, U of Toronto, Canada	(Zhang et al., 2018)
<i>D. melanogaster</i> : <i>mbs</i> RNAi	Bloomington stock center	#41625,RRID:BDS C_41625
<i>D. melanogaster</i> : UASp-RHOGEF2	Bloomington stock center	#9386,RRID:BDSC _9386
<i>D. melanogaster</i> : <i>Sqh-Sqh</i> Cherry, <i>mat67-Gal4</i> ; <i>Ubi-DE-cad-GFP</i> , <i>mat15-Gal4/TM3Sb</i>	Adam C. Martin, MIT, MA, USA	(Mason et al., 2016)
<i>D. melanogaster</i> : <i>nanos-Gal4</i>	Bloomington stock center	N/A
<i>D. melanogaster</i> : <i>maternal α-tubulin Gal4-VP16 (mat-Gal4)</i>	Girish Ratnaparkhi, IISER, Pune, India	N/A
<i>D. melanogaster</i> : <i>baz</i> RNAi	Bloomington stock center	#35002
<i>D. melanogaster</i> : UASp-Baz Δ 969-1464-GFP	Andreas Wodarz	(Krahn et al., 2010)
<i>D. melanogaster</i> : UASp-Baz Δ 1-904-GFP	Andreas Wodarz	(Krahn et al., 2010)
<i>D. melanogaster</i> : <i>pnut</i> RNAi	Bloomington stock center	#65157
<i>D. melanogaster</i> : DE-cadherin RNAi	Bloomington stock center	#38207
<i>D. melanogaster</i> : <i>w</i> ¹¹¹⁸ ; UASp-shg. Δ JM	Bloomington stock center	#58444
<i>D. melanogaster</i> : UASp-shg. Δ p120	Bloomington stock center	#58434
<i>D. melanogaster</i> : UASp-shg. Δ β -cat	Bloomington stock center	#58497

<i>D. melanogaster</i> : endo-DE-Cadherin-GFP	Bloomington stock center	#60584
<i>D. melanogaster</i> : UASp-Pnut-mCherry	Manos Mavrakis	N/A
<i>D. melanogaster</i> : ovo ^D , FRT G13/CyO	Bloomington stock center	#2125
<i>D. melanogaster</i> : pnut ^{XP} FRT G13/CyO	Manos Mavrakis	(Mavrakis et al., 2014)
<i>D. melanogaster</i> : Small embryos	Cecelia Miles and Jun Ma	(Miles et al., 2011)

Table 2.1 Fly strains

2.2 Immunostaining

F1 flies were maintained in cages and 0-2.5hrs old embryos were collected on sucrose agar plates, washed and dechorionated with 100% bleach for 1 min. Embryos were then fixed using 1:1 mixture of 4% paraformaldehyde (PFA) and heptane for 20 min. Fixed embryos were then either hand-de-vitellinized or MeOH de-vitellinized (for phalloidin staining), washed thrice in 1X PBST (1X PBS with 0.3% Triton X-100) and blocked in 2% BSA (Sigma-Aldrich) in 1X PBST for 1 hr. Primary antibody was then added with appropriate dilution and incubated overnight, followed by three 1X PBST washes, and 1hr incubation in appropriate fluorescently coupled secondary antibodies at 1:1000 (Molecular probes) (Rothwell and Sullivan, 2007; Swedlow, 2011a, 2011b). Hoechst 33258 (1:1000, Molecular Probes) was added for 5 min in 1X PBST. Finally, the embryos were washed three times in 1X PBST and mounted in Slow fade Gold antifade reagent (Molecular Probes). For Zipper and Dlg immunostainings, heat fixation was done by adding dechorionated embryos in boiling 1X washing buffer (10X -7% NaCl and 0.5% Triton X) and instantly adding ice cold 1X washing buffer, followed by MeOH de-vitellinization. The primary antibodies used were: mouse anti-Dlg (1:100), rat anti-DE-cad (1:5, DSHB) and rabbit anti-Zipper (1:1000, gift from Thomas Jeffrey, Texas tech University, TX, USA). DNA was stained with Hoechst 33258.

2.3 Antibodies and Reagents

The antibodies and reagents used are listed in Table 2.2

Antibodies	SOURCE	IDENTIFIER
Rabbit anti-Bazooka	Andreas Wodarz	(Wodarz et al., 1999)
Mouse anti-Peanut	DSHB	4C9H4
Rat anti-DE-cadherin	DSHB	DCAD2, RRID:AB_528120
Rabbit anti-Patj	Hugo Bellen	N/A
Rabbit anti-Arp2	William Theurkauf	(Stevenson et al., 2002; Wodarz et al., 1999)
Rabbit anti-Dia	Steve Wasserman	(Afshar et al., 2000)
Mouse anti-Dlg	DSHB	4F3, RRID:AB_528203
Rabbit anti-Zipper	Thomas Jeffrey, Texas Tech University, TX, USA	(Chougule et al., 2016)
Alexa 488 coupled Goat anti-Mouse	Molecular Probes	A-1100, RRID:AB_2534069
Alexa 488 coupled Goat anti-Rabbit	Molecular Probes	A-11008, RRID:AB_143165
Alexa 568 coupled Goat anti-Mouse	Molecular Probes	A-11004, RRID:AB_141371
Alexa 568 coupled Goat anti-Rabbit	Molecular Probes	A-1101, RRID:AB_143157
Chemicals and dyes	SOURCE	IDENTIFIER
Hoechst 33258	Molecular Probes	H-3569
Slow Fade Gold	Molecular Probes	S-36937
CaCl ₂	Sigma Aldrich	449709-10G
EGTA	Sigma Aldrich	E3889-25G
Alexa 488 coupled Phalloidin	Molecular Probes	A-12379,

		RRID:AB_2315147
Alexa 568 coupled Phalloidin	Molecular Probes	A-12380, RRID:AB_2759224
Alexa 647 coupled Phalloidin	Molecular Probes	A-22287, RRID:AB_2620155

Table 2.2 Antibodies and reagents

2.4 Live Imaging of *Drosophila* embryos

F1 flies were maintained in cages and 1-1.5hrs old embryos were collected and dechorionated with 100% bleach for 1 min, and mounted on coverslip-bottomed LabTek chambers. The chambers were then filled with 1X PBS (Mavrakis et al., 2008) and imaged on either Zeiss Plan Apochromat 40X/ 1.4 NA oil objective or Leica SP8 40X/1.4 NA oil objective.

2.5 Microscopy specifications

Live or fixed embryos were imaged using the Zeiss laser scanning confocal microscope LSM710, LSM780 and Leica laser scanning confocal microscope SP8. The 40X objective with NA 1.4 was used to image living and fixed embryos. Care was taken to maintain the laser power and gain with the range indicator mode such that the 8-bit image acquired did not show any saturation and was within the 0-255 range. Averaging of 2 was used for both fixed and live imaging. Images were acquired with an optical section of 1.08 μm in all stainings.

2.6 Fluorescence Recovery after Photobleaching (FRAP)

FRAPs were performed on live embryos with 63X oil immersion objective with NA1.4 using Zeiss laser scanning confocal microscope LSM710. 488 nm laser was used at 100% power for photobleaching GFP tagged proteins with 80 iterations at zoom 2.5 and 2 averaging with maximum speed. The pinhole was opened to 160 μm .

3 frames were captured before the photobleaching followed by time lapse imaging for 1 minute. Please refer to the Image analysis section for estimation of the mobile fractions.

2.7 Quantification and statistical analysis

2.7.1 Quantification of relative fluorescent signal

Either single grazing sections or sum intensity Z projections from each time point were used for intensity analysis as per requirement. ROIs were drawn manually using the segmented line tool of ImageJ (National Institutes of Health) with thickness upto 6 points around minimum 5 cells per embryo to obtain raw intensity values. Normalizations were either done to the maximum or minimum value or the values from the apical section of interphase to depict a fold change. Please refer to the materials and methods of individual chapters to see specifics of normalization and quantification in each chapter.

2.7.3 Quantification of circularity

10 cells from each time point or furrow length were outlined with the polygon tool and circularity was calculated using the ImageJ shape descriptor tool. Circularity has the following formula:

$$\text{Circularity} = 4\pi (\text{Area}/\text{Perimeter}^2)$$

2.7.4 Polygon analysis

The most taut and bright grazing section from metaphase of each NC per embryo was used to quantify polygons using the Packing analyzer software (provided by Benoit Aigouy, (Classen et al., 2005), <https://idisk-srv1.mpi-cbg.de/~eaton/>). The software allows outlining each cell and colour coding it based on the polygon type. It also provides an excel sheet with the area, perimeter and polygon type of each cell in the field. Three or more embryos were used per NC and all the cells in the field were analysed this way to obtain the polygon distribution per cycle.

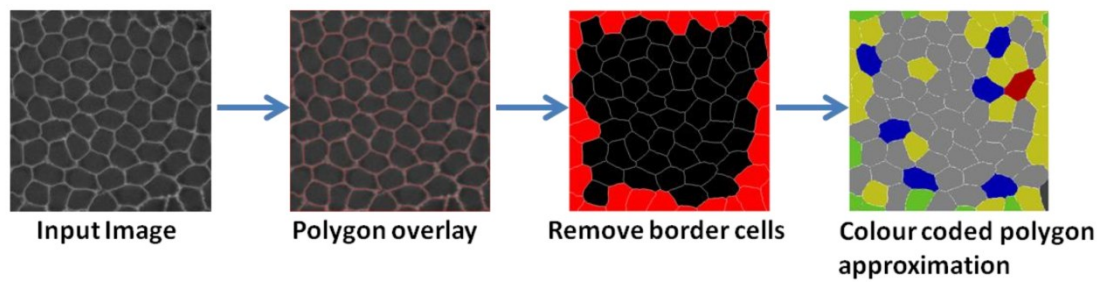


Figure 2.1 Steps involved in quantifying polygon distribution in tissues using packing analyser software.

2.7.5 Quantification of the furrow length

Furrow lengths were quantified from the orthogonal sections for different time points and NCs using the Zen blue software. Approximately 5-8 furrows were measured per time point per embryo. These lengths were further confirmed by estimating the number of z stacks spanning the entire furrow length of syncytial cells in the field of view.

2.7.8 Statistical analysis

All data are represented as mean \pm SD. Statistical significance was determined using the unpaired, two-tailed, Student's t-test for comparison between two means. One way ANOVA with Dunnett's Multiple Comparison Test was used when comparing three or more means together and comparing all points to a control point. One way ANOVA with Tukey's Multiple Comparison Test was used when comparing multiple means together and comparing all points with each other. Smoothing of circularity versus furrow length and DE-cad and Sqh intensity analysis curves were done using 2nd order, 3 neighbour "Savitsky-Golay" smoothing algorithm for better representation.

CHAPTER 3

Circular to polygonal transition correlates with lateral membrane length in the syncytial *Drosophila* embryo.

3.1 Introduction

Certain assumptions are often made while studying the property of hexagon dominance in epithelial tissues. Firstly, most studies are done in an already formed epithelium with polygonal organization, where various perturbations that only tweak the distribution are studied. This excludes understanding of how the transition from circular to polygonal cells occurs in the first place. The second major assumption is that most of these studies, including the theoretical models, approximate the epithelial sheet as a two dimensional array where only the apical section or a cross section of the cells is represented. Thus, the third dimension of cell height or lateral membrane length is completely ignored. Many 3D vertex models have been introduced with detailed description of forces acting along the apical, lateral and basal surfaces, in order to describe morphogenesis in 3D (Hannezo et al., 2014; Okuda et al., 2015; Alt et al., 2017). However, none of these models have been used to study the contribution of the lateral membrane in regulating the polygonal architecture of epithelial cells.

As mentioned in sections 1.1.1 and 1.1.2, the third dimension of an epithelial cell, that is, the lateral membrane houses some of the most important set of molecules that define an epithelial cell. These molecules include the junctional complexes, polarity regulators and cytoskeletal proteins associated with them. Therefore, the extent of stabilization of the lateral membrane could be an important factor contributing to the polygonal architecture. Here, we analyse the role of the lateral membrane length in transition of cell shape from circular to polygonal during early *Drosophila* embryogenesis. The *Drosophila* embryo is particularly suited for this due to the presence of a dynamic lateral membrane in the form of a furrow. During the syncytial nuclear division cycles, the plasma membrane between the nuclei

ingresses perpendicular to the embryo surface in the form of a furrow. This furrow initiates at interphase/prophase of each cycle, reaching a maximum at metaphase and retracts during anaphase/telophase (Figure 3.1, Silverman-Gavrila et al., 2008; Holly et al., 2015; Sherlekar and Rikhy, 2016). Mutations in several actin regulatory proteins show a decrease in the furrow length (Afshar et al., 2000; Stevenson et al., 2002). This property of extensive lateral membrane remodelling along with the availability of mutants that affect furrow length allows an analysis of lateral membrane length in the initiation of polygonal architecture.

3.2 Materials and methods

3.2.1 Fly stocks

Flies were raised in regular cornmeal agar at 25 °C. tGPH expressing flies were used for live imaging.

Stock name	Source	ID
<i>D. melanogaster</i> : CantonS	L.S. Shashidhara	
<i>D. melanogaster</i> : tGPH	Bloomington stock center	#8163,RRID:BDSC_8163

Table 3.1 Fly strains used

3.2.2 Live imaging

F1 flies were maintained in cages at 25 °C and 1-1.5hrs old embryos were collected and processed for imaging as mentioned in materials and methods section of chapter 2 (2.4).

3.2.3 Analysis

3.2.3.1 Quantification for circularity versus length graph

For each time point, the Z stack before the last visible stack towards the embryo interior was used for quantifying circularity using ImageJ as mentioned in chapter 2 (2.8.3). The furrow lengths for each time point were quantified using the zen blue software from orthogonal sections as mentioned in chapter 2 (2.8.5). The lengths were then grouped into class intervals of $1\mu\text{m}$ and the respective circularity values were plotted against it. Smoothing of the curve was done using 2nd order, 3 neighbour "Savitsky-Golay" smoothing algorithm for better representation.

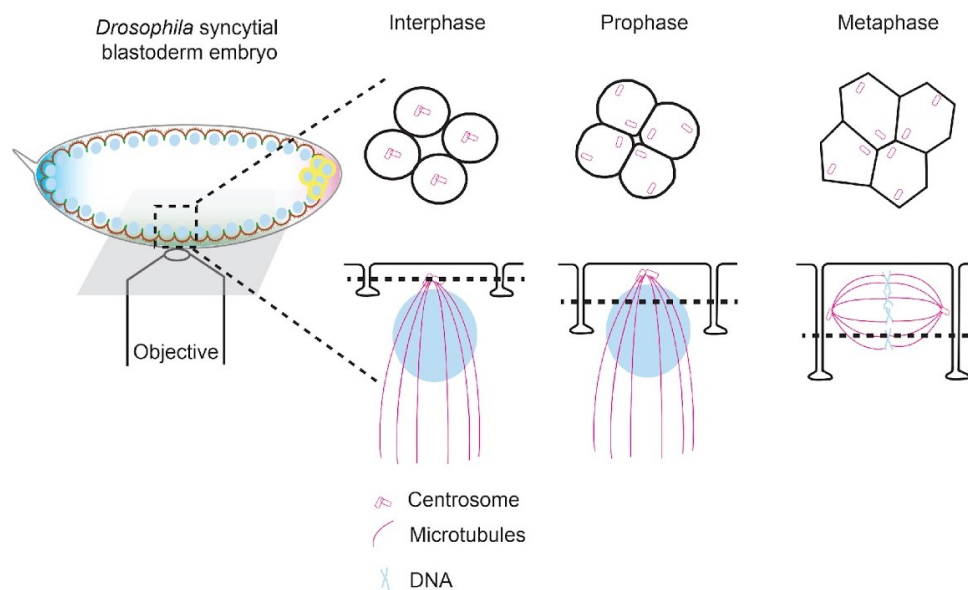


Figure 3.1 Schematic overview of confocal imaging of the syncytial blastoderm in *Drosophila* embryos.

The syncytial blastoderm division cycles show the presence of cortical nuclei with apical centrosomes giving rise to vertical microtubules. The centrosomes migrate to the lateral PM in prophase and metaphase coincident with extension of the PM to form an LM furrow. The LM furrow increases in length in the NC from interphase to metaphase. The schematics depict the PM organization in grazing and sagittal sections from interphase to metaphase. The dotted line in the sagittal view shows the section at which the grazing section is drawn in the schematic.

3.3 Results

3.3.1 A threshold plasma membrane ingression length correlates with the onset of polygonal architecture

Each nucleo-cytoplasmic domain of the syncytial *Drosophila* blastoderm

embryo shows compartmentalization of molecules and organelles in the plasma membrane and cytoplasm (Frescas et al., 2006; Mavrakis et al., 2009a). Hence, we refer to these domains as “syncytial cells”. The plasma membrane of syncytial cells is organised into polygons even before complete cell formation in cellularization (Holly et al., 2015b; Mavrakis et al., 2009b; McCartney et al., 2001a; Zhang et al., 1996a). To determine the temporal emergence of this polygonal architecture with respect to furrow or lateral membrane length in the syncytial embryo, we imaged living embryos (Figure 3.1) expressing the GFP tagged PH domain of GRP1 (tGPH). tGPH preferentially binds PIP3 in the plasma membrane (Britton et al., 2002) and labelled apical and lateral regions uniformly (Movie 3.1). We started with characterizing furrow length dynamics in the cortical syncytial cycles. The metaphase furrow length increased with each NC reaching approximately 6 μm in NC11, 9 μm in NC12 and 12 μm in NC13 (Figure 3.2A) and these values were similar to previous reports (Holly et al., 2015c; Silverman-Gavrila et al., 2008b). Within each NC, furrow length increased with respect to time from interphase to metaphase (Figure 3.2 B) . In NC13, there was an increase in furrow length with a slower phase until prophase and a faster phase from late prophase to metaphase (Figure 3.2C). These phases have been recently found to occur due to the onset of zygotic gene expression (Xie and Blankenship, 2018).

We next tracked the change in shape of syncytial cell plasma membrane with respect to furrow length. The plasma membrane organization changed from circular to polygonal as the furrow length increased in each NC (Figure 3.2D). To quantify this, we estimated circularity (C) of the plasma membrane in syncytial cells, as a measure of cell shape, with changing furrow lengths in NC13. $C=1$ for a perfect circle and $C<1$ for angular shapes, however for regular polygons which tend towards circles, $0.7<C<1$ (Xue and Sokac, 2016). Circularity decreased with increase in furrow length in NC11-13 (Figure 3.2D and E, Movie 3.2). Syncytial cells in interphase with short furrows (approximately $\leq 4 \mu\text{m}$), had almost circular plasma membrane organization ($C=0.95$) and transformed to a polygonal shape ($C= 0.7-0.85$) in metaphase with longer furrow lengths (approximately $\geq 10 \mu\text{m}$) (Figure 3.2F). This was also true for NC11-12 (Figure 3.2E). Polygonality was seen when the furrows ingressed beyond a threshold length range of 4.75-5.75 μm (Figure 3.2E, F). This threshold length range was taken as a testable limit for consistent change to polygonality in the syncytial *Drosophila* blastoderm embryo.

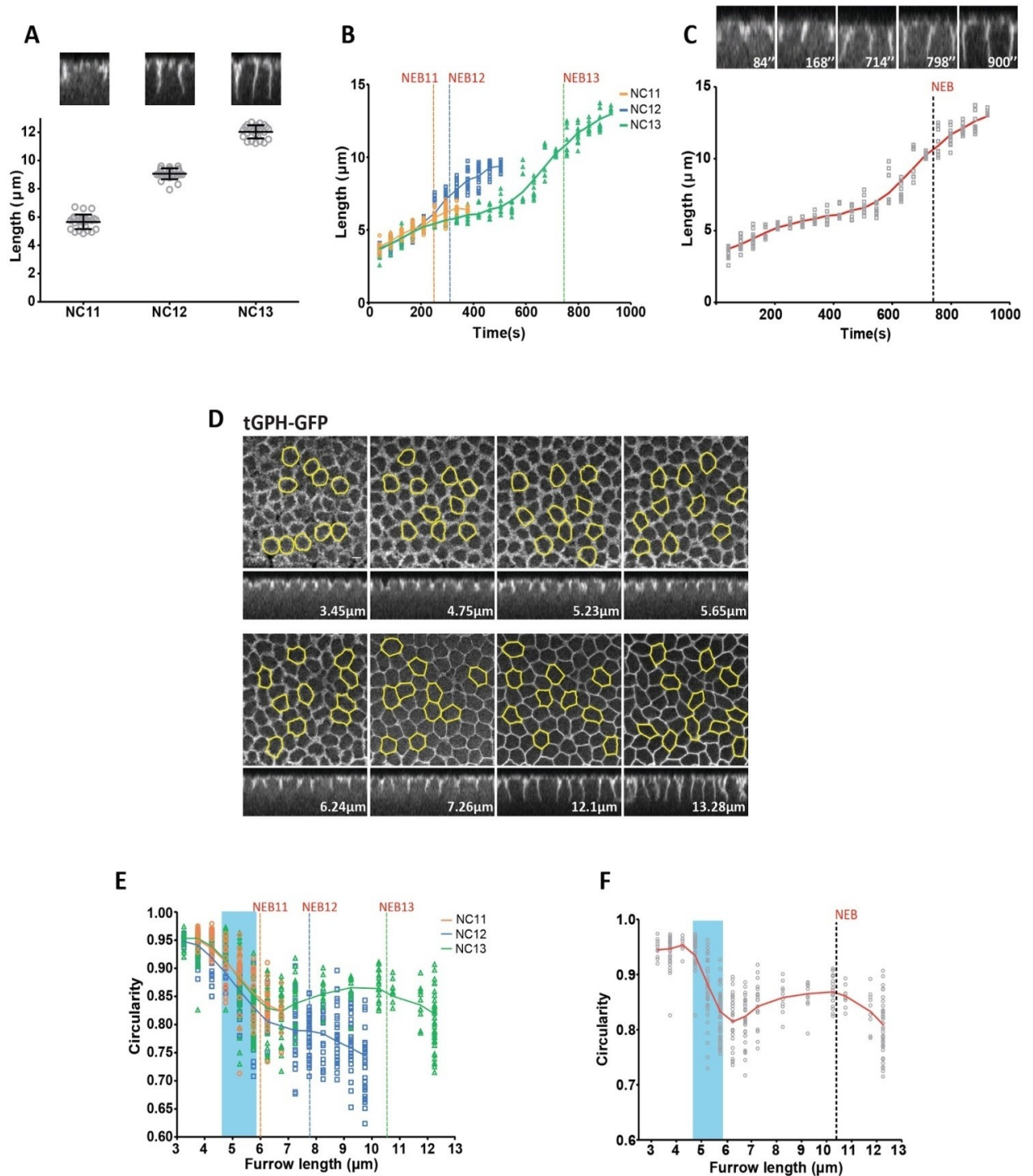


Figure 3.2 Circularity of syncytial cells decreases with increase in furrow lengths. Metaphase furrow length increases from NC11-13 (**A**). Furrow length increases with respect to time during NC11-13 (n=15; 5 furrows per embryo, 3 embryos) (**B**). Note that similar to Figure 1A, the final length that the furrow reaches in metaphase increases in the subsequent NCs. Furrow length increases with time in NC13 from interphase to metaphase (n=15; 5 furrows/embryo, 3 embryos) (**C**). Grazing and sagittal sections of tGPH expressing embryos at different furrow lengths ranging from 3.45 μm at the beginning of interphase to 13.28 μm at the end of metaphase (**D**). Yellow ROIs mark the cell shapes that are used to calculate the circularity at a given furrow length. Graph showing decrease in circularity with increase in furrow length in NC11-13 (**E**). Note the similar decrease in

circularity with respect to length in all cycles irrespective of the final length (n=30; 10 cells/embryo, 3 embryos). Graph showing circularity decreases with furrow length increase in NC13 (**F**) (n=30; 10 cells/embryo, 3 embryos). The blue region in **E** and **F** shows the threshold range, i.e., it is the range during which the PM organization changes from circular to polygonal. Dashed lines represent the nuclear envelope breakdown (NEB) point for the respective nuclear division cycles

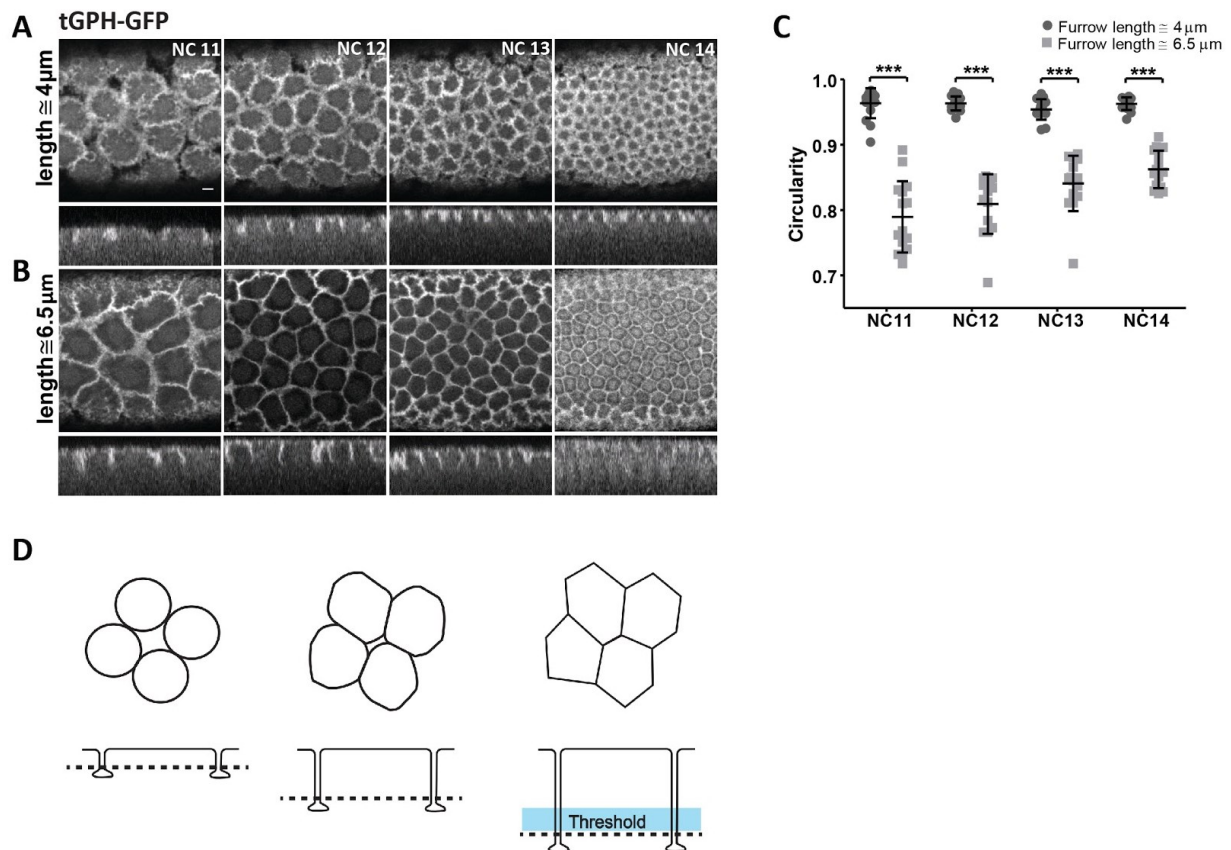


Figure 3.3 Polygons are seen above a threshold lateral membrane length irrespective of cell size and crowding. tGPH embryos grazing (XY) and sagittal (XZ) sections in NC11-14 at furrow length $<4.75\mu\text{m}$ (the furrows selected are $\sim 4\mu\text{m}$) (**A**) and $>5.75\mu\text{m}$ (the furrows selected are $\sim 6.5\mu\text{m}$) (**B**). Quantification of circularity at lengths in **E** and **F** (**C**) (n=15; 5 cells/embryo, 3 embryos). (**D**) Schematic summarising polygonality onset after crossing the threshold furrow length range. Data is represented as mean \pm SD, * $p < 0.05$, ** $p < 0.01$, and *** $p < 0.001$, Student's t test, paired, two tailed. Scale bar: $5\mu\text{m}$.

3.3.2 The onset of polygonality is dependent on threshold irrespective of cell crowding, size and edge lengths.

As the embryo progressed through NC11-14, the number of syncytial cells increased while the cell size and edge length decreased. We, therefore, asked whether polygonality onset was correlated with increase in crowding as a result of increased syncytial cell numbers. For this, we measured the circularity of syncytial

cells across NC11-14 at two different furrow lengths, i.e. at a length below and above the threshold range, irrespective of the cell cycle phase (Figure 3.3A-B). The plasma membrane around syncytial cells remained circular in all NCs, when the lateral membrane length was less than the threshold at approximately 4 μm (Figure 3.3A, C). Only at furrow length greater than the threshold, at approximately 6.5 μm , the plasma membrane was polygonal in NC11-14 (Figure 3.3B, C). Polygonality in the syncytial *Drosophila* embryo was, therefore, a function of furrow length, independent of number of syncytial cells or edge lengths (Figure 3.3D).

3.4 Discussion and conclusion

Based on the study, we propose a lateral membrane length-based model for the initiation of polygonal epithelial-like architecture, in the earliest morphogenetic event of syncytial blastoderm development in *Drosophila* embryogenesis. Because of a dynamic lateral membrane furrow, the syncytial blastoderm forms an effective model system to elucidate the mechanism by which key molecular components regulate polygon shape transition. We show that ingression of furrows above a threshold lateral membrane length range allows the coincident formation of edges between adjacent plasma membrane regions and transition of syncytial cell shapes from circular to polygonal (Figure 3.3D). Polygonal plasma membrane organization occurs at the threshold lateral membrane length, irrespective of the cell cycle phase, NC, cell crowding and cell size. The plasma membrane shape changes from circular to polygonal in NC11, when the threshold lateral membrane length is crossed for the first time during syncytial development. This study shows for the first time the contribution of the third dimension of epithelial cells in polygon formation.

CHAPTER 4

Onset of epithelial-like hexagon-dominated polygon distribution in the syncytial *Drosophila* embryo

4.1 Introduction

Hexagon-dominated polygonal packing is a conserved property of all epithelia across various organisms ranging from the diploblastic *Hydra* to the triploblastic *Xenopus* (Gibson et al., 2006). This kind of organization has also been seen to evolve over developmental stages in some cases. For example, in the wing disc of *D. melanogaster*, there is an increase in the percentage of hexagons from 60% to 80% from larval to pupal stages (Classen et al., 2005; Sánchez-Gutiérrez et al., 2013).

There are various physical as well as molecular factors that influence this distribution. Most theoretical models use surface free energy minimization as the constraint that leads to hexagonal packing. Surface energy minimization for a group of epithelial cells is a cumulative result of minimizing the surface area of each cell exposed to the surrounding while maximizing contacts between them, just like molecules in a fluid bulk (Lecuit and Lenne, 2007). If cells have asynchronous divisions but uniform cell division rates, then hexagon dominated polygon packing can arise simply as a result of cell division (Gibson et al., 2006). Farhadifar et al., on the other hand, also include mechanical properties of the cell in a 2D vertex model and incorporate cell rearrangements, in addition to cell divisions and show that both contribute to the hexagon-dominated polygon distribution (Farhadifar et al., 2007). Another model shows that mechanical-force-dependent growth rates along with cellular rearrangements result in a distribution that best matches experimental data for hexagon dominance (Aegerter-Wilmsen et al., 2010)

Tissue level anisotropy of forces also direct polygon distribution. Increased tension in the pupal wing epithelial tissue along the proximal-distal (PD) axis increases the frequency of hexagonal cells and their alignment along the PD axis.

This is corroborated by the fact that when the wings are cut from the hinge, the anisotropy of tension along PD axis is reduced which correlates with the decrease in the number of hexagonal cells (Sugimura and Ishihara, 2013).

Very few molecular factors have been reported to influence hexagon dominance. One of the most common one is the junctional molecule E-cadherin (E-cad). Overstabilization or lack of E-cad recycling results in decreasing the frequency of hexagons in *Drosophila* wing discs. This E-cad recycling is shown to be regulated by planar cell polarity (PCP) proteins and the loss of PCP proteins, in turn, shows a decrease in the number of hexagons in the epithelium (Classen et al., 2005). In animal cell cultures, it has been observed that loss of ROCK1 and ROCK2, which are important regulators of Myosin II activity, result in shortening of lateral cell height and decrease in the percentage of hexagons (Kalaji et al., 2012). Therefore, a range of adhesion, contractility and polarity molecules may affect this distribution.

Tissue geometry also influences the way epithelial cells are organized in 3 dimensions. In *Drosophila* cellularization, contacts between neighbouring cells change along the apico-basal axis at the anterior pole, as opposed to cells in the embryo trunk where the frequency of such changes is low (Rupprecht et al., 2017). This kind of contact rearrangement in space along the apico-basal axis is now known to be a property of highly curved or tubular tissues and the 3D shapes, thus, formed are referred to as scutoids (Gómez-Gálvez et al., 2018). Whether such changes in tissue geometry also alter the polygonal distribution is still unclear. Based on pure mathematical considerations, a flat surface can be most optimally packed with regular hexagons, while a spherical surface needs to have a combination of both pentagons and hexagons, like that on a football. In biological samples, most tissues are not flat and, thus, have a combination of hexagons, pentagons and heptagons, with hexagons dominating. However, it will be interesting to see if the polygon distribution varies with the tissue geometry.

The plasma membrane of syncytial *Drosophila* embryos is organised into polygons even before complete cell formation in cellularization (Holly et al., 2015d; Mavrakakis et al., 2009c; McCartney et al., 2001b; Zhang et al., 1996b). However, the temporal emergence of this architecture as well as the frequency distribution they attain during development is not documented. As shown in Chapter 3, the onset of polygonal architecture occurs when the lateral membrane length reaches a threshold length in each NC. Further, we went ahead to quantify the frequency distribution of

the polygonal architecture achieved at the maximum lateral membrane length in each NC i.e. at metaphase (which is longer than the threshold lateral membrane length). Here, we look at the effect of various factors like, lateral membrane length, crowding of cells and tissue geometry on the polygonal distribution.

4.2 Materials and methods

4.2.1 Fly stocks

Flies were raised in regular cornmeal agar at 25 °C. tGPH expressing flies were used for live imaging while small embryos and CantonS were used for fixed imagings and stainings.

Stock name	Source	ID
<i>D. melanogaster</i> : CantonS	L.S. Shashidhara	
<i>D. melanogaster</i> : tGPH	Bloomington stock center	#8163,RRID:BDSC_8163
<i>D. melanogaster</i> : Small embryos		

Table 4.1 Fly strains used

4.2.2 Live imaging

F1 flies were maintained in cages at 25 °C and 1-1.5hrs old embryos were collected and processed for imaging as mentioned in materials and methods section of chapter 2 (2.4).

4.2.3 Immunostaining

F1 flies were maintained in cages at 25 °C and 2.5-3hrs old embryos were collected and fixed with 4% PFA as mentioned in Chapter 2 (2.2). For phalloidin staining, embryos were hand-devitellinized followed by three washes in PBST for 5 mins each. Phalloidin was added at a concentration of 1:100 and incubated for

45mins. Finally, the embryos were washed three times in 1X PBST including one wash with Hoechst 33258 (1:1000, Molecular Probes) in 1X PBST, for 5 min and mounted in Slow fade Gold antifade reagent (Molecular Probes)

4.2.4 Analysis and Quantification

4.2.4.1 Polygon analysis

The brightest Z-stack amongst the last few lateral sections at metaphase were used for polygonal approximation using packing analyzer as mentioned in Chapter 2 (2.8.4). The percentage of each polygon type was then plotted for each embryo to obtain an average polygon distribution for the population.

4.3 Results

4.3.1 Hexagon dominated plasma membrane organization emerges at nuclear cycle 12

We started with quantifying the polygon distribution of syncytial cells at metaphase of each NC. Towards this we performed live imaging of tGPH expressing embryos and used the packing analyzer software to quantify the polygon distribution from the images. The syncytial cells were relatively far apart in NC10 metaphase and seen as separated caps at the embryo surface. In metaphase of NC11, the plasma membrane was organized into a polygonal array for the first time in *Drosophila* embryo development (Figure 4.1A). NC11 was also the point at which the furrow length (6 μm) extended beyond the threshold for the first time during development (Figures 3.2 and 3.3). NC11 showed almost equal numbers of pentagons and hexagons (Figure 4.1B,C). The polygonal array became hexagon-dominated at NC12 metaphase and this persisted in NC13-14 (Figure 4.1B,C). Thus, epithelial-like hexagon dominance first occurs at NC12, even before complete cells are formed in cellularization.

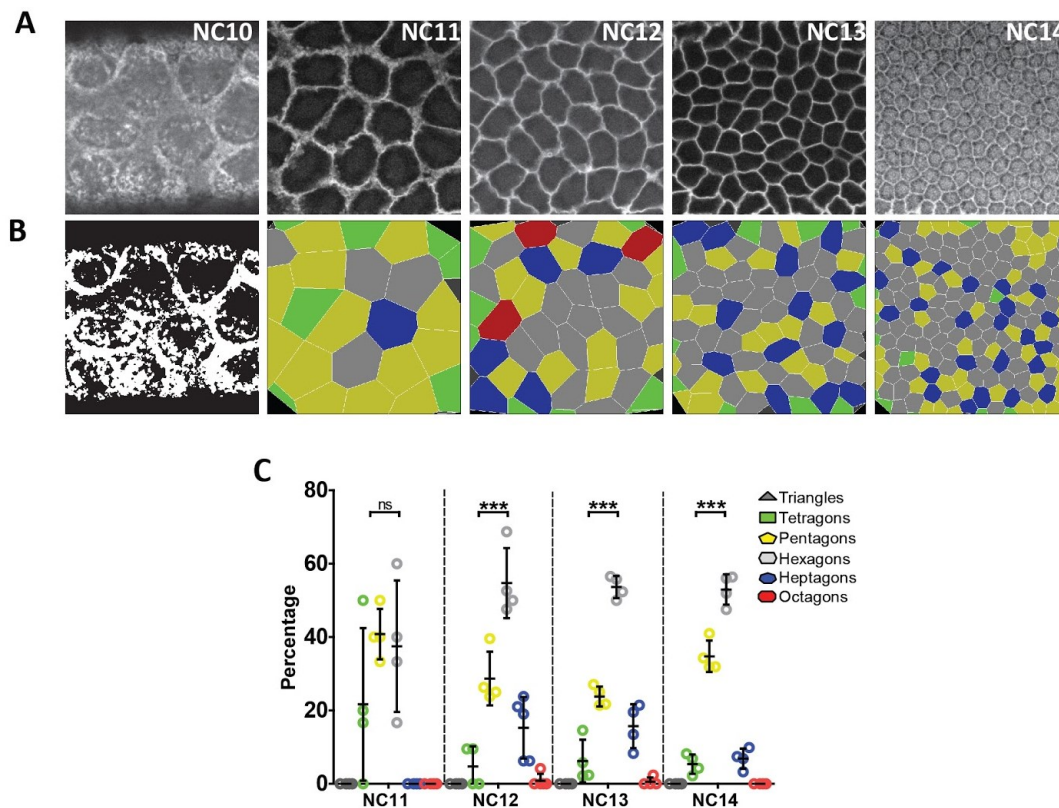


Figure 4.1 Hexagon dominated plasma membrane organization emerges at NC12 . Grazing sections of tGPH expressing embryos from NC10-14 at metaphase (A). Colour-coded polygon rendering using the packing analyzer software (B). Quantitative analysis of polygon distribution in NC11-14 (n=4 embryos) (C). Data is represented as mean \pm SD, * p <0.05, ** p <0.01, and *** p <0.001. NC11 polygon distribution is significantly different from NC12-14 and NC12-14 are similar to each other, Multinomial chi square test (*** p <0.001). Two tailed, unpaired Student's t test to compare pentagons and hexagons.

4.3.2 Both lateral membrane length and crowding influence onset of hexagon-dominance

Since the onset of polygonal architecture in the syncytial cells occurs with the lateral membrane length crossing a threshold length range (Chapter 3), we were curious to see if hexagon dominance also depended on lateral membrane length. Towards this, we quantified the polygonal distribution for each NC just above the threshold (at lateral membrane length equal to $6.5\mu\text{m}$) when the polygonal shape is initiated, using the same tGPH movies (Figure 4.2B, C). The onset of hexagon dominance occurred at NC13 at this length as opposed to at NC12 at maximum lateral length during metaphase (Figure 4.2D). If hexagon dominance was dependent only on lateral membrane length, then the onset would have occurred at

the same length across NC11-14. However, that is not the case and the onset of hexagon dominance occurs at different lengths for different NCs. Since the only thing that is changing across NC11-14 at length 6.5 microns is the cell size and crowding, these can be additional factors influencing the number of contacts per individual cell and, hence, the polygonal distribution of the tissue.

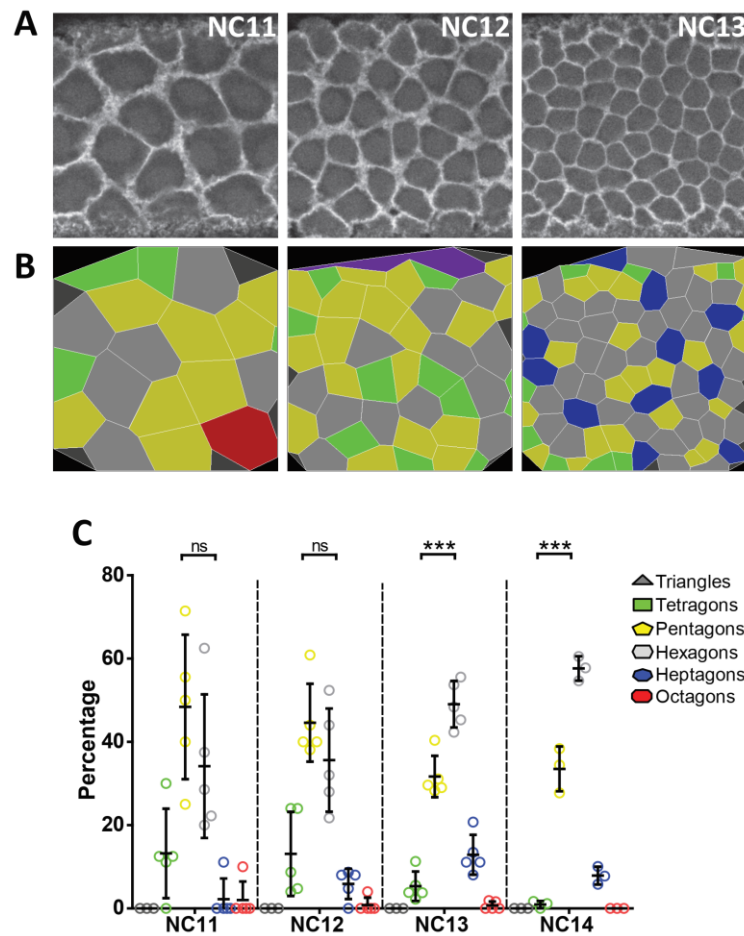


Figure 4.2 NC12 does not show hexagon dominance at a furrow length just above the threshold.

Grazing sections of tGPH expressing embryos from NC11-13 at furrow length just above the threshold (approximately 6.5 μ m) (A). Colour-coded polygon rendering using the packing analyzer software (B). NC14 was quantified manually. Quantitative analysis of polygon distribution in NC11-14 (n=4 embryos) (C). NC11-12 polygon distributions are significantly different from NC13-14. Data is represented as mean \pm SD, *p<0.05, **p<0.01, and ***p<0.001. Multinomial chi square test (***p<0.001). Two tailed, unpaired Student's t test to compare pentagons and hexagons.

4.3.3 Small embryos show a delay in the onset of hexagon-dominated polygon distribution

In order to further look at the influence of cell crowding and cell sizes on the polygonal distribution, we quantified the polygonal distribution in small and large embryos (Miles et al., 2011). The length, as measured along the antero-posterior axis, was significantly shorter than the wild-type in small embryos while for the large embryos we didn't find a larger size (Figure 4.3A). Thus, we proceeded with the analysis of only the small embryos as a comparison to wildtype CS embryos. These embryos were fixed and stained for F-actin with Phalloidin and imaged using confocal microscopy. We expected that because of scaling, the smaller embryos might have either decrease in cell numbers or have the same cell numbers but decreased cell areas in a given field of the tissue. But we found that they had similar cell numbers and cell areas as compared to wildtype (Figure 4.3B and 4.4A,D). However, the onset of hexagon dominance was delayed and occurred at NC13 instead of NC12 as in wildtype (Figure 4.4A-F). Thus, changing the size of the tissue slightly delays the onset of hexagon-dominance but still achieves the conserved hexagon-dominated distribution by NC13.

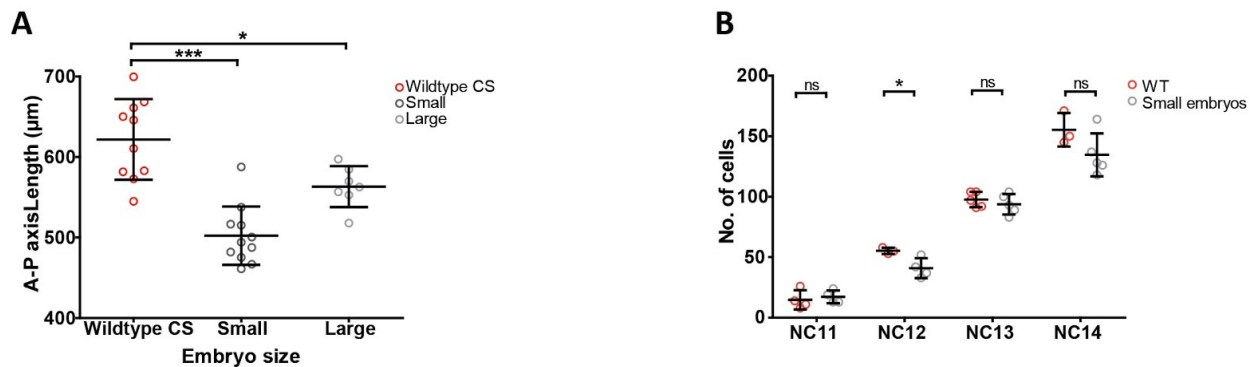


Figure 4.3 Comparison between small, large and wildtype embryos.

Graph comparing the length along A-P axis of small, large and wildtype embryos (**A**). Graph comparing the cell numbers between small and wildtype embryos (**B**). Data is represented as mean \pm SD, * $p < 0.05$, ** $p < 0.01$, and *** $p < 0.001$. Two tailed, unpaired Student's t test to compare pentagons and hexagons.

4.4 Conclusion and discussion

Here, we show that the syncytial blastoderm shows onset of hexagon dominance at NC12, much before complete cells are formed during cellularization. Unlike previous reports from tissues with asynchronous divisions, synchronous divisions of syncytial blastoderm also give rise to the conserved hexagon-dominated distribution. There is no fixed lateral membrane length threshold to achieve hexagon dominance, as NC12 does not show hexagon dominance just above the threshold at $6.5\mu\text{m}$, while NC13-14 do. However, lateral length has some contribution as the distribution at NC12 eventually becomes hexagon-dominated with further lateral membrane extension to $9\mu\text{m}$ at metaphase. At a fixed lateral membrane length, the only variable across NCs is the cell number and cell size. Thus, it is possible that a combination of cell crowding, cell size and lateral membrane length contribute to hexagon dominance.

Interestingly, tissue geometry does not drastically affect this distribution. This is in agreement with the finding that various epithelia in metazoans show the conserved hexagon-dominated distribution, irrespective of the geometry of the epithelial tissue (Gibson et al., 2006; Miles et al., 2011). In addition, the anterior pole of the *Drosophila* embryo still shows hexagon-dominance similar to the trunk region in cellularization. This could be further corroborated by studying the polygon distribution in mutants where the embryo shape is drastically changed. One of the ways to do this is to knockdown the atypical cadherin molecule Fat2 which gives rise to spherical embryos (Rupprecht et al., 2017). In spite of this, the marginal difference of delay in hexagon-dominance seen in small embryos might be due to differences in the protein concentration on the plasma membrane of key molecules that regulate shape change. A screen for such molecules can help us narrow down the protein complexes that regulate this distribution.

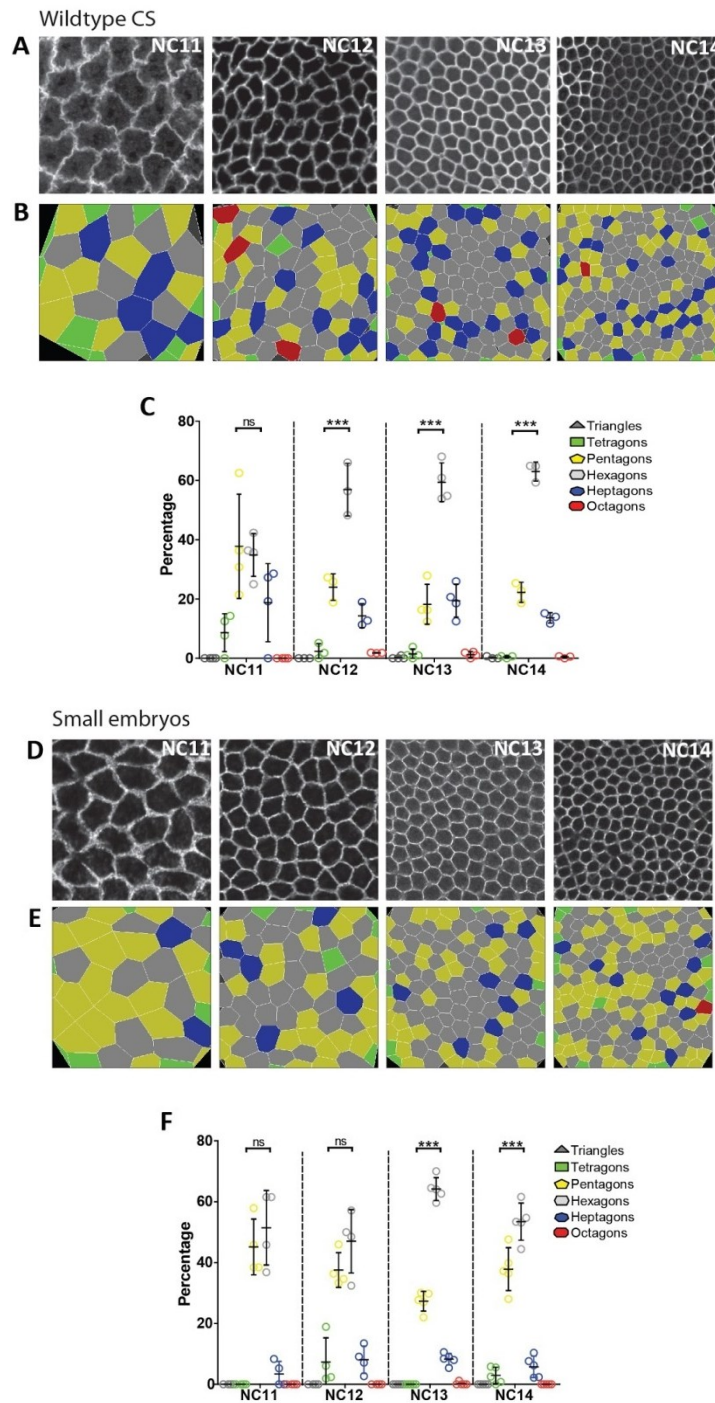


Figure 4.4 Small embryos show a delay in the onset of hexagon dominance.

Grazing sections of phalloidin stained wildtype embryos from NC11-14 at metaphase (**A**). Colour-coded polygon rendering using the packing analyzer software (**B**). Quantitative analysis of polygon distribution in NC11-14 (n=4 embryos) (**C**). Grazing sections of phalloidin stained small embryos from NC11-14 at metaphase (**D**). Colour-coded polygon rendering using the packing analyzer software (**E**). Quantitative analysis of polygon distribution in NC11-14 (n=4 embryos) (**F**). Data is represented as mean \pm SD, * $p < 0.05$, ** $p < 0.01$, and *** $p < 0.001$. Two tailed, unpaired Student's t test to compare pentagons and hexagons.

CHAPTER 5

Onset of epithelial-like plasma membrane polarity in the syncytial *Drosophila* embryo

5.1 Introduction

Epithelial polarity in *Drosophila* embryos is distinctly present at the end of cellularization when epithelial cells are first formed (Harris and Peifer, 2004). However, the syncytial cells have several features that resemble an epithelial cell, for example, apical villi-like projections and a nascent plasma membrane ingression that resembles the lateral membrane of epithelial cells. It is known that polarity proteins such as Bazooka, DE-cadherin, PatJ and Dlg are already present on the membrane before cellularization, i.e. in the syncytial cycles, and molecular asymmetries with respect to some of these proteins have been noted (Mavrakis et al., 2009d; Schmidt and Grosshans, 2018). The asymmetry is, however, found to be quite different from that of mature epithelial cells.

To begin with, the *Drosophila* embryo is cortically uniform at the pre-blastoderm stage, both morphologically and molecularly. The first cortical differentiation occurs at the syncytial blastoderm stage where the cortex is divided into two domains during interphase; the cap and intercap regions. The cap region is enriched in F-actin and actin associated proteins like Arp2/3, SCAR, Moesin, ELMO, Sponge and α -spectrin, while the intercap region is marked by Myosin II, Toll and Slam. Subsequently, during metaphase, the cortex is further segregated into 3 domains; apical, lateral and basal domain. In the case of a syncytial cell, basal domain refers to the furrow tip since syncytial cells lack a basal membrane. The apical-lateral region is occupied by Canoe, Peanut, Scrambled, DE-cad, Bazooka; lateral by Dlg and Toll; and the furrow tip by PatJ, Amphiphysin, Anilin, Dia and Syndapin. Unlike mammalian epithelial cells however, lipid asymmetries in PIP2 and PIP3 are not seen very clearly in the syncytial system (Foe et al., 2000; Mavrakis et al., 2009c; Pesacreta et al., 1989; Schmidt and Grosshans, 2018; Schmidt et al.,

2018; Stevenson et al., 2002; Thomas and Williams, 1999; Zallen et al., 2002). This is summarized in Table 5.1.

In terms of morphological features, the caps are enriched in multiple villi-like projections as compared to the intercap region. These projections are reduced at metaphase when the caps are flattened (Figard et al., 2013, 2016; Turner and Mahowald, 1976). Thus, the syncytial system already shows molecular and morphological asymmetries and can be said to be polarized to some extent. However, the function of polarity in the early syncytial system is not thoroughly explored.

Besides the usual apico-basal polarity, epithelial cells also show asymmetries in other planes. One such example is of planar cell polarity (PCP), which refers to polarized distribution of cellular components along the plane of the epithelial sheet, i.e. perpendicular to the apico-basal axis. A simplistic version of this is asymmetric distribution of proteins along the edges and vertices of a polygonal epithelial cell which, unlike PCP, lacks any polarity axis. Vertices are points in an epithelial sheet where three cells meet, also referred to as tricellular junctions. Edges, on the other hand, are the points where two cells meet, also referred to as bicellular junctions. One of the examples of such asymmetry are molecules of tricellular junctions in invertebrate epithelia, namely, Gliotactin, Sidekick and Anakonda (Byri et al., 2015; Lye et al., 2014; Schulte et al., 2003). They are essential for the morphology and barrier function of epithelia. The vertebrate counterparts of these are tricellulins and angulins (Higashi et al., 2013; Ikenouchi et al., 2005; Masuda et al., 2011). Myosin II and vinculins are also seen at the vertices sometimes in response to mechanical tension (Higashi and Miller, 2017). In *Drosophila* germ band extension, F-actin and non-muscle Myosin II are specifically enriched along the dorso-ventrally oriented junctions, while the adherens junction components and Baz are enriched along the antero-posterior junctions (Kong et al., 2017). Whether such asymmetries exist in the syncytial system is not known till date.

Thus, with the hints of epithelial-like apico-basal polarity already existing, we decided to quantitatively describe these asymmetries in the syncytial cells. We also decided to carefully observe asymmetries, if any, in the plane of the epithelium.

Cell cycle phase	Position	Polarity regulators
Interphase	Cap	F-actin, Arp2/3, SCAR, Moesin, and β -spectrin, ELMO, Sponge
	Intercap	α -spectrin, β_{Heavy} -spectrin, Myosin II, Toll, Anillin, E-cad and Slam
Metaphase	Apicolateral	Bazooka, Peanut, Canoe, Scrambled, E-cad, Baz
	Lateral	Dlg, Toll,
	Basal (Furrow tip)	PatJ, Amphiphysin, Anilin, Dia, Syndapin

Table 5.1 Summary of polarity in the syncytial *Drosophila* embryo

5.2 Materials and Methods

5.2.1 Fly stocks

Flies were raised in regular cornmeal agar at 25 °C. tGPH, endo-DE-Cadherin-GFP, UASp-Baz-GFP, UASp-Pnut-mCherry, UASp-Sep1-GFP and UASp-Sep2-GFP were used for live imaging. UASp-Baz-GFP, UASp-Pnut-mCherry, UASp-Sep1-GFP and UASp-Sep2-GFP were crossed to *nanos-gal4* at 25 °C to maternally express the tagged proteins in the F2 embryos.

Stock name	Source	ID
<i>D. melanogaster</i> : tGPH	Bloomington stock center	#8163,RRID:BDSC_8163
<i>D. melanogaster</i> : CantonS	L.S. Shashidhara	
<i>D. melanogaster</i> : UASp-Baz-GFP	Bloomington stock center	#65845

<i>D. melanogaster</i> : endo-DE-Cadherin-GFP	Bloomington stock center	#60584
<i>D. melanogaster</i> : UASp-Pnut-mCherry	Manos Mavrakis	N/A
<i>D. melanogaster</i> : UASp-Sep1-GFP	Bloomington stock center	
<i>D. melanogaster</i> : UASp-Sep2-GFP	Bloomington stock center	
<i>D. melanogaster</i> : <i>nanos</i> -Gal4	Bloomington stock center	N/A

Table 5.1 Fly strains used

5.2.2 Live imaging

F1 flies were maintained in cages at 25 °C and 1-1.5hrs old embryos were collected and processed for imaging as mentioned in Chapter 2 (2.4).

5.2.3 Immunostaining

F1 flies were maintained in cages at 25 °C and 2.5-3hrs old embryos were collected and fixed with 4% PFA as mentioned in Chapter 2 (2.2). Embryos were fixed with 1mM EGTA IN 4%PFA for DE-cad staining. Following antibodies were used for detecting asymmetries: Dlg (1:100), DCAD2 (1:5), Pnut (1:5), Sep1(1:100), Sep2 (1:250), Scrib(1:2000). Finally, the embryos were washed three times in 1X PBST including one wash with Hoechst 33258 (1:1000, Molecular Probes) in 1X PBST for 5 min and mounted in Slow fade Gold antifade reagent (Molecular Probes).

5.2.4 Analysis and quantification

5.2.4.1 Quantification of relative fluorescent signal across depth and in planar sections of the plasma membrane

The grazing sections at metaphase across depth expressing various polarity transgenes were used for this analysis. ROIs were drawn at 5 edges and 5 vertices for NC11, and 10 edges and 10 vertices for NC12-13, in each stack from apical to

basal sections. The mean intensities from these ROIs were measured using ImageJ. The intensities from each stack were background subtracted. The graphs shown in Figure 2 represent mean intensities obtained across the depth of the furrow normalized to the mean intensity of the apical-most stack in NC11.

For calculating relative fold change of fluorescence for DE-cad-GFP, Baz-GFP and Pnut-mCherry in the furrow in NC11 to NC13, total intensities across the furrow length were computed by summation of the mean intensity across the number of optical stacks in NC11, 12 and 13. The total intensities obtained for the entire furrow in NC12 and 13 were divided by the total intensity obtained in NC11 to obtain fold change.

Enrichment in the basolateral region and edge/vertex were computed by performing statistical analysis for the fluorescence values on the length of the furrow using two way ANOVA to test how the intensity of signals varied with either edge/vertex or apical/basal regions of the furrow.

5.3 Results

5.3.1 XZ Polarity in the syncytial *Drosophila* embryo

Since the syncytial embryo plasma membrane was organized into epithelial-like polygonal array starting from NC11, we determined if polarity proteins were progressively and quantitatively enriched in the lateral furrows in NC11-13. Presence of DE-cadherin (DE-cad, *shotgun*, *shg*), Bazooka (Baz), Crumbs, Stardust, Dlg and PatJ was first confirmed with immunostaining. Crumbs and Stardust were not expressed in the early embryo (data not shown). As previously observed, DE-cad, Baz and Dlg were present along the lateral membrane while PatJ was enriched at the tip (Figure 5.1A, C). On careful observation, Dlg was seen to be enriched in the basolateral part of the furrow (Figure 5.1A). Scribble (Scrib), which is part of the same polarity complex as Dlg was also found to be present laterally (Figure 5.1B). The septin family proteins Peanut (Pnut), Sep1 and Sep2 were also studied as Pnut is present at the lateral membrane in syncytial stages and functions in actin organization and furrow extension (Silverman-Gavrila et al., 2008b).

In order to characterize the temporal distribution of DE-cad, Baz and Pnut as

compared to tGPH, we performed live imaging of embryos expressing DE-cad-GFP (Huang et al., 2009), Baz-GFP (Benton and St Johnston, 2003) and Pnut-mCherry (Guillot and Lecuit, 2013) (Figure 5.2A-D). We quantified the fluorescently tagged protein in edges and vertices of the polygonal array in NC11-13 along the entire metaphase furrow length and plotted the fold change with respect to the apical section of NC11 (Figure 5.2E-H). DE-cad was spread on the entire metaphase furrow throughout NC11-13 and also increased in levels during the NCs (Figure 5.2B-B", F-F"). Baz and Pnut were enriched towards the basolateral region of the furrow throughout the syncytial cycles and this asymmetry was enhanced with the subsequent cycles (Figure 5.2C-C", G'-G", 5.2D-D", H-H"). Baz and Pnut also showed increased furrow recruitment from NC11-12. However, the fold change of DE-cad across the syncytial cycles was more than Baz and Pnut (Figure 5.2F" compared to 5.2G", H").

5.3.2 XY Polarity in the syncytial *Drosophila* embryo (Done in collaboration with Tirthasree Das)

As mentioned in section 5.1, the epithelial plasma membrane shows a distinct distribution of proteins along tricellular junctions, which function in sealing the intercellular space (Ikenouchi et al., 2005; Schulte et al., 2003). Interestingly, we also observed asymmetries in the XY plane apart from that along the XZ plane. DE-cad and Baz were enriched along the edges of the polygonal syncytial cells, while Pnut was enriched at the vertex (Figure 5.2F", H"). The relative enrichments for Baz and Pnut started at NC11 (Figure 5.2G, H), while that for DE-cad appeared only at NC13 (Figure 5.2F"). Edge enrichment was also seen for Dlg and vertex enrichment was additionally observed in Sep1 and Sep2 (Figure 5.1E-H). In contrast to these asymmetrically localized proteins, tGPH showed uniform fluorescence without significant asymmetries in the XZ and XY planes (Figure 5.2A-A", E-E").

5.4 Conclusion and Discussion

Collectively, these data helped characterizing the onset of molecular asymmetry in the lateral furrow of syncytial *Drosophila* embryos before cellularization

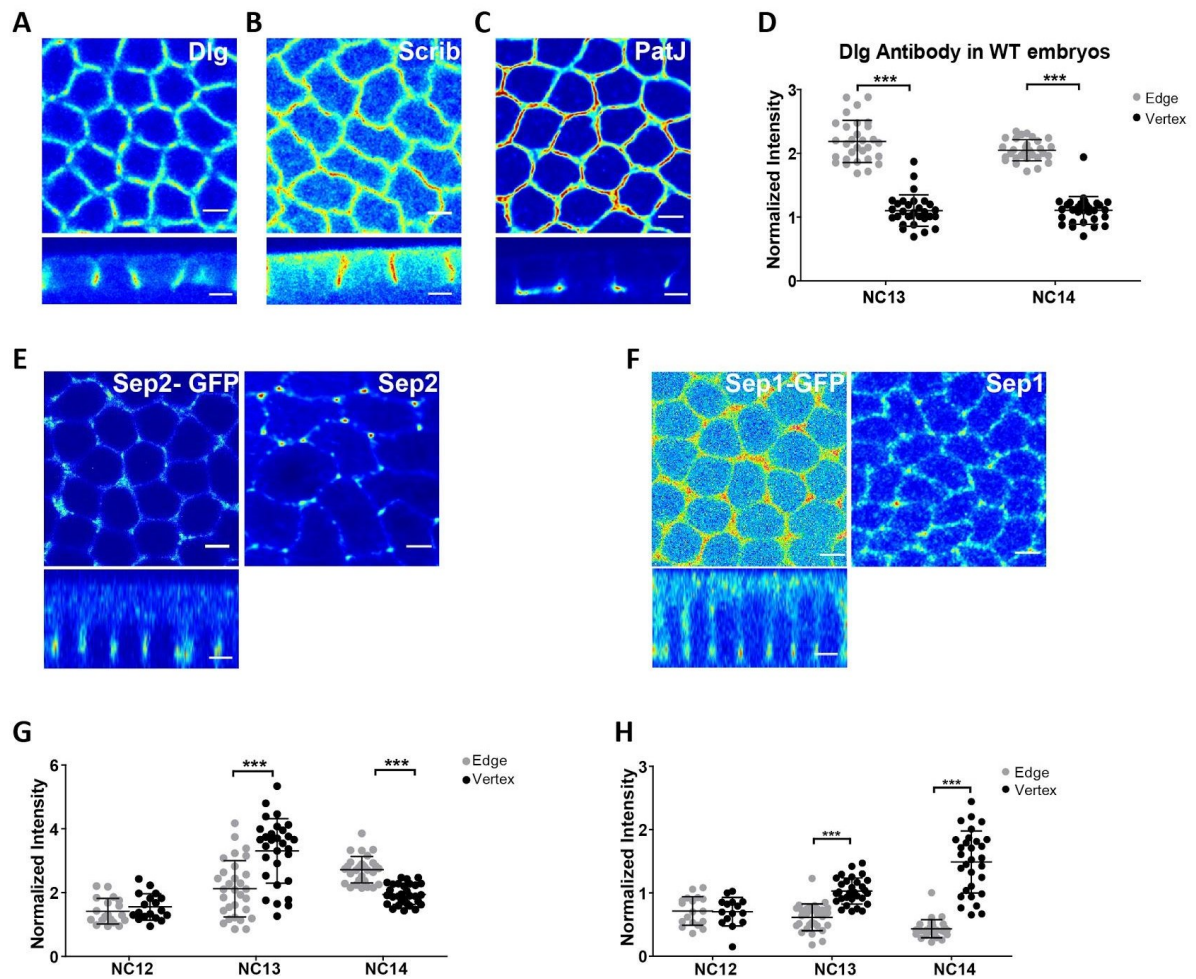


Figure 5.1 Asymmetric localization of polarity regulators and septin family proteins in the syncytial embryo .

Grazing and sagittal sections of wildtype embryos stained with Dlg (**A**), Scrib (**B**) and PatJ at NC13. Graph showing edge enrichment of Dlg (**D**). Note the sagittal section in Dlg staining shows basolateral enrichment while Patj shows basal tip enrichment. (**E-H**)The septin family proteins Sep1 and Sep2 show vertex enrichment in the syncytial plasma membrane in NC13-14. Grazing sections of embryos expressing Sep2-GFP along with the antibody staining (**E**) and Sep1-GFP along with the antibody staining (**F**) in wild type embryos at NC13 (**A**). Graphs show the comparison of signal on edge versus vertex in Sep2-GFP (**G**) and Sep1-GFP (**H**) expression embryos at single optical section (n=15, 5 edges and vertices from each embryo; 3 embryos). Data is represented as mean \pm SD, *p<0.05, **p<0.01, and ***p<0.001, Student's t test with Welch's correction. Scale Bar = 5 μ m.

(Figure 5.3). In summary, Baz and Pnut asymmetrically distributed between edges and vertices, respectively, by NC12. By this time, Baz and Pnut were also collectively enriched in the basolateral furrow region. DE-cad was enriched along the edges in NC13 and was spread throughout the lateral domain from NC11-13. These molecular asymmetries in syncytial cells were in the form of relative enrichments along the lateral furrow length or edges and vertices. This was different from later

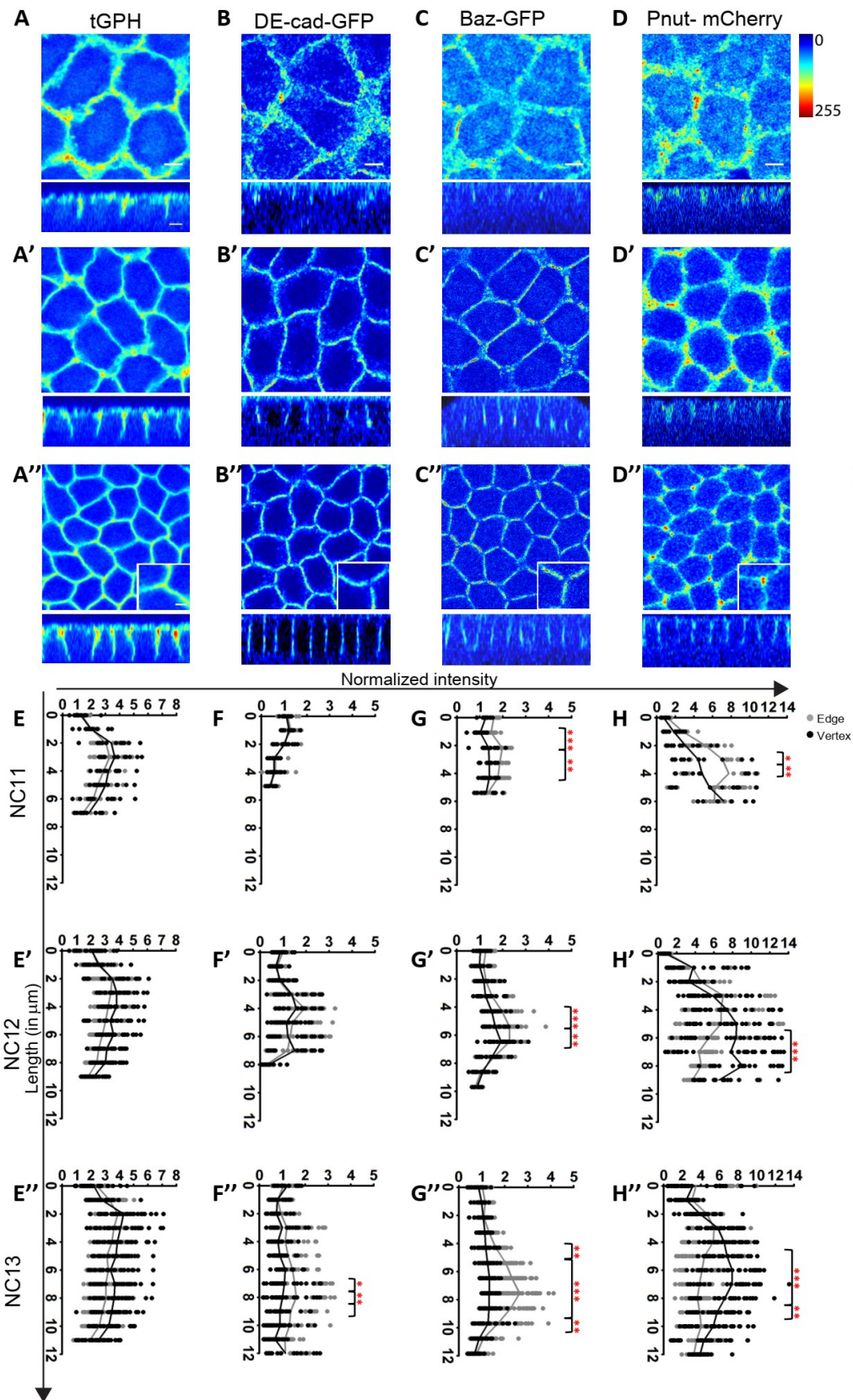


Figure 5.2 DE-cad, Baz and Pnut show polarized distribution in the syncytial cells.

(A-D) Distribution of tGPH (A: NC11, A': NC12 and A'': NC13), DE-cad-GFP (B: NC11, B': NC12 and B'': NC13), Baz-GFP (C: NC11, C': NC12 and C'': NC13) and Pnut-mCherry (D: NC11, D': NC12 and

D'': NC13) in grazing and sagittal views in syncytial NC11-13. The Jet rainbow scale from ImageJ is used to show fluorescent intensities. tGPH (**A''**) shows uniform localization on the entire plasma membrane, DE-cad (**B''**) and Baz (**C''**) show edge enrichment and Pnut shows vertex enrichment in NC13 (**D''**) (insets show zoomed images). (**E-H**) Quantification of intensities normalized to the apical section of NC11 in edges (black) and vertices (grey) along the metaphase furrow length for tGPH (**E**: NC11, **E'**: NC12, **E''**: NC13), DE-cad-GFP (**F**: NC11, **F'**: NC12, **F''**: NC13), Baz-GFP (**G**: NC11, **G'**: NC12, **G''**: NC13) and Pnut-mCherry (**H**: NC11, **H'**: NC12, **H''**: NC13) in NC11-13 (n=3 embryos each). Baz is enriched on the edge NC11 onwards while Pnut is enriched on the vertex NC12 onwards. DE-cad is enriched at edges in NC13. The scatter plots contain a line connecting the means, *p<0.05, **p<0.01, and ***p<0.001, Two way ANOVA with Bonferroni post tests. Bazooka and tGPH show 1.5 fold enrichment on the membrane from NC11-12, Pnut and DE-cad show 2 fold enrichment from NC11-12. DE-cad shows 3 fold enrichment on the lateral membrane at NC13 while others do not show further increase

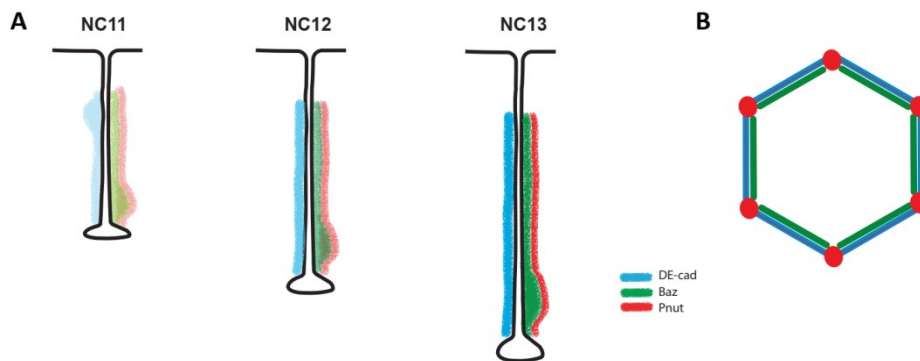


Figure 5.3 Schematic representing the polarized localization of proteins in XZ and XY planes.

Asymmetric distribution of DE-cad, Baz and Pnut across NC11-13 along the XZ plane(**A**). While DE-cad spreads all across the length, Baz and Pnut are enriched in the basolateral region. Note the general increase in the levels of all three proteins across the syncytial cycles. Asymmetric distribution of DE-cad, Baz and Pnut between edges and vertices in the XY plane (**B**)

stages in fully formed epithelial cells where there are distinct domains marked by mutually exclusive localizations of polarity complexes (Bilder et al., 2000, 2003; Harris and Peifer, 2004). In addition to the existing literature for the syncytium, our quantitation provides details of finer asymmetries along the lateral furrow. Previous reports group Dlg, E-cad, Toll and Bazooka into one domain that uniformly spans the entire lateral membrane (Mavrakakis et al., 2009; Schmidt and Grosshans, 2018). In contrast, our data showed enrichment of Baz and Pnut in the basolateral membrane and E-cad spread throughout the lateral membrane. Immunostainings of Dlg also showed that it was enriched in the basolateral region. Plasma membrane polarity is

known to be important in maintaining cell morphology (Bilder and Perrimon, 2000; Hayashi and Carthew, 2004; Letizia et al., 2013). It would, therefore, be interesting to follow the functions of these cortical domains in the syncytium and their impact on cell morphology.

The levels of polarity proteins also increased on the syncytial membrane differentially for each protein from NC11-13. While Baz and Pnut showed up to two-fold increase in recruitment from NC11 to NC12, DE-cad showed further three-fold increase by NC13. Directed membrane addition through exocytosis contributes to increased lengths and numbers of furrows over the successive NCs (Holly et al., 2015; Mavor et al., 2016). It is possible, therefore, that DE-cad being a transmembrane protein gets recruited more in each cycle. Increased levels of DE-cad may be required for increased adhesion between the furrow membranes as the furrow lengths increase in successive NCs, thereby, requiring DE-cad to span a larger region of the membrane.

In addition, the syncytial cycles are highly dynamic and require quick formation and dissociation of contacts during furrow formation and retraction. Excessive adhesion may lead to strong and static contacts, leading to a jammed state where cells are relatively frozen in place. This would impede the fluidity and dynamicity of the syncytial cycles. This may be the reason why polarity complexes gradually increased over the syncytial division cycles towards cellularization, where stronger contacts are required to withstand the forces in gastrulation.

Septins are a conserved family of cytoskeletal GTP-binding proteins in eukaryotes that have diverse functions in cell polarity, cytokinesis and membrane remodelling (Kinoshita, 2006; Mostowy and Cossart, 2012). Vertex enrichment of septins in the syncytial cells was an interesting finding, as septins usually function as diffusion barriers for proteins embedded in the plasma and endoplasmic reticulum (ER) membrane (Luedeke et al., 2005; Takizawa et al., 2000). They also act as scaffolds for the recruitment of a wide variety of proteins, for example, a large repertoire of cell division machinery in yeast is recruited in a septin-dependent manner at the cytokinetic ring. Therefore, it is possible that Septins localize at the vertex to serve as a barrier for diffusion of proteins across the edge. At the same time, Septins at the vertex may also act as a scaffold for the recruitment of other tricellular junction proteins. Further experiments in this direction will be necessary to answer these open questions. *Drosophila melanogaster* has five septin family

proteins, namely- Sep1, Sep2, Sep4, Sep5 and Pnut. Of these, Pnut, Sep1 and Sep2 form a heteromeric six-subunit complex consisting of two copies of each septin (Field et al., 1996). This is in agreement with the observation that all three showed vertex enrichment in NC13 of the syncytial embryo.

It is interesting to observe that the *Drosophila* syncytial plasma membrane showed epithelial-like polarity even in the absence of a basal membrane. In mammalian epithelial cells, basal membranes play an important role in supporting the initiation of polarity. This occurs mainly via re-organization of cytoskeletal regulators upon adhesion between Integrins in the basal membrane and the extra-cellular matrix (ECM). In the absence of cell-ECM adhesion, polarity is, nevertheless, initiated with the help of E-cad mediated cell-cell adhesion but the tight junctions formed are spread throughout the lateral domain. Only upon restoring the cell-ECM adhesion, tight junctions get restricted to the apico-lateral boundary. Cell-ECM adhesion through the basal membrane is also essential to re-orient the polarity axis. If a cell aggregate with apical surface exposed to the surrounding is covered with ECM, the apical surface transforms into the basal domain and vice-versa. In such cases, the tight junctions then migrate to the new apico-lateral position (Drubin and Nelson, 1996; Vega-Salas, 1987; Wang et al., 1990a, 1990b). It is, therefore, possible that absence of a basal membrane results in gross asymmetries in the syncytial plasma membrane, unlike finer asymmetries observed in later stages where the basal membrane is present (Harris and Peifer, 2004).

CHAPTER 6

Adhesion and contractility balance at the threshold lateral membrane length regulates circular to polygonal transition

6.1 Introduction

Two fundamental forces that drive cell shape changes and, therefore, tissue morphogenesis are actomyosin based contractions and cadherin mediated cell-cell adhesion. These two forces play opposing roles with adhesion facilitating expansion of the contact area between cells while actomyosin contractions working to reduce it (Heisenberg and Bellaïche, 2013; Maître and Heisenberg, 2013). A change in the balance of these two forces transforms the shapes of cells. Cellular force generation typically relies on molecular motors like Myosin II which can bind to and reorganize actin filaments in the cell. The cytoskeletal changes within a cell are then transmitted to other cells via cell-cell and cell matrix adhesion molecules like cadherins and integrins. For example, during *Drosophila* ventral furrow invagination, apical constriction of mesodermal cells occurs due to apical myosin pulling on to the cadherin based junctions, thus, reducing the apical surface area (Martin et al., 2009; Roh-Johnson et al., 2012). Similarly, coupling of actomyosin to cadherin based junctions during germ band extension allows shrinking of dorso-ventrally oriented junctions (Rauzi et al., 2010). On the other hand, resolution of multicellular rosettes in germ band extension, is facilitated by DE-cadherin accumulation in the absence of Myosin II on the newly formed contact (Blankenship et al., 2006).

Both adhesion and contractility, individually are also responsible for lateral membrane length or cell height. Suppression of Myosin II based contractility along lateral membranes is essential for junction maturation and thus, proper cell height formation in mammalian cells (Yu et al., 2016a). On the contrary, epithelial cell height in *Drosophila* wing disc is shortened by hyperactivity and spread of Rho1 and Myosin II along the entire lateral membrane length (Widmann and Dahmann, 2009). Loss of AJ components, like Armadillo and E-cad, during gastrulation also result in

cells losing adhesion to neighbouring cells, thereby, rounding up and losing their columnar shape (Cox et al., 1996; Harris and Peifer, 2004). As opposed to this, overexpression of cell adhesion molecules like Fas2 prevents the shrinking of lateral membranes during cuboidal to squamous transition in the *Drosophila* follicular epithelium (Gomez et al., 2012). This is also observed with increased expression of DE-cad, DN-cad and Arm in the same system (Melani et al., 2008). On the other hand, Arm loss in the early stage follicle cells, which are normally cuboidal, causes them to assume a flattened squamous shape (Tanentzapf et al., 2000). It is, therefore, possible that an interplay of adhesion and contractility regulates lateral membrane length and stability.

Thus, to evaluate the role of key molecular players in achieving the shape transition through a threshold lateral membrane extension, we focused our attention to the roles of DE-cadherin (DE-cad) in lateral membrane adhesion and Myosin II (MyoII) in regulating contractility in the lateral membrane.

6.2 Material and Methods

6.2.1 Fly stocks

All flies were raised in regular cornmeal agar and all crosses were maintained at 25 °C, except *rhoGEF2*ⁱ which was maintained at 29 °C and *shg*ⁱ which was maintained at 18 °C. *maternal α4 tubulin-Gal4-VP16* was used for all RNAi and overexpression experiments except for *shg*ⁱ and *mbs*ⁱ for live imaging with tGPH. *shg*ⁱ was crossed to a single chromosomal copy of *nos-Gal4* and maintained at 18 °C. F1 flies expressing *shg*ⁱ with *nos-Gal4* laid embryos that were arrested early in the pre-blastoderm stage of development when the cross was grown at 25 or 29 °C and, hence, the experiments were performed at 18 °C to allow for Gal4 dilution. The lethality of *shg*ⁱ embryos was 100% (n=150) at 25 °C and 29 °C and 70% (n=200) at 18 °C after 24 hours. The *shg*ⁱ expressing embryos laid from the cross at 18 °C gave an opportunity to test the effect of loss of DE-cad in the syncytial blastoderm embryo. For live imaging, tGPH *mat-Gal4-VP16*; *mat-Gal4-VP16* or *Sqh-Sqh Cherry*, *mat67-Gal4*; *Ubi-DE-cad-GFP*, *mat15-Gal4/TM3Sb* were crossed to all RNAi lines except *mbs*ⁱ which was crossed to tGPH *nos-Gal4*. This was done to reduce the severity of

effects caused due to tagged transgenes with two copies of Gal4, which increased the lethality of these embryos and ff arrested them in pre-blastoderm.

Stock name	Source	ID
<i>D. melanogaster</i> : CantonS	L.S. Shashidhara	
<i>D. melanogaster</i> : tGPH	Bloomington stock center	#8163,RRID:BDSC_8163
<i>D. melanogaster</i> : <i>shg</i> RNAi	Bloomington stock center	#38207,RRID:BDS C_38207
<i>D. melanogaster</i> : <i>rhogef2</i> RNAi	Bloomington stock center	#34643,RRID:BDS C_34643
<i>D. melanogaster</i> : <i>rok</i> RNAi	Tony J. Harris, U of Toronto, Canada	(Zhang et al., 2018)
<i>D. melanogaster</i> : <i>mbs</i> RNAi	Bloomington stock center	#41625,RRID:BDS C_41625
<i>D. melanogaster</i> : <i>UASp-RHOGEF2</i>	Bloomington stock center	#9386,RRID:BDSC_9386
<i>D. melanogaster</i> : <i>Sqh-Sqh</i> Cherry, <i>mat67-Gal4</i> ; <i>Ubi-DE-cad-GFP</i> , <i>mat15-Gal4/TM3Sb</i>	Adam C. Martin, MIT, MA, USA	(Mason et al., 2016)
<i>D. melanogaster</i> : <i>nanos-Gal4</i>	Bloomington stock center	N/A
<i>D. melanogaster</i> : <i>maternal α-tubulin Gal4-VP16 (mat-Gal4)</i>	Girish Ratnaparkhi, IISER, Pune, India	N/A
<i>D. melanogaster</i> : <i>endo-DE-cadherin-GFP</i>	Bloomington stock centre	#60584,RRID:BDS C_60584

Table 6.1 Fly strains used

6.2.2 Live imaging

F1 flies were maintained in cages at 25 °C or 29 °C or 18 °C as per requirement, and 1-1.5hrs old embryos were collected and processed for imaging as mentioned in Chapter 2 (2.4).

6.2.3 Immunostaining

F1 flies were maintained in cages at 25 °C or 29 °C or 18 °C and 2.5-3hrs old embryos were collected and fixed with 4% PFA as mentioned in Chapter 2 (2.2). Embryos were fixed with 1mM EGTA in 4%PFA for DE-cad staining or were heat fixed for Dlg and Zipper staining as mentioned in Chapter 2. Following antibodies were used: Dlg (1:100), DCAD2 (1:5), Zipper (1:100). Phalloidin (1:100) was only used after hand-devitellinization. Finally, the embryos were washed three times in 1X PBST including one wash with Hoechst 33258 (1:1000, Molecular Probes) in 1X PBST for 5 min and mounted in Slow fade Gold antifade reagent (Molecular Probes).

6.2.4 Fluorescence Recovery after Photobleaching (FRAP)

FRAPs were performed on live E-cad-GFP and Sqh-GFP embryos as mentioned in Chapter 2 (2.6). ROI sizes of 2µm and 3µm in diameter were used for E-cad-GFP and Sqh-GFP, respectively. FRAPs were performed at two different stages for comparison; below threshold (as observed with circular membrane morphology) and above threshold (as observed with polygonality onset). See section 6.2.5.3 for quantification and analysis

6.2.5 Laser Ablation

tGPH GFP or DE-cad GFP expressing live embryos were used for visualizing the membrane for laser ablation experiments using the Leica TCS SP8 MP or Zeiss LSM780. ROIs of size 0.4µm in diameter were created on junctions below threshold (as observed with circular membrane morphology), above threshold (as observed with polygonality onset) and Metaphase. Ablations were performed with 800nm multiphoton laser at 80% power with 10 iterations under 40X water immersion objective on Leica TCS SP8 MP or 30-45% laser power with 30 iterations under 63X oil immersion objective on Zeiss LSM780 MaiTai laser. Please refer to the Image analysis section for estimation of recoil velocities from control and ablated regions

6.2.6 Analysis and quantification

6.2.6.1 Quantification of the metaphase furrow length

Metaphase was identified as the time point when maximum extension took place. The furrow lengths in metaphase for each NC were quantified using the Zen blue software from orthogonal sections as mentioned in chapter 2 (2.8.5). Statistical significance was determined using the unpaired, two-tailed, Student's t-test for comparison between controls and mutants.

6.2.6.2 Quantification of relative fluorescent signal for DE-cad-GFP and Sqh-mCherry across time from interphase to metaphase.

Sum intensity z projections of all z stacks with membrane signal for Sqh-mCherry and DE-cad-GFP were obtained using ImageJ for each time point from interphase to metaphase. ROIs were drawn around 6 syncytial cells to get total intensity values for each time point using ImageJ as mentioned in Chapter 2 (2.8.1). The total intensity at each time point was normalised to the maximum value and plotted as Normalized intensity versus time graph.

6.2.6.3 Estimation of mobile fractions from FRAP experiments

FRAP was monitored in the bleached region with respect to the bleached edge and the neighboring edges in contact with the bleached edge (Bleached edge+4 neighboring edges=total ROI). The raw intensity values from the bleached ROI and the total ROI across time were obtained using the Zen software, FRAP module. The raw intensity values in the ROI were first subtracted by the raw intensity values at first times point after the bleach time point to set the bleach point to zero. The values, thus obtained were normalized to the average of pre-bleach intensity in both the bleached ROI and Total ROI. Finally these values were then normalized to the total to obtain the FRAP curve data points on a 0-1 scale. These data points were then used for a one-phase association curve fitting using Graphpad Prism 5 which provides the mobile fractions as an output. Following is the equation for one-phase exponential association curve:

$Y = Y_0 + (\text{Plateau} - Y_0) (1 - \exp(-Kx))$,
where Plateau - Y_0 is the mobile fraction.

6.2.6.4 Quantification of recoil velocities after laser ablation

The XY coordinates of vertices from control and ablated edges were obtained using the MtrackJ plugin of ImageJ software. The distances between the two vertices were calculated using these XY coordinates with the following formula:

$$\text{Distance} = \sqrt{(X_2 - X_1)^2 + (Y_2 - Y_1)^2},$$

Where (X1, Y1) and (X2, Y2) are the coordinates of vertex1 and vertex2, respectively.

A distance versus time graph was plotted followed by linear fitting. The slopes of the vertex distance versus time graph represented the recoil velocities (Liang et al., 2016). The recoil velocities, thus, obtained were then plotted for comparison between the control and ablated edges below threshold, above threshold and metaphase. In order to normalize for inherent differences between controls of below threshold, above threshold and metaphase, all the points of the control and ablated edge of a given stage was divided by the average of the control of that stage. This brought all the controls to the same level and allowed comparison across the three different stages.

6.3 Results

6.3.1 Myosin II levels decrease while DE-cadherin levels increase at the lateral plasma membrane with length above the threshold

DE-cad has been previously observed to be present at the polygonal plasma membrane in syncytial embryos (Harris and Peifer, 2004; McCartney et al., 2001a) and MyoII recruits to the furrow in interphase and prophase and is lost from the

furrow in metaphase of the syncytial cycle (Foe et al., 2000; Royou et al., 2002a, 2002b). We started with further determining the relative dynamics of DE-cad and MyoII in a quantitative manner within one syncytial NC. We performed live imaging of embryos co-expressing mCherry tagged Myosin regulatory light chain, Spaghetti squash (Sqh-mCherry) and GFP tagged DE-cadherin (DE-cad-GFP) and quantified their intensities on the plasma membrane from interphase to metaphase of NC13 (Movie 6.1). We observed that there was an increase in DE-cad intensity throughout the NC until metaphase (Figure 6.1A, D). Conversely, MyoII intensity dropped consistently from interphase to metaphase (Figure 6.1B, D). In addition, at metaphase MyoII was completely lost from the furrow membrane and became cytosolic while DE-cad was retained on the plasma membrane. MyoII again got recruited to the plasma membrane during late telophase at the sites of new furrow formation followed by DE-cad accumulation (Figure 6.1C). Therefore, MyoII appears to be dispensable for furrow stability at the point of maximum extension at metaphase.

6.3.2 Myosin II is stabilized more after crossing the threshold whereas DE-cadherin dynamics remain unchanged

Further, we studied the mobility of both DE-cad and MyoII at the lateral membrane below and above the threshold with Fluorescence recovery after photobleaching (FRAP). DE-cad mobility didn't show significant differences in mobile fractions below and above the threshold in our experimental setup. This suggested that the organization possibly doesn't change drastically during this transition (Figure 6.2 A- D). However, MyoII mobile fraction was reduced significantly after crossing the threshold suggesting that the MyoII gets more organized on the plasma membrane (Figure 6.1E-H).

6.3.3 The lateral furrow plasma membrane with length above the threshold has higher tension

Since there was a transition of plasma membrane shape from circular to

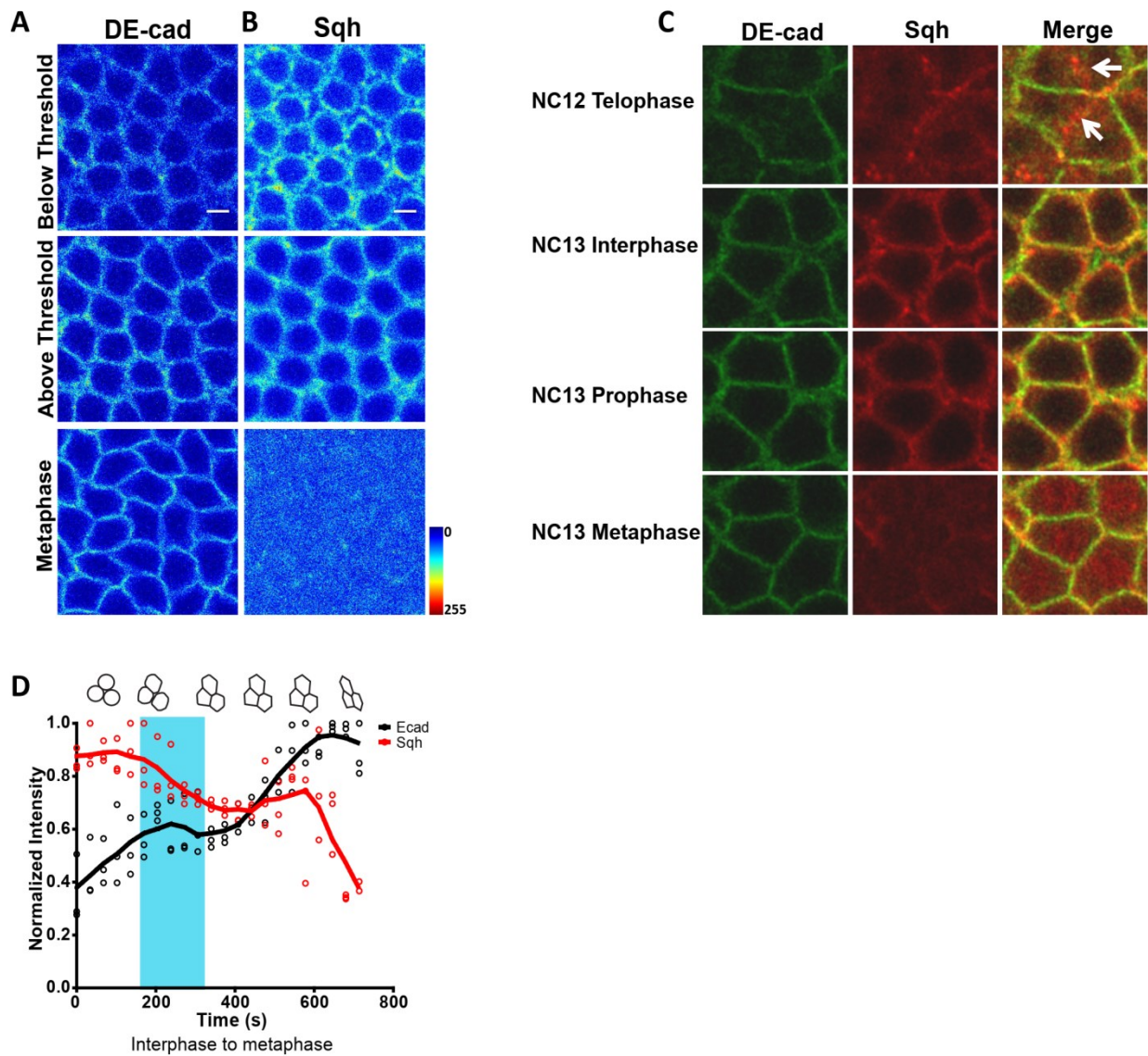


Figure 6.1 DE-cad levels increase while MyoII levels decrease at the plasma membrane in NC13 during furrow extension. (A-C) DE-cad increases and MyoII decreases in NC13: Grazing sections of an embryo expressing DE-cad-GFP (**A**) and Sqh-mCherry (**B**) showing total intensity of the membrane signal across the lateral furrow below threshold lateral membrane length, above threshold lateral membrane length, and at metaphase. (**C**) Grazing sections of an embryo co-expressing DE-cad-GFP and Sqh-mCherry from NC12 telophase to NC13 metaphase. The white arrows point to the locations of appearance of Sqh-mCherry at the end of telophase. (**D**) Quantification of total membrane intensities across the Z stack normalized to the maximum value for DE-cad-GFP (black) and Sqh-mCherry (red) ($n=18$, 6 cells/embryo, 3 embryos). The blue region in (**C**) is the threshold range of transition from circular to polygonal. Scale bar: 5 μm .

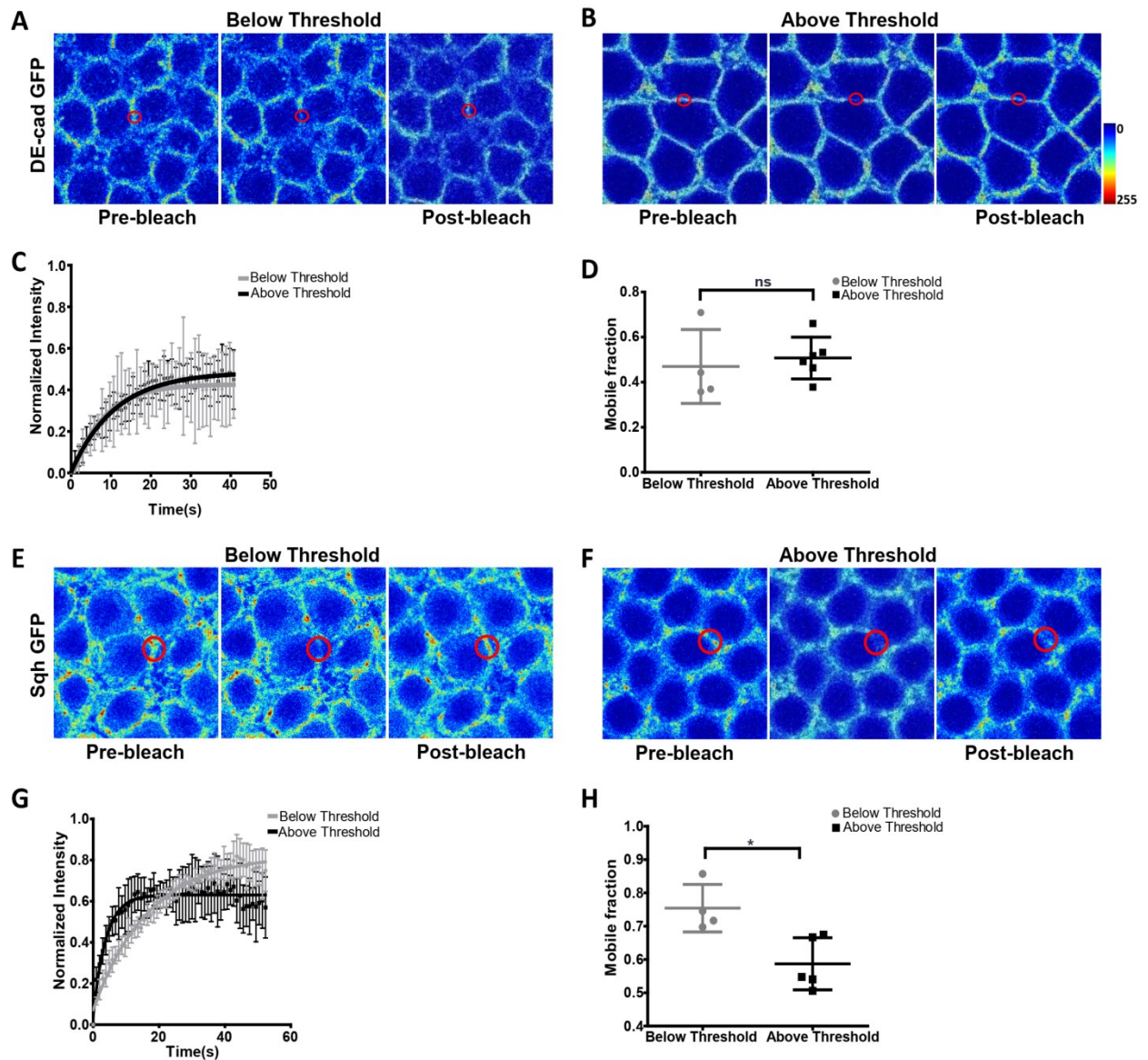


Figure 6.2 Myosin II is stabilized on the lateral membrane above the threshold

(A-D) DE-cad dynamics remain the same during lateral membrane extension: Snap shots during FRAP analysis of DE-cad-GFP expressing embryos pre-bleach, bleach and post bleach, below (A) and above the threshold (B). (C) FRAP curves and mobile fractions (D) below (grey; n=4 embryos) and above threshold lateral membrane length (black, n=6 embryos) show no significant difference. (E-H) MyoII becomes less mobile at the lateral membrane above the threshold. Snap shots during FRAP analysis of Sqh-GFP expressing embryos at pre-bleach, bleach and post bleach below (E) and above the threshold lateral membrane length (F). (G) FRAP curves show reduced recovery above threshold (black, n=5 embryos) compared to below threshold (grey, n=5 embryos) and mobile fraction (H) significantly decreases above the threshold. Data is represented as mean \pm SD, * p <0.05, ** p <0.01, and *** p <0.001, Student's t test, unpaired, two tailed.

polygonal after a threshold lateral membrane length range, we checked if there was a change in the tension at the edges or junctions above the threshold length. In order to do this, we performed focal laser ablations at the point of contact between syncytial cells below and above the threshold length range (Figure 6.3A-D, G). The recoil velocity was greater in edges of syncytial cells above the threshold lateral membrane length, while no significant difference in recoil velocity was observed in the edges of syncytial cells below the threshold when compared to the control un-ablated neighbouring edges (Figure 6.3C-D, G). Junctional tension was also probed at metaphase when the lateral membrane length was the maximum, but no significant recoil was observed at this stage compared to control un-ablated neighbouring junctions (Figure 6.3E-G). This shows that edges formed above threshold lateral membrane length have higher tension than the points of contact between circular syncytial cells below the threshold or even at metaphase. Together with increase in junctional tension at the threshold, this suggests that with increased DE-cad levels, MyoII gets organized and immobilized on the junction at the threshold. In order to test how the forces generated by these two molecules regulate the lateral membrane length, we studied mutants of DE-cad and MyoII activity regulators.

6.3.4 DE-cadherin depletion results in decreased lateral furrow length and increased circularity causing a loss of polygonal architecture formation

We assessed DE-cad mutant embryos for lateral membrane length and circularity in the syncytial cycles. *shg* RNAi (*shg^j*) was maternally expressed in embryos (see methods section for details). Embryos developing to syncytial stages had significantly reduced DE-cad staining (Figure 6.4A-C). The MyoII organization as estimated by immunostaining for Zipper, the MyoII heavy chain subunit showed a decrease but using live imaging with Sqh-GFP did not show any significant change in DE-cad knockdown embryos (Figure 6.4A'-B', D-E). Live imaging of *shg^j* embryos with tGPH showed defects during syncytial division cycles which could be categorised into 3 classes: 22% embryos showed disruption of polygonal architecture (Movie 6.2), 17% showed polygonal organization with loose plasma membrane seen in the form of a spread tGPH signal (Movie 6.3) and 61% showed polygonal organization of the plasma membrane (Movie 6.4) (Figure 6.4F-G). This

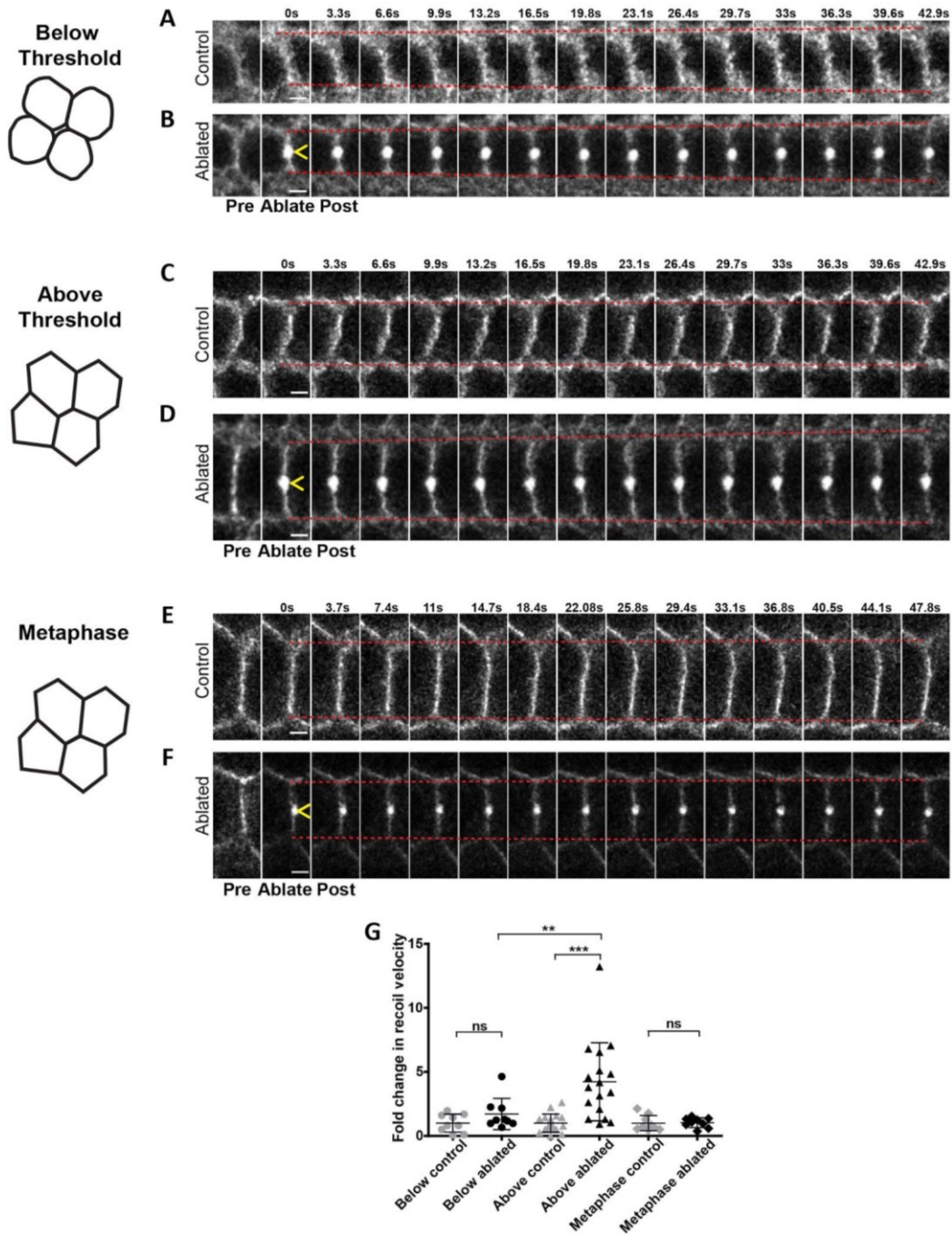


Figure 6.3 Junctional tension is higher at lateral membrane length above the threshold. (A-D) Laser ablation is performed at edges below threshold, above threshold and at metaphase: Time series of control un-ablated edges (**A,C,E**) and laser ablated edges (yellow marks the ROI for ablation) (**B,D,F**) of DE-cad GFP expressing embryos below threshold (**A-B**), above threshold (**C-D**) and at metaphase (**E-F**). Junctional tension is increased after the threshold lateral membrane length. Quantification of recoil velocities of vertices between control un-ablated junctions and laser ablated junctions below threshold (n=9 junctions, 1 junction per embryo, 9 embryos), above threshold lateral membrane length (n=17 junctions, 1 junction per embryo, 17 embryos) and at metaphase (n=9 junctions, 1 junction per embryo, 9 embryos)(**G**). Data is represented as mean \pm SD, *p<0.05, **p<0.01, and ***p<0.001, One way ANOVA. Scale bar: 2.5 μ m.

variation in architecture could be attributed to partial knockdown of DE-cad. The *shgⁱ* embryos that showed a disruption of polygonal architecture did not show formation of furrows. All categories of embryos were estimated for furrow length and it was found to be considerably shorter than the control embryos across syncytial cycles 11-13 (Figure 6.4H). There was also a consistent increase in circularity of the metaphase syncytial cell shapes of all NCs (Figure 6.4I). Circularity comparison at maximum furrow length in NC13 metaphase showed that *shgⁱ* embryos with furrows below the threshold lateral membrane length were circular as compared to those above the threshold (Figure 6.4J). The loss of furrows seen in *shgⁱ* is similar to that reported in a preliminary analysis of DE-cad mutants in syncytial stages (Wang et al., 2004).

Actin caps in interphase are known to show expansion till they meet and stabilize their area (Afshar et al., 2000; Cao et al., 2010; Stevenson et al., 2002; Zhang et al., 2018). The area of the cap increased in control embryos after the threshold lateral membrane was achieved. Consistent with lack of effect on recruitment of MyoII, DE-cad loss did not affect cap expansion and the area of the cap increased similar to control embryos at the threshold length (Figure 6.7). Taken together, DE-cad plays a significant role in keeping adjacent lateral membranes together for the formation of edges and appropriate extension in order to achieve onset of polygonality in the syncytial *Drosophila* embryo.

6.3.5 Depleting Myosin II activity leads to polygon architecture formation below the threshold lateral membrane length

In order to change the balance of contractility and adhesion during shape transition, we depleted levels of activated MyoII by altering the levels of the MyoII regulators. Rho-GTP is an important regulator of MyoII activity. RhoGEF2, the GTP exchange factor (GEF), functions in furrow elongation in the syncytial cycles and during cellularization (Cao et al., 2010; Crest et al., 2012; Padash Barmchi et al., 2005a). Rho-GTP activates ROCK (*Drosophila* Rok) and Rok, in turn, activates MyoII and deactivates the Myosin phosphatase by phosphorylation. MyoII is deactivated by dephosphorylation with Myosin phosphatase and this is defective in mutants of the Myosin binding subunit (MBS) of Myosin phosphatase (Mizuno et al., 1999, 2002; Royou et al., 2002; Tan et al., 2003; Zhang et al., 2018). We analysed the effect of reducing MyoII-based contractility on the onset of polygon formation. To

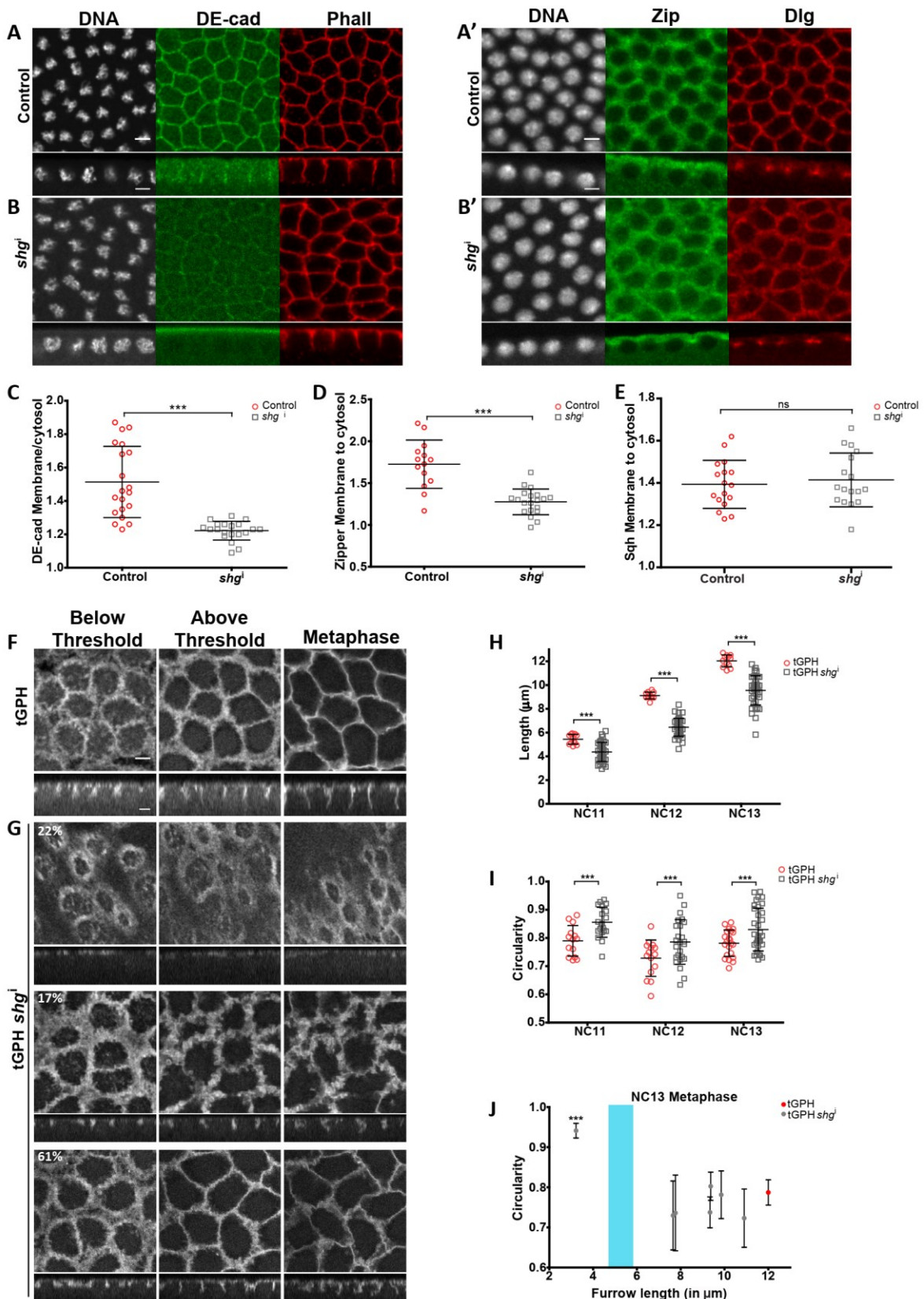


Figure 6.4 DE-cad depletion leads to short furrows, increased circularity and no effect on Zipper levels. (A-D) DE-cad is lowered and Zipper remains unchanged in *shg^j* embryos. *shg^j* and *nanos-Gal4/+* (n=10) are stained with DE-cad (green) and phalloidin (red) in metaphase (A-B); Zip (green) and Dlg (red) in prophase (A'-

B'). *shg^j* shows lowering of DE-cad (86%, n=21 embryos) and zipper staining is at comparable levels. Graph showing the E-cad intensities in control and knockdowns (n= 20 cells, 4 embryos, 5 cells per embryo) (**C**). Quantification of Zipper membrane to cytosol ratios in control and knockdowns (n= 20 cells, 4 embryos, 5 cells per embryo) (**D**). Quantification of SqhGFP membrane to cytosol ratios in control and knockdowns (n= 20 cells, 4 embryos, 5 cells per embryo) (**E**). (**F-G**) *shg^j* embryos have decreased furrow length. tGPH grazing sections from control (n=4 embryos) (**F**) and *shg^j* with disruption of polygonal architecture (22%, n=18 embryos), with loose membrane (17%, n=18 embryos) and short furrow lengths in NC12 (61%, n=18 embryos) at three different time points: below threshold, above threshold and metaphase at NC12 (**G**). Quantification of metaphase furrow lengths in *shg^j* and tGPH/+ (n=32, 7 furrows/embryo; 8 embryos) (**H**). (**I-J**) *shg^j* shows increased circularity. Graph showing circularity in *shg^j* embryos at metaphase of NC11-13 (n=25-35, 5 cells/embryo; 5-7 embryos) (**I**). Graphs showing circularity in *shg^j* embryos with different furrow lengths at metaphase at NC13. Each point represents circularity measurements (n=7 syncytial cells/ furrow length) from one embryo having the indicated furrow length at metaphase (average of n=5 furrows/ embryo) (**J**). The red dot represents the control tGPH/+ embryo with 12µm furrow length while the knockdowns are shown in grey dots. Data is represented as mean ± SD, *p<0.05, **p<0.01, and ***p<0.001, Student's t test, unpaired, two tailed (F-G). One way ANOVA with Dunnett's Multiple Comparison Test, each point of the mutant compared to the control (H). Scale bar: 5 µm.

this end, *rhoGEF2* RNAi (*rhoGEF2^j*) was maternally expressed in the embryos (see methods for details). All embryos expressing *rhoGEF2^j* showed lowering of Sqh as seen with live imaging and cytosolic Zipper staining (Figure 6.5 A'-B'). DE-cad levels remain unchanged as compared to controls as observed with live imaging using DE-cad-GFP (Figure 6.5 A-D). In order to deplete active MyoII more directly, we knocked down Rok. Rok depletion did not show a significant defect in DE-cad distribution on the membrane but showed cytosolic Zipper staining in interphase of all NCs (Figure 6.5A-D, A', C', E).

Live imaging of *rhoGEF2^j* and *rokⁱ* embryos with tGPH showed that the furrows are slightly but significantly shorter than the controls (Figure 6.5 I, Movie 6.5, 6.6). These embryos also showed irregular furrows throughout the embryo as reported earlier and (Figure 6.5F-H) (Sherlekar and Rikhy, 2016; Zhang et al., 2018) *rokⁱ* embryos showed a higher severity of this irregular furrow phenotype. The variation in the furrow lengths was greater in *rokⁱ* embryos, partly because of different regions of the embryos proceeding in different NCs, which reflects problems in nuclear axial expansion (Foe et al., 2000; Royou et al., 2002c). The plasma membrane in *rhoGEF2^j* and *rokⁱ* embryos also showed undulations, suggesting lowering of tension in the cortex. Further, the actin cap area measurement was used as an indicator of contractility in the cortex. The loss of contractility in *rhoGEF2^j* was reflected in larger cap areas in interphase at the lateral membrane length below threshold, without a significant further expansion above the threshold (Figure 6.7).

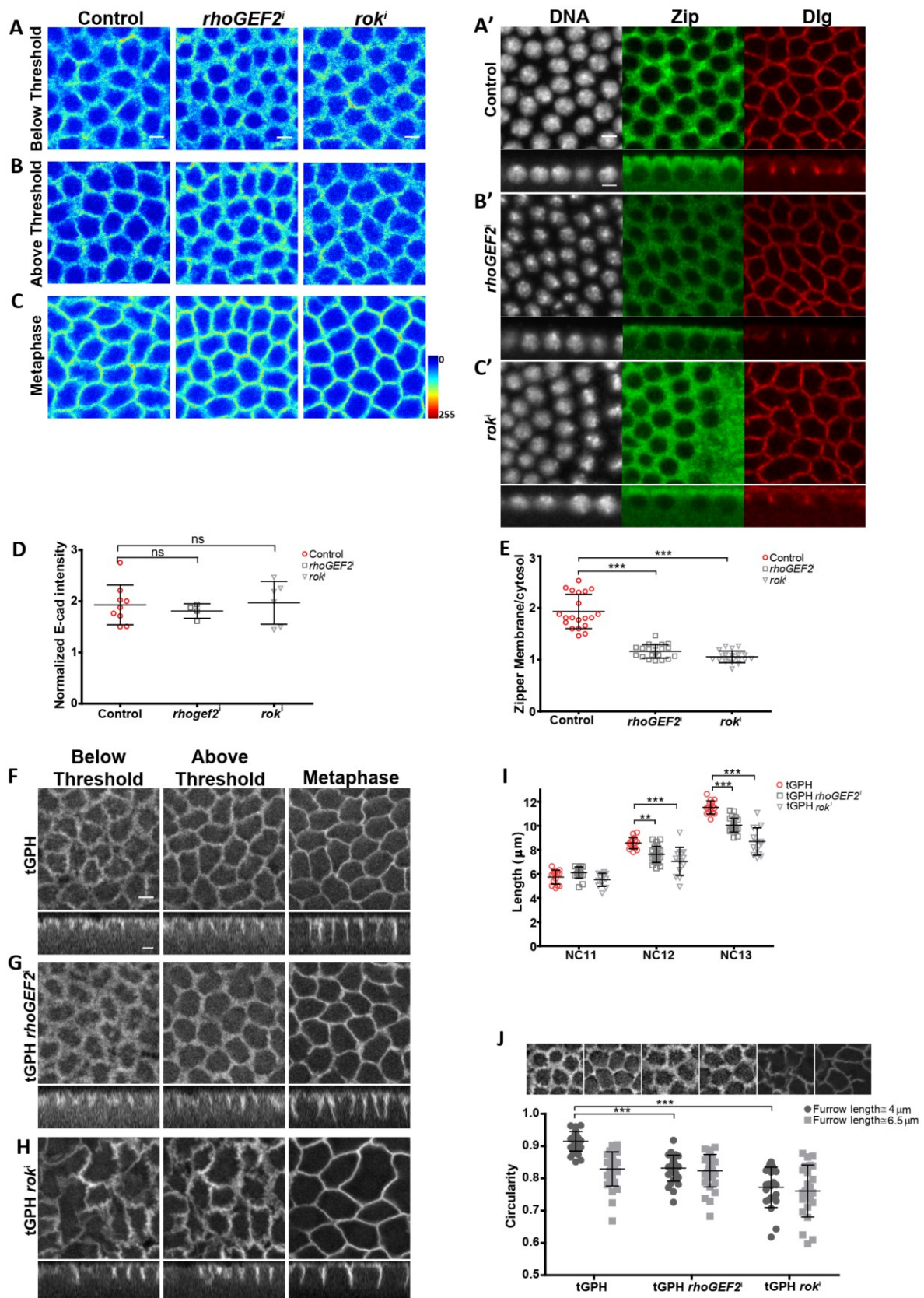


Figure 6.5 RhoGEF2 and Rok depletion reduces MyoII activity and changes the lateral membrane threshold for polygonality. (A-E) DE-cad is unchanged and Zipper is cytosolic in *rhoGEF2ⁱ* and *rok¹* embryos. *mat-gal4/+* Control (n=4 embryos) (A), *rhoGEF2ⁱ* (n=4 embryos) (B) and *rok¹* (n=6 embryos) (C) embryos

expressing DE-cad-GFP; *mat-gal4/+* (n=10) (**A'**), *rhoGEF2^j* (57% cytosolic Zipper, n=7 interphase/prophase embryos) (**B'**) and *rok^j* (95% cytosolic Zipper, n=22 interphase/prophase embryos) (**C'**) embryos co-stained with Zipper (green) and Dlg (red) (**A'-C'**). Graph showing DE-cad-GFP levels are comparable in *rhoGEF2^j* and *rok^j* embryos (n=24 cells, 6 cells per embryo, 4 embryos) (**D**). Graph showing lowered Zipper levels on the membrane in *rhoGEF2^j* and *rok^j* embryos compared to controls (n=20 cells, 5 cells per embryo, 4 embryos) (**E**). (**F-I**) *rhoGEF2^j* and *rok^j* embryos show decreased furrow length. tGPH grazing sections from control (**F**), *rhoGEF2^j* (100%, n=6 embryos) (**G**) and *rok^j* (100%, n=5 embryos) (**H**) expressing embryos at three different time points: below threshold, above threshold and metaphase at NC13. Quantification of metaphase furrow lengths in tGPH/+ (n=15, 5 furrows/ embryo, 3 embryos), *rhoGEF2^j* (NC11: n=20, 5 furrows/ embryo, 4 embryos; NC12-13: n=25 5 furrows/ embryo, 5 embryos) and *rok^j* (n=15, 5 furrows/ embryo, 3 embryos) (**I**). (**J**) *rhoGEF2^j* embryos achieve polygonality at lateral membrane lengths below the threshold. Quantification of circularity in *rhoGEF2^j* embryos compared to tGPH/+ embryos at furrow length <4.75 μ m (~4 μ m) and >5.75 μ m (~6.5 μ m) (n=30, 10 syncytial cells per embryo, 3 embryos). Data is represented as mean \pm SD, *p<0.05, **p<0.01, and ***p<0.001, Student's t test, unpaired, two tailed. Scale bar: 5 μ m.

If the increase in contractility was balanced by increased adhesion to form the polygonal architecture at the threshold lateral membrane length, then decreasing contractility provided a paradigm to ask if adhesion or edge formation could occur below the threshold lateral membrane length. An alteration in the extent of adhesion with respect to contractility would lead to change in circularity and we, therefore, measured circularity at lateral membrane length below (at approximately 4 μ m) and above the threshold (at approximately 6.5 μ m) in *rhoGEF2^j* and *rok^j* expressing embryos similar to the control (Figure 3.3A-C). Interestingly, the circularity at lateral membrane length below the threshold was already low (C=0.832 at approximately 4 μ m) in *rhoGEF2^j* and *rok^j* expressing embryos (Figure 6.5J). This corresponded to the polygonal shape and was similar to that achieved in control embryos beyond the threshold (C=0.829 at approximately 6.5 μ m). This suggested that with lowering of MyoII activity, polygonality was achieved at lateral membrane length below the threshold or in other words, the threshold shifted to a lower lateral membrane length.

Thus, lowering MyoII based contractility did not affect furrow initiation but allowed furrow adhesion to take place earlier and, thus, polygonality occurred at a shorter lateral membrane length.

6.3.6 Increased Myosin II activity shows unbalanced cap contraction, loss of DE-cadherin and abrogation of polygonal architecture

Next, we checked for alteration of syncytial cell plasma membrane

morphology on increased MyoII activity. To this end, we analyzed embryos maternally overexpressing RhoGEF2 (RhoGEF2-OE) or expressing an RNAi against the MBS (*mbsⁱ*) (see methods for details). As expected, RhoGEF2-OE and *mbsⁱ* embryos showed retention of Zipper on the apical plasma membrane in patches, even in metaphase, indicating an increase in MyoII activity in these mutants (Figure 6.6A'-C', E). Interestingly, this Zipper increase corresponded to a complete loss of furrow extension and circular cells with no polygonal organization as seen with phalloidin staining (Figure 6.6A-C). The RhoGEF2-OE and *mbsⁱ* embryos also showed complete loss of DE-cad from the membrane (Figure 6.6A-D). Further, live imaging of RhoGEF2-OE and *mbsⁱ* embryos with DE-cad-GFP and Sqh-mCherry showed that some DE-cad-GFP remained on the membrane in between caps and was unable to organize into the junctions (data not shown), possibly due to inability of the caps to expand and touch with increased contractility (Figure 6.7).

Live imaging of RhoGEF2-OE and *mbsⁱ* embryos along with tGPH showed that syncytial cells were unable to transition into a polygonal state with very short furrow lengths, well below the threshold in NC11-13 (Figure 6.6F-I, Movie 6.7, 6.8). Plotting the circularity of the cells with different metaphase furrow lengths in RhoGEF2-OE embryos showed that furrow lengths below the threshold were abundant and they showed a high circularity. The RhoGEF2-OE embryos occasionally had longer lateral membranes and they showed an increased circularity compared to the control embryos despite crossing the threshold (Figure 6.6J). Increased contractility of the cortex was also reflected in cap area measurements which showed smaller caps in interphase as compared to control embryos which do not undergo much further expansion (Figure 6.7). Thus, increased Myosin II activity led to loss of cap expansion and inability to initiate furrows. Lack of furrow extension beyond the threshold gave rise to circular cells.

6.4 Conclusion and Discussion

Based on our study, we propose a lateral membrane length based model for the initiation of polygonal epithelial-like architecture, in the earliest morphogenetic event of syncytial blastoderm development in *Drosophila* embryogenesis. Because of a dynamic lateral membrane furrow, the syncytial blastoderm forms an effective

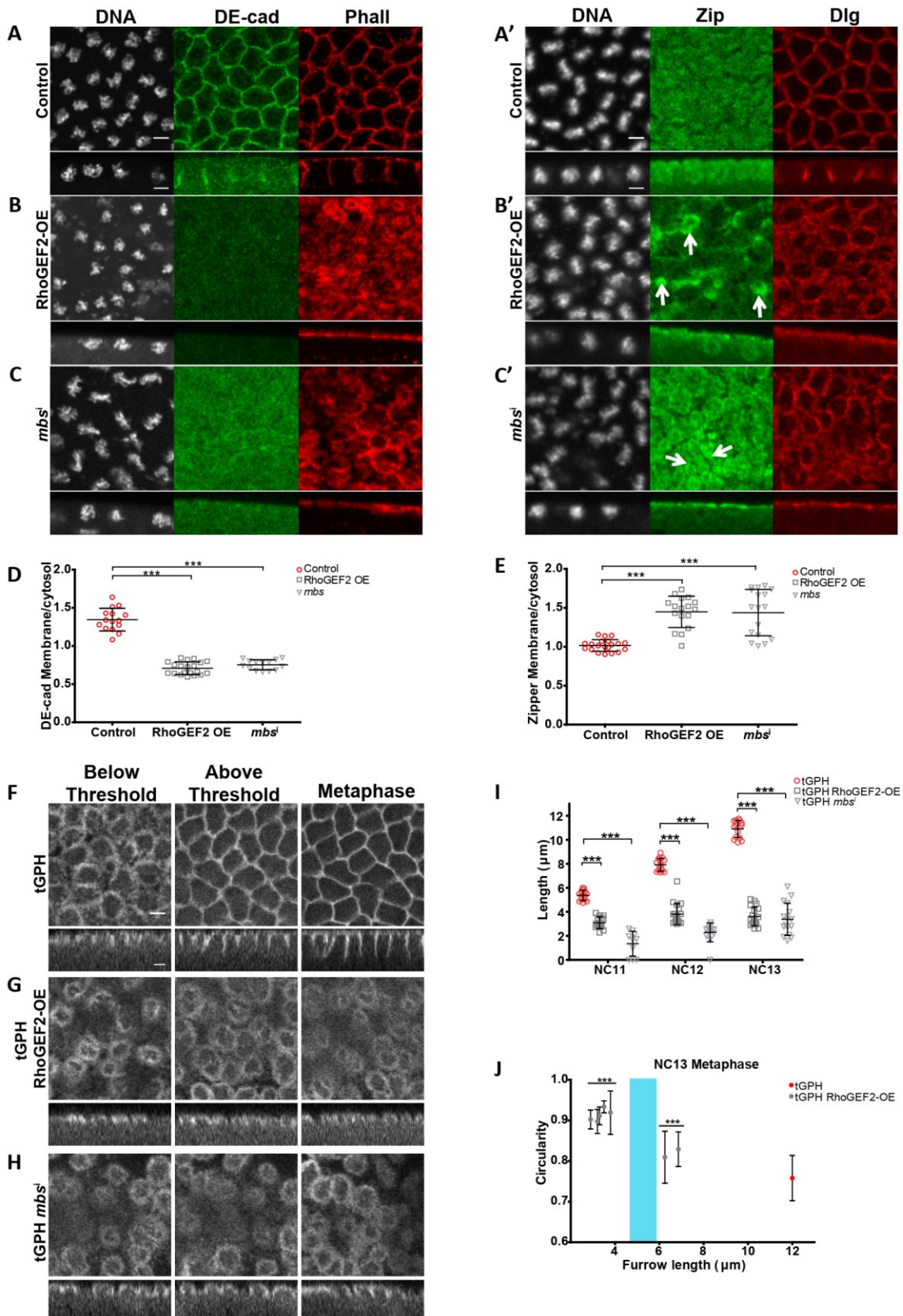


Figure 6.6 RhoGEF2 overexpression and MBS depletion leads to retention of MyoII in patches in metaphase and abrogation of polygonal architecture. (A-E) DE-cad is lost from membranes in RhoGEF2 and *mbsⁱ* embryos while Zipper is retained at metaphase unlike controls. *mat-gal4/+* (n=10) (A), RhoGEF2-OE (100%

show loss of DE-cad, n=30 embryos) **(B)** and *mbs¹* (100% show loss of DE-cad, n=10 embryos) **(C)** embryos co-stained with DE-cad (green) and phalloidin (red); *mat-gal4/+* (n=19) **(A')**, RhoGEF2-OE (92% show Zipper patches, n=13 metaphase embryos) **(B')** and *mbs¹* (86% show Zipper patches, n=7 metaphase embryos) **(C')** co-stained with Zipper (green) and Dlg (red). Arrows show Zipper patches on the apical membrane at metaphase. Graph showing loss of DE-cad from syncytial membrane (n=20 cells, 5 cells per embryo, 4 cells) **(D)**. Graph showing retention of Zipper as patches on the apical membrane in metaphase (n=20 cells, 5 cells per embryo, 4 cells) **(E)**. **(F-I)** RhoGEF2 over-expression and *mbs¹* show circular membranes with no furrow extension. tGPH grazing sections from control **(F)**, RhoGEF2-OE (83%, n=12 embryos) **(G)** and *mbs¹* (86%, n=7 embryos) **(H)** expressing embryos at three different time points: below threshold, above threshold and metaphase at NC13. Quantification of metaphase furrow lengths in tGPH/+, RhoGEF2-OE (n=19, 4-5 furrows per embryo, 4 embryos) and *mbs¹* (n=15, 4-5 furrows per embryo, 3 embryos) **(I)**. Data is mean \pm SD, *p<0.05, **p<0.01, and ***p<0.001, Student's t test, unpaired, two tailed. **(J)** Graph showing circularity in RhoGEF2-OE embryos with respect to furrow lengths at metaphase at NC13. Each point represents circularity measurements (5 syncytial cells/ furrow length) from one embryo having the indicated furrow length at metaphase (average of n=5 furrows for each point). Data is represented as mean \pm SD, *p<0.05, **p<0.01, and ***p<0.001, One way ANOVA with Dunnett's Multiple Comparison Test, each point of the mutant compared to the control. Scale bar: 5 μ m.

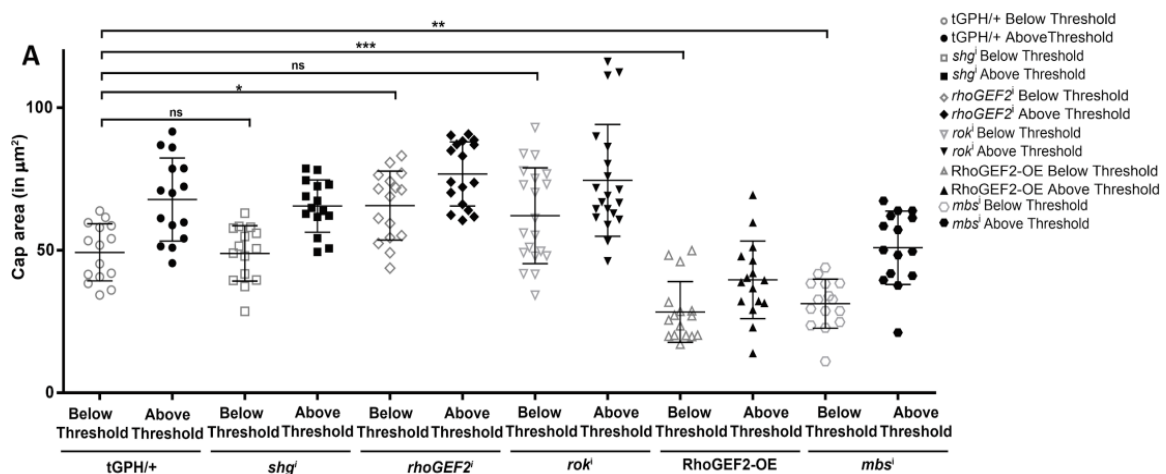


Figure 6.7 Actin cap area expansion as an indicator of MyoII based cortical contractility

Cap areas are smaller in RhoGEF2 overexpression embryos and larger on RhoGEF2 depletion. Quantification of cap areas below and above the threshold in tGPH/+, *shg¹*, *rhoGEF2¹*, *rok¹*, RhoGEF2-OE and *mbs¹* embryos (n=15, 5 syncytial cells per embryo, 3 embryos).

model system to elucidate the mechanism by which key components of adhesion and contractility regulate polygon shape transition. We show that ingression of furrows above a threshold lateral membrane length range allows the coincident formation of edges between adjacent plasma membrane regions and transition of syncytial cell shapes from circular to polygonal. This threshold length is presumably determined by fine tuning the concentration and stabilization of MyoII relative to DE-cad in the lateral membrane. The threshold is likely to be the point at which MyoII

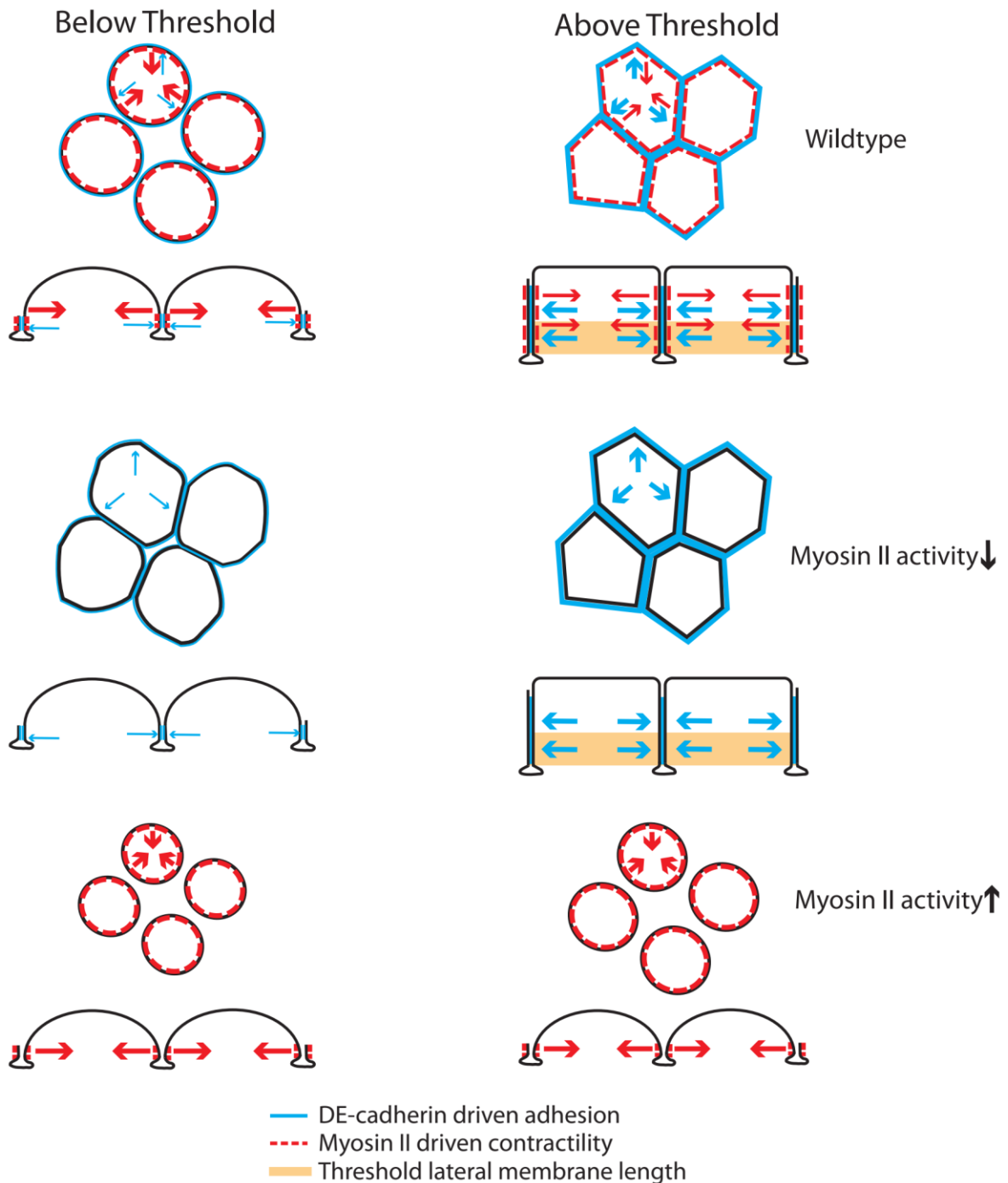


Figure 6.8 Summary model showing the role of DE-cad and MyoII balance in formation of polygonal epithelial architecture. The lateral membrane furrow in between adjacent syncytial nuclei is organized as a polygon when the length exceeds the threshold of 4.75-5.75 μm . DE-cad increases whereas MyoII decreases when the lateral membrane exceeds the threshold length. MyoII is less dynamic above the threshold length. DE-cad depletion leads to loss of furrow length and increase in circularity. Depletion of MyoII driven contractility leads to polygon architecture formation at a lower lateral membrane length. Increase in MyoII driven contractility leads to circular PM organization, loss of adhesion and loss of lateral membrane furrow formation. Thus the syncytial cycle shows onset of polygonal shape due to a balance in DE-cad-MyoII adhesive-contractile forces at the threshold lateral membrane length.

based contractility is balanced appropriately by adhesion in the lateral membrane. This is supported by the fact that decrease in MyoII activity allowed the threshold to be achieved earlier than the control, while increase in MyoII activity removed DE-cad from the membrane preventing the threshold from being achieved (Figure 6.8).

Such a model also predicts that lowering adhesion may allow contractile forces to dominate and thus, phenocopy increased MyoII activity. However, lowering adhesion resulted in increased circularity and disruption of polygonal architecture in only a small percentage of embryos, as compared to increasing MyoII activity, where circular plasma membrane organization was more prevalent. This may indicate either incomplete abrogation of adhesion due to partial loss of DE-cad in the knockdowns or the presence of other transmembrane adhesion molecules in the system at this stage that contribute to adhesive forces. Echinoid is one such cell adhesion molecule that cooperates with DE-cad to mediate adhesion in the wing epithelium. Loss of Echinoid is compensated for by the upregulation of DE-cad in the Echinoid mutant cells (Wei et al., 2005). It is possible that loss of adhesion by depletion of DE-cad is partly compensated by the expression of Echinoid in the early embryo. Further studies testing the role of Echinoid in the syncytium may clarify this in the future.

Actin polymerization has a key role in furrow extension and loss of actin regulators like Rhogef2, Diaphanous, Arp2/3 and SCAR decrease furrow lengths (Stevenson et al., 2002; Zallen et al., 2002; Padash Barmchi et al., 2005; Sherlekar and Rikhy, 2016). It is known that Arp2/3 based branched actin polymerization is essential for actin cap expansion in the syncytial embryo, while MyoII based contractility tends to restrict it. Attachment of the growing actin network to the MyoII borders of the cap allows buckling of cap borders to initiate furrows (Zhang et al., 2018). However, loss of MyoII activity does not affect furrow initiation. Our study focuses on the step of furrow extension, which allows the transition of the shape of the syncytial cells from spherical to polygonal. To begin with, in the actin caps contractility dominates over adhesion, followed by increase in DE-cad and decrease in MyoII levels that balance each other to reach the threshold membrane ingression. Reduction of contractility alone, allows adhesive forces to dominate and prematurely transition to a polygonal shape. On the other hand, increasing MyoII activity from the beginning results in contractile forces to dominate, preventing cap expansion. In addition, the complete loss of E-cad molecules in this scenario results in unbalanced

and excessive contraction, preventing the threshold lateral membrane length from being achieved and results in formation of circular syncytial cells (Figure 6.8).

Change in E-cad and MyoII mobility or levels allows for plasticity of cell shape. Decrease in MyoII mobile fraction as observed with FRAP is usually indicative of increased pool of stable MyoII on the membrane resulting in increased tension (Munjaj et al., 2015). Increase in the mobile fraction of DE-cad also corresponds to increased turnover that facilitates junctional remodelling during wing development (Classen et al., 2005; Iyer et al., 2018). In our study, we saw a decrease in the mobile fraction of MyoII and a corresponding increase in tension after crossing the threshold. DE-cad mobility, on the other hand, remained unchanged but the levels of DE-cad on the lateral membrane increased above the threshold. E-cad is under constitutive tension because of the linkage to the underlying actomyosin (Borghi et al., 2012). When subjected to forces, conformational modulation of α -catenin occurs at E-cad based junctions, which recruits vinculin to promote junction stability (Borghi et al., 2012; Yonemura et al., 2010). Thus, even though E-cad mobility itself does not change drastically in our study or in the time scales across which the threshold length and polygonal transition is obtained, a change in the underlying MyoII organization could indirectly lead to increased tension on the junctions via E-cad.

E-cad adhesion sites are also sites of active Rho signalling, as well as sites of actin polymerization via recruitment of actin nucleators like Arp2/3, formins and cortactin. This enables them to, in turn, contribute to the biogenesis and regulation of the underlying actomyosin (Lecuit and Yap, 2015). During junction maturation in mammalian cells, interaction of E-cad with binding partners such as p120-catenin plays a crucial role in inhibiting Rho1 and active MyoII levels to decrease contractility along the lateral membrane in these cells (Yu et al., 2016). Therefore, one possibility is that increased DE-cad levels in the syncytial cycle of the *Drosophila* embryo allows for recruitment of embryo specific cytoskeletal regulators that organize the underlying MyoII network causing increased tension during lateral membrane extension beyond the threshold. The cytoskeletal regulators linking DE-cad adhesion and MyoII contractility remain to be identified. The increase in adhesion may, thus, indirectly result in the change in tension to contribute to the transition of the cell shape from circular to polygonal.

E-cad and MyoII enrichment usually occurs in a complementary manner. For example, the dorso-ventral borders have higher levels of DE-cad, while antero-

posterior borders have higher MyoII in *Drosophila* embryos undergoing germband extension. Loss of DE-cad with simultaneous increase in medial and junctional MyoII levels results in loss of contacts between cells of the neuroectoderm, thus, giving rise to *Drosophila* neuroblast ingression (Lecuit and Yap, 2015b; Simões et al., 2017). Shrinking of junctions to form rosettes and T1-T2 transitions during cell intercalations also occur due to enrichment of MyoII (Bertet et al., 2004; Blankenship et al., 2006). Similarly, in our study, as the syncytial cells progressed towards a taut and stable polygonal array from interphase to metaphase, the levels of DE-cad increased, while levels of MyoII decreased. The point of transition from circular to polygonal possibly represents the optimal levels of both molecules that contribute forces which can counterbalance each other and give rise to a stable lateral membrane.

The concept of minimal lateral membrane attachment is particularly of interest when considering reverse shape changes from polygonal to spherical during epithelial to mesenchymal transition (EMT). EMT is an important step in cell migration during development and disease, involving dynamic modulations in cell-cell adhesion. For example, in *Drosophila* border cells, expansion of the sub-apical adherens junction complex containing DE-cad results in loss of detachment from the follicle cell epithelium (McDonald et al., 2008; Pinheiro and Montell, 2004). EMT involves a transition from strong junctional complexes that favour static epithelial character, to increase in Rho GTPase activity, that favour cell motility (Lamouille et al., 2014). A fine balance of Rho GTPase activity at the adherens junctions results in either their stability or disassembly (Lamouille et al., 2014; Quiros and Nusrat, 2014). This is also seen in our study as increasing or decreasing active RhoGTP levels impacts the polygon formation. It is possible that a critical RhoGTP level regulates one state versus the other. An analysis of our threshold lateral membrane attachment model during these scenarios might reveal the point at which this balance tips off to either stability or disassembly. In conclusion, the lateral membrane length could be an important parameter to alter during epithelial remodelling in *Drosophila* development and in epithelia across different organisms.

CHAPTER 7

Plasma membrane polarity proteins regulate the onset of hexagon-dominated polygonal architecture

7.1 Introduction

Asymmetric distribution of polarity complexes is important for cell shape, tissue integrity and tissue remodelling (Bilder and Perrimon, 2000; Hayashi and Carthew, 2004; Letizia et al., 2013) (Section 4.1 and 5.1). For example, in *Drosophila* stage10 embryo ectoderm, over-expression of Crumbs causes expansion of the sub-apical domain at the expense of the free apical domain and gives rise to a columnar epithelial morphology. Conversely, Crumbs knockdown causes shrinking of the sub-apical region with simultaneous expansion of the apical region, giving rise to a cuboidal morphology (Letizia et al., 2013). Loss of adherens junction components like DE-cad and β -catenin in *Drosophila* gastrulation results in a pear shaped cell with an expanded apical domain (Harris and Peifer, 2004). Differential expression of DE- and DN-cadherin in the cone cells of *Drosophila* retinal epithelium regulates their typical soap bubble-like shape and arrangement (Hayashi and Carthew, 2004). Besides one report on planar cell polarity mutants showing a decrease in the frequency of hexagons in the wing epithelium, no other report on the analysis of the role of polarity proteins in regulating the polygonal distribution of epithelia exists (Classen et al., 2005).

The small Ras-like GTPase, Rap1, is a versatile regulator of morphogenesis which regulates diverse processes like cell polarity, cell-matrix and cell-cell adhesion. In the *Drosophila* wing epithelium, loss of Rap1 leads to formation of non-hexagonal cells, which are by and large pentagonal. This is due to the uneven distribution of E-cad around the cell circumference. The same mechanism facilitates the formation of trapezoidal and pentagonal cells of the adult wing vein cells (Knox and Brown, 2002; O'Keefe et al., 2012). Rap1 and its downstream effector Canoe are also required to position Baz and AJs apically in *Drosophila* cellularization and,

thus, are essential for establishment of apico-basal polarity. In addition, Rap1 is also important for the columnar shape of epithelial cells in a Canoe independent manner (Choi et al., 2013). Thus, known polarity proteins as well as their various regulators play an important role in regulating epithelial cell shapes.

As noted in Chapter 5, the syncytial *Drosophila* embryo shows asymmetric distribution of various polarity and cytoskeletal proteins. Besides the conventional apico-basal polarity, the syncytial cells also show asymmetries in the XY plane, i.e. between edges and vertices (Section 5.3.1 and 5.3.2). This led us to believe that these asymmetries may be important in regulating the polygonal distribution of the cells. To the best of our knowledge, no such analysis about the effect of polarity regulators on polygon distribution exists. Thus, we looked at the effect of Baz, Pnut, DE-cad and catenins on polygonal distribution.

Several cell culture studies implicate formation of AJs as the polarity cue (Vega-Salas, 1987; Wang et al., 1990; Nelson and James Nelson, 1991), however, a study in *Drosophila* cellularization shows Baz to be at the top of the polarity program instead of DE-cad. They show that in the absence of AJs, Baz localization is unaffected but in the absence of Baz, apical spot AJs fail to form (Harris and Peifer, 2004). Therefore, these two were particularly interesting candidates to study how they affect cell shape and localization of other polarity proteins in the syncytial stages. In addition, we also looked at the effect of the septin family protein, Pnut in polygon formation, since it showed an interesting enrichment at the vertex in the syncytium (Figure 5.2D-D", H-H").

7.2 Material and Methods

7.2.1 Fly stocks

All flies were raised in regular cornmeal agar and all crosses were maintained at 29 °C, except *shgⁱ* which was maintained at 18 °C. *maternal α4 tubulin-Gal4-VP16* was used for all RNAis except for *shgⁱ*. *shgⁱ* was crossed to a single chromosomal copy of *nos-Gal4* and maintained at 18 °C as mentioned in Chapter 6 (6.2.1). tGPH *mat-Gal4*;

Stock name	Source	ID
<i>D. melanogaster</i> : tGPH	Bloomington stock center	#8163,RRID:BD SC_8163
<i>D. melanogaster</i> : CantonS	L.S. Shashidhara	
<i>D. melanogaster</i> : baz RNAi	Bloomington stock center	#35002
<i>D. melanogaster</i> : UASp-Baz Δ 969-1464-GFP	Andreas Wodarz (Krahn et al, 2010)	N/A
<i>D. melanogaster</i> : UASp-Baz Δ 1-904-GFP	Andreas Wodarz (Krahn et al, 2010)	N/A
<i>D. melanogaster</i> : pnut RNAi	Bloomington stock center	#65157
<i>D. melanogaster</i> : DE-cadherin RNAi	Bloomington stock center	#38207
<i>D. melanogaster</i> : UASp-shg. Δ JM	Bloomington stock center	#58444
<i>D. melanogaster</i> : ovo ^D , FRT G13/CyO	Bloomington stock center	#2125
<i>D. melanogaster</i> : pnut ^{XP} FRT G13/CyO	Manos Mavrakis (Mavrakis et al, 2014)	N/A
<i>D. melanogaster</i> : UASp-shg. Δ p120	Bloomington stock center	#58434
<i>D. melanogaster</i> : UASp-shg. Δ β -cat	Bloomington stock center	#58497
<i>D. melanogaster</i> : nanos-Gal4	Bloomington stock center	N/A
<i>D. melanogaster</i> : maternal α -tubulin Gal4-VP16 (<i>mat-Gal4</i>)	Girish Ratnaparkhi	N/A

Table 7.1 Fly strains used

7.2.2 Live imaging

F1 flies were maintained in cages at 28 °C or 18 °C and 1-1.5hrs old embryos were collected and processed for imaging as mentioned in materials and methods section of chapter 2 (2.4).

7.2.3 Immunostaining

F1 flies were maintained in cages at 29 °C or 18 °C and 2.5-3hrs old embryos were collected and fixed with 4% PFA as mentioned in Chapter 2 (2.2). Embryos were fixed with 1mM EGTA in 4%PFA for DE-cad staining or with 1mM CaCl₂ in 4%PFA for p120 catenin staining. Heat fixation was done for α-cat staining. Following antibodies were used with the concentrations mentioned inside brackets: Baz (1:1000), DCAD2 (1:5), Pnut (1:5), GFP (1:1000), p120-cat (1:8), α-cat (1:1000), arp2 (1:500) and Dia (1:1000). Phalloidin (1:100) was only used after hand-devitellinization. Finally, the embryos were washed three times in 1X PBST including one wash with Hoechst 33258 (1:1000, Molecular Probes) in 1X PBST for 5 min and mounted in Slow fade Gold antifade reagent (Molecular Probes).

7.2.4 Analysis and quantification

7.2.4.1 Quantification of the metaphase furrow length

Metaphase was identified as the time point when maximum extension took place. The furrow lengths in metaphase for each NC were quantified using the zen blue software from orthogonal sections as mentioned in chapter 2 (2.8.5). Statistical significance was determined using the unpaired, two-tailed, Student's t-test for comparison between controls and mutants.

7.2.4.2 Quantification of circularity for different metaphase furrow length mutant embryos

For each embryo at metaphase, the Z stack before the last visible stack towards the embryo interior was used for quantifying circularity using ImageJ as mentioned in chapter 2 (section 2.8.3). The furrow lengths for the same time point in metaphase were quantified using the zen blue software from orthogonal sections as mentioned in chapter 2 (section 2.8.5). The average circularity for each embryo was then plotted against the respective average furrow length at metaphase.

7.3 Results

7.3.1 Baz affects Pnut recruitment to the plasma membrane and depletion of both result in shorter furrow lengths

We investigated whether mutations in Baz and Pnut affected furrow lengths and polygonal plasma membrane organization. To this end, we maternally expressed *baz* RNAi (*baz^j*) (see Chapter 2 for further details), which resulted in lowered Baz protein levels compared to controls as observed with immunostaining (Figure 7.1A-B). These embryos were also 100% lethal (n=300) as previously reported (Krahn et al., 2010). Interestingly, with the knockdown of this edge enriched protein, the vertex associated protein, Pnut was also lowered. However, the actin organization observed using phalloidin staining remained unaffected and appeared similar to control embryos (Figure 7.1A'-B'). To verify if appropriate Pnut localization depended on Baz association to the syncytial plasma membrane, we maternally overexpressed a C-terminal truncation mutant of Baz, Baz Δ 969-1464-GFP, which is defective in plasma membrane recruitment (Krahn et al., 2010). Baz Δ 969-1464-GFP had a cytosolic localization and caused diffused distribution of the endogenous Baz protein (Figure 7.2A-B). This is because Baz forms oligomers *in vivo* and the oligomerization domain in this mutant could remove endogenous Baz from the plasma membrane (Benton and St Johnston, 2003). Like *baz^j*, these embryos also showed lowering of Pnut (Figure 7.2A-B). On the other hand, when the Baz N-terminal truncation mutant, Baz Δ 1-904-GFP, was maternally overexpressed, Pnut distribution was closer to wild-type (Figure 7.2C). Thus, the C-terminal domain of Baz was important not only for its own recruitment on the plasma membrane but also for Pnut localization. As Baz function is important for formation of spot adherens junctions in cellularization (Harris and Peifer, 2004), we checked DE-cad distribution in *baz^j* embryos and found that it was not affected in the syncytium (Figure 7.1A'-B').

To determine the effect of loss of Pnut on Baz and DE-cad localization, we generated germline clones of null mutants of Pnut (*pnut^{XP}*) (Neufeld and Rubin, 1994). The embryos were 100% (n=290) lethal and showed complete loss of Pnut (Figure 7.1A, C). However, Baz and DE-cad localization were similar to wild-type in these embryos (Figure 7.1 A, C, A', C'). Thus, Pnut is not important for Baz localization on the syncytial plasma membrane. Neither Baz nor Pnut depletion affects DE-cad distribution on the syncytial plasma membrane. However, on careful examination using live imaging with DE-cad GFP, we found that DE-cad levels

increase in NC13 in both *baz*^l and *pnut*^l embryos with respect to controls (Figure 7.2D-E). Loss of Pnut is reported to result in shorter metaphase furrows in the syncytial *Drosophila* embryos (Sherlekar and Rikhy, 2016; Silverman-Gavrila et al., 2008b). We analyzed furrow length in Baz and Pnut knockdown embryos (*pnut*^l), by live imaging with tGPH (Movie 7.1, 7.2). *baz*^l and *pnut*^l embryos showed a marginal but significant decrease in furrow lengths in NC11-13 as compared to controls (Figure 7.1D-E). However, the lengths achieved were significantly above the threshold. We also checked the rate of furrow ingression in these knockdowns and found them to be similar to controls (Figure 7.1G). Thus, Baz and Pnut loss are not major contributors of lateral membrane length stability or ingression.

In order to test if Baz and Pnut are part of the same pathway or are in parallel pathways we studied embryos with double knockdowns of both Baz and Pnut. These embryos showed similar extents of furrow shortening as the single knockdowns (Figure 7.1D, F). Thus, together with the data about Baz facilitating Pnut recruitment on the membrane, this suggests that Baz and Pnut most likely function in the same pathway.

7.3.2 Baz and Pnut depletion results in delayed hexagon dominance in syncytial cells

We next examined the polygonal distribution in *baz* and *pnut* mutant embryos stained with phalloidin in NC12 when hexagon dominated plasma membrane architecture first appears. We found that *baz*^l and *pnut*^{XP} showed a significant increase in the frequency of pentagons at NC12 (Figure 7.3A-B, I). However, the hexagon-dominance recovered at NC13 in both the cases to match the controls (Figure 7.3E-F, I). Thus, although Baz and Pnut mutants do not drastically affect lateral membrane length and polygonal architecture of the syncytial cells, the polygon distribution achieved shows a delay in the onset of hexagon dominance. The recovery in the hexagon dominance at NC13 can possibly be correlated with an increase in the levels of DE-cad in NC13 as compared to controls (Figure 7.2D-E). This suggests that DE-cad increase may compensate for loss of Baz and Pnut and is, possibly, more important for regulating the polygon distribution. Thus, we assessed the role of DE-cad in the onset of hexagon dominance next.

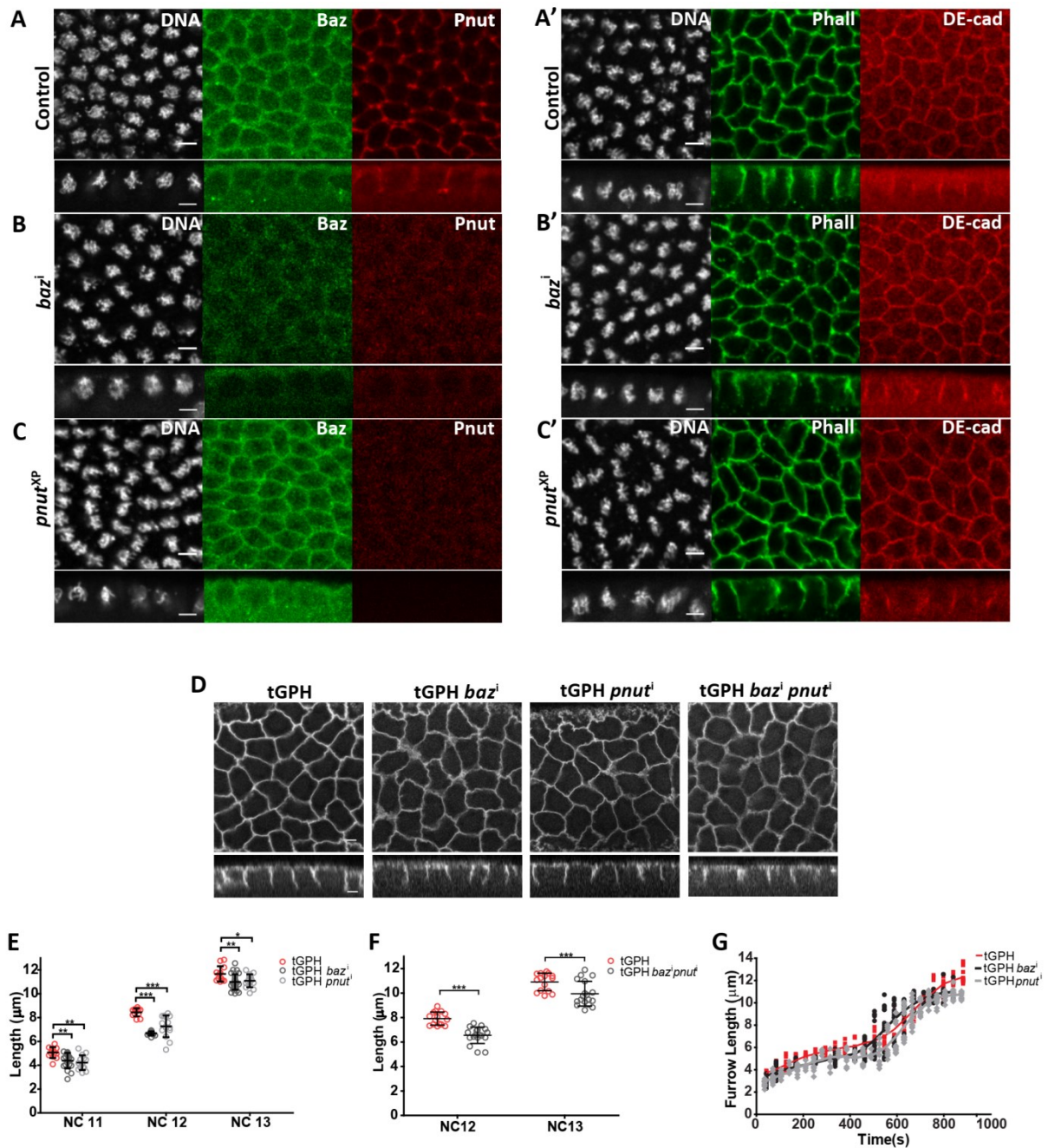


Figure 7.1 Baz and Pnut depletions show decrease in lateral membrane length and delay in hexagon dominance. (A-C) DE-cad is not affected in *baz* and *pnut* mutant embryos. *mat-Gal4/+* (A) control (n=20), *baz*¹ (B) and *pnut*^{xP} (C) embryos co-stained with Baz (green) and Pnut (red) (A-B); DE-cad (red) and phalloidin (green) (A'-B'). *baz*¹ shows a decrease in Baz and Pnut (100%, n=20) (B), DE-cad is unaffected (100%, n=10) (B'). *pnut*^{xP} shows loss of Pnut (100%, n=17) (C); Baz (100%, n=11) and DE-cad (100%, n=15) are unaffected (C-C'). (D-F) *baz* and *pnut* mutant embryos show decreased furrow length. tGPH grazing sections in control, *baz*¹ and *pnut*¹ in NC12 (D). Quantification of metaphase furrow lengths in *baz*¹, *pnut*¹ and tGPH/+ in NC11-13 (n=12, 4 furrows; 3 embryos) (E). Quantification of metaphase furrow lengths in *baz*¹ *pnut*¹ double knockdown and tGPH/+ in NC12-13 (n=12, 4 furrows; 3 embryos) (F). Graph showing furrow ingression rates in *baz*¹ and *pnut*¹ (G). Data is represented as mean \pm SD, *p<0.05, **p<0.01, and ***p<0.001, unpaired Student's t test. Scale bar: 5 μ m.

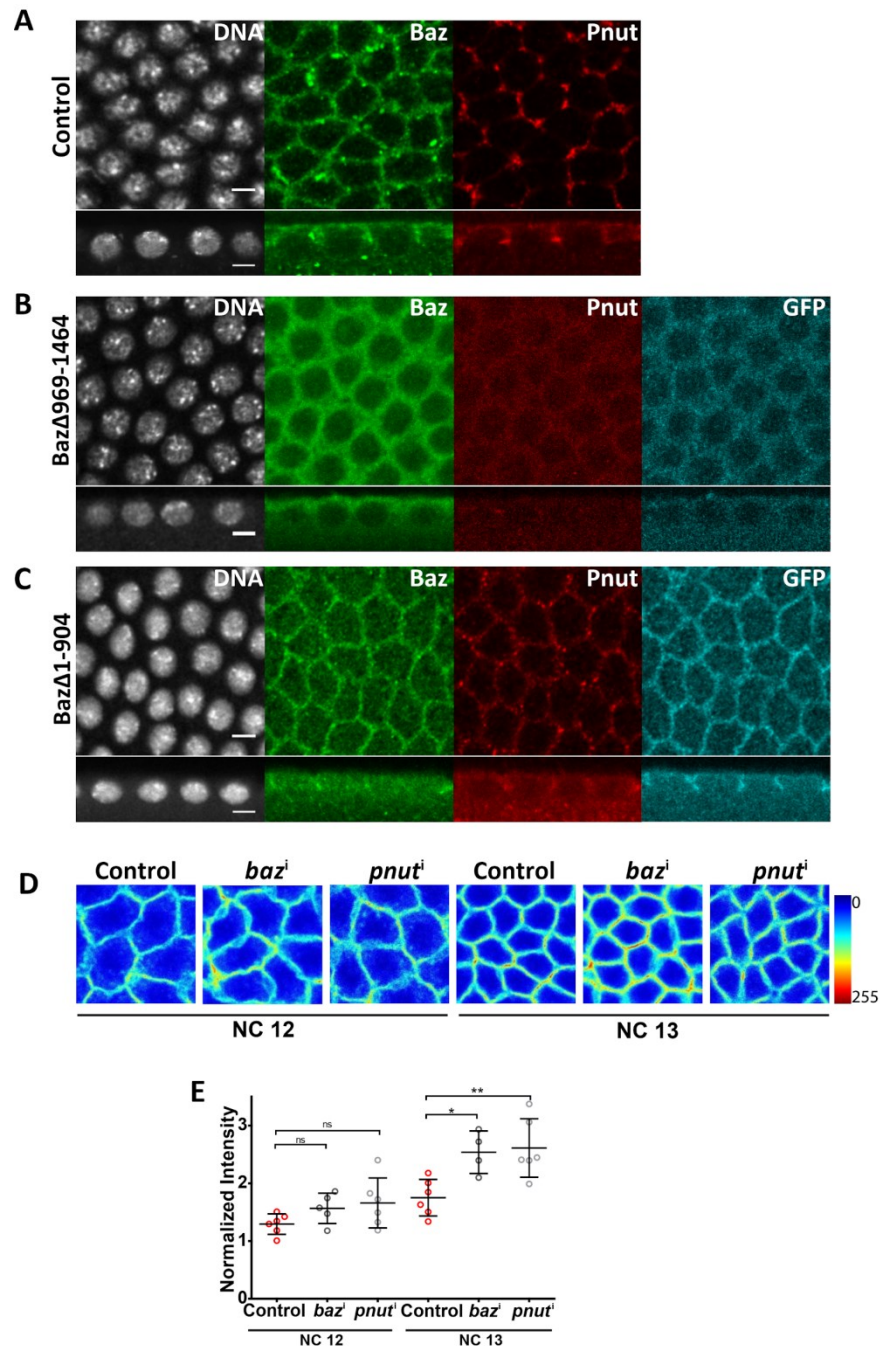


Figure 7.2 Characterization of Baz truncation mutants for Pnut localization.

(A-C) Baz plasma membrane depletion decreases Pnut levels. Control (n=10 embryos) **(A)**, *Baz* Δ 969-1464-GFP **(B)** and *Baz* Δ 1-904-GFP **(C)** expressing embryos co-stained with Baz (green), Pnut (red) and GFP (cyan). *Baz* Δ 969-1464-GFP **(B)** and Baz antibody show cytosolic localization. These embryos also show loss of Pnut from the membrane (87%, n=24 embryos). *Baz* Δ 1-904-GFP **(C)** and Baz antibody shows membrane localization. Pnut distribution is slightly reduced but vertex enrichment is present (64%, n=14 embryos). **(D-E)** DE-cad levels in Baz and Pnut knockdowns is increased at NC13. Sum intensity projections of DE-cad-GFP in control, *baz*ⁱ and *pnut*ⁱ embryos at NC12-13 metaphase **(D)**. Graph showing fold change in DE-cad intensity with respect to NC12 apical section **(E)**. Data is represented as mean \pm SD, *p<0.05, **p<0.01, and ***p<0.001, unpaired Student's t test. Scale Bar = 5 μ m.

7.3.3 DE-cad knockdown results in greater disruption in furrow length and loss of hexagon dominance in syncytial cells

We next knocked down DE-cad in embryos to probe for localization of Baz and Pnut along with lateral membrane length and polygon onset in the syncytial cycles. As shown previously in Chapter 6, *shgⁱ* embryos had reduced DE-cad staining. The *shgⁱ* embryos had diffuse F-actin distribution as seen by phalloidin staining (Figure 7.4A-B). Pnut was spread into the edges and not at the vertex and Baz staining was diffuse as compared to wild-type (Figure 7.4A'-B').

Live imaging of *shgⁱ* embryos with tGPH showed defects during syncytial division cycles which could be categorised into 3 classes: 22% embryos showed disruption of polygonal architecture, 17% showed polygonal organization with loose plasma membrane and 61% showed polygonal organization of the plasma membrane (Figure 7.4C, D). As shown previously, all categories of embryos were estimated for furrow length and it was found to be considerably shorter than control, compared to Baz and Pnut knockdowns (Figure 6.3F compared to 7.1D-E). Finally, the polygon distribution was estimated for *shgⁱ* embryos with furrow length more than the threshold. *shgⁱ* embryos showed pentagon dominance at NC12 (Figure 7.3C-D,J) and hexagon dominance was not recovered in NC13 (Figure 7.3G-H,J). Taken together, DE-cad plays a significant role in keeping adjacent lateral membranes together for the formation of edges and appropriate extension in order to achieve onset of polygonality in the syncytial *Drosophila* embryo.

7.3.4 p120-catenin is more important for regulation of furrow length stabilization as compared to other catenins in the syncytial embryo

With the aim to understand how DE-cad was mechanistically regulating furrow extension along with polygonal distribution, we attempted to test the role of DE-cad binding partners, the catenins, in syncytial plasma membrane organization. The syncytial embryo contains p120-catenin (p120), α -catenin and β -catenin (McCartney et al., 2001a; Pacquelet et al., 2003). β -catenin mutant embryos show loss of spindle attachment to the cortex in small regions but do not show defects in plasma membrane or actin organization in syncytial stages (McCartney et al., 2001a). Also, overexpression of *Shg $\Delta\beta$ cat* (Pacquelet and Rørth, 2005), in which the

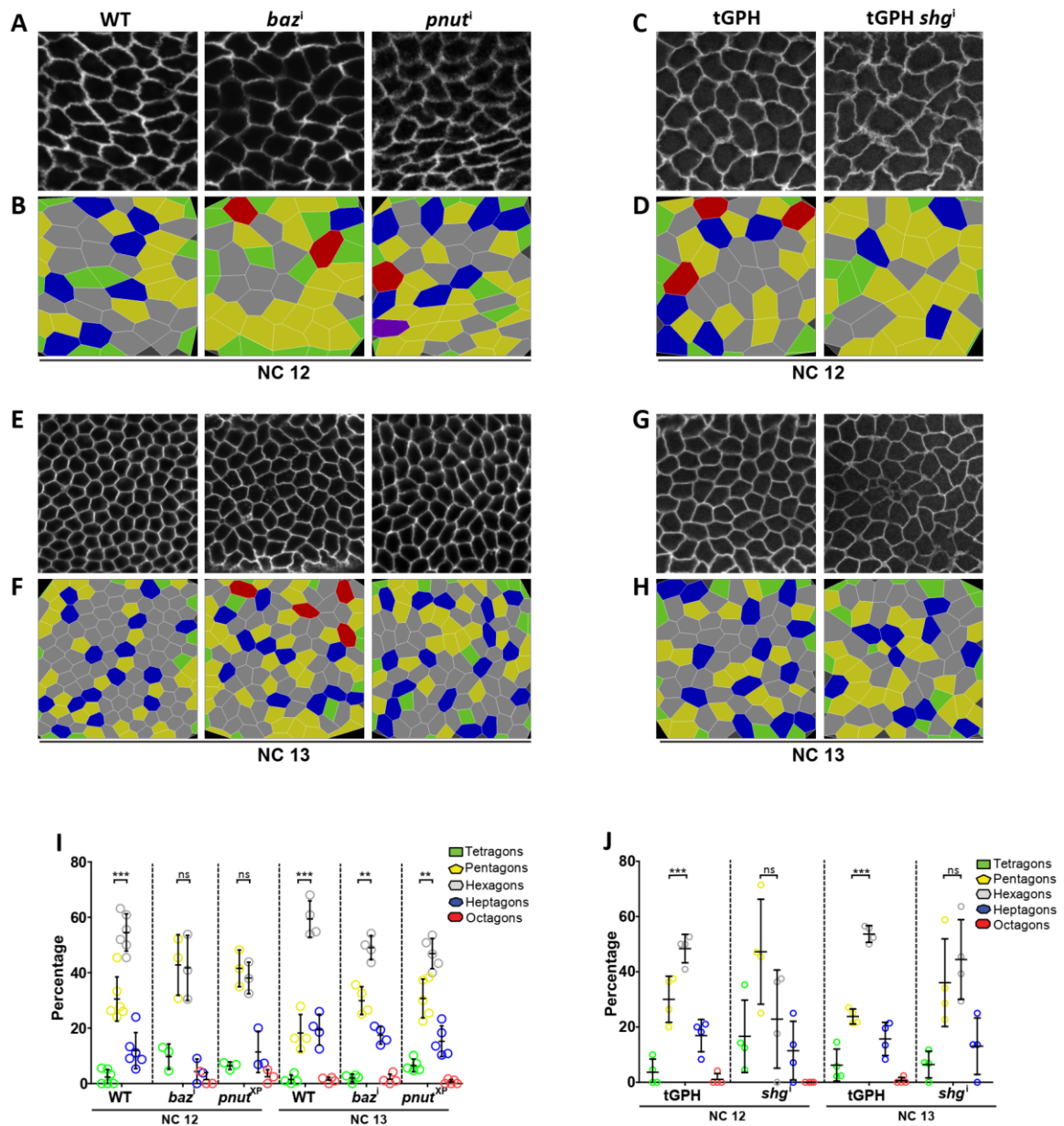


Figure 7.3 Baz and Pnut depletion show delay in hexagon dominance while DE-cad depletion results in loss of hexagon dominance. Wild-type, *baz*¹ and *pnut*^{XP} embryos stained with phalloidin in NC12-13 (**A,E**) along with the respective colour-coded polygon renderings (**B,F**). Polygon distribution in the mutants and wild-type stained with phalloidin in NC12-13 (**I**). Polygon distributions of wild-type and *baz*¹ and *pnut*^{XP} embryos are significantly different from each other (* $p < 0.05$) at NC12 but not at NC13. Multinomial chi square test ($n = \text{approx. } 60\text{--}80$ syncytial cells, 20-30 cells/embryo; 4-5 embryos). Hexagon dominance in *baz*¹ and *pnut*^{XP} recovers in NC13. (**C-D, G-H, J**) *shg*¹ shows pentagon dominance. tGPH/+ and tGPH *shg*¹ embryos in NC12-13 (**C,G**) along with the respective colour-coded polygon renderings (**D,H**). Polygonal distribution in *shg*¹ in NC12-13 (**J**). The polygon distributions of *shg*¹ are significantly different from control (* $p < 0.05$) using Chi square test ($n = \text{approx. } 120$ syncytial cells, 20-30 cells/embryo; 4 embryos). Hexagon dominance doesn't recover at NC13. Pentagons and hexagons are compared in each cycle using the unpaired Student's t test. Mean \pm SD is shown, * $p < 0.05$, ** $p < 0.01$, and *** $p < 0.001$.

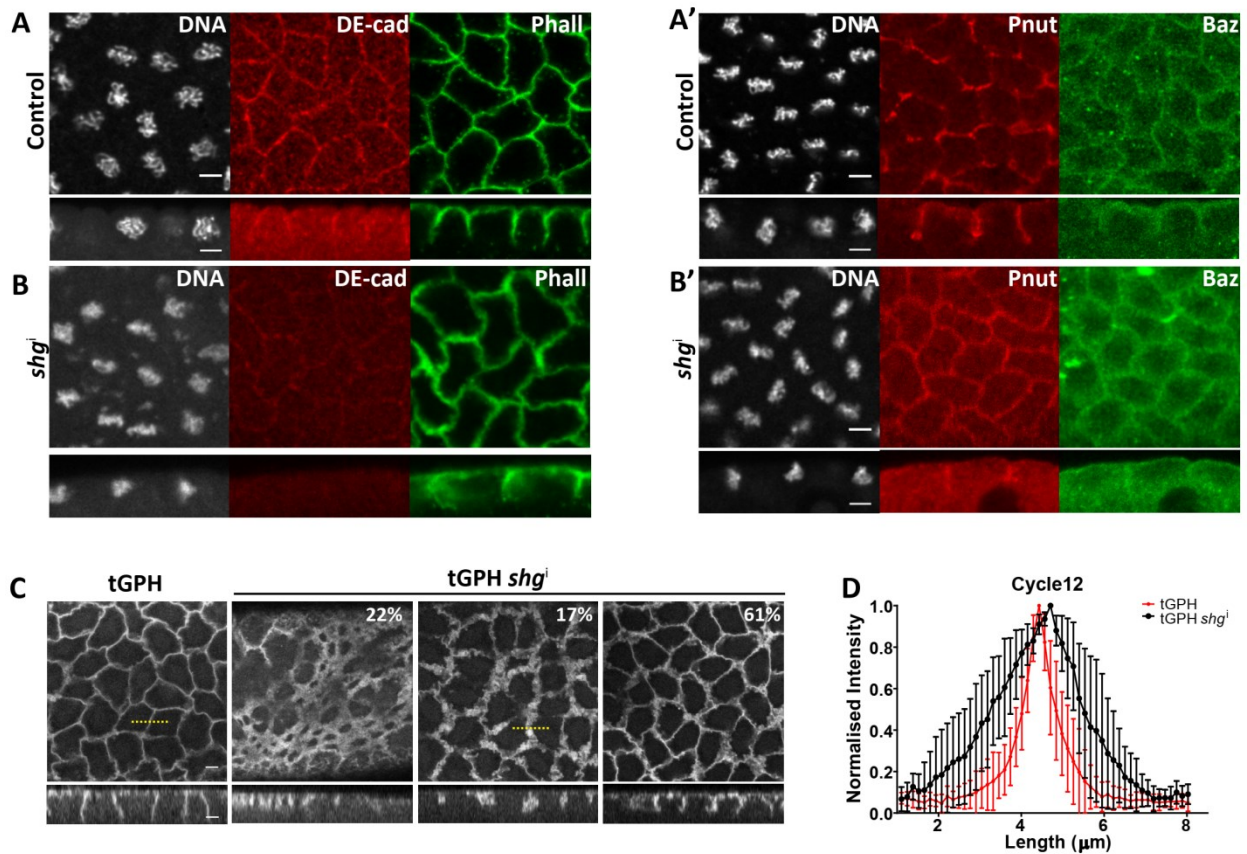


Figure 7.4 DE-cad depletion results in mislocalization of Baz and Pnut and loose membrane morphology.

DE-cad is lowered in *shg^j* embryos. *shg^j* (B, 86%, n=21) and *nanos-Gal4/+* (n=10) are stained with DE-cad (red) and phalloidin (green) (A-B); Baz (green) and Pnut (red) (A'-B'). Baz and Pnut are more spread in *shg^j* embryos (94%, n=16). Note the general disorganization of cells in *shg^j*. (C-D) *shg^j* embryos show decreased furrow length with loose and ruffled membrane in syncytial cells. tGPH grazing sections from control (n=4 embryos) and *shg^j* with disruption of polygonal architecture (22%, n=18 embryos), with loose membrane (17%, n=18 embryos) and short furrow lengths in NC12 (61%, n=18 embryos) (C). Line profiles of (yellow dashed lines in C) control and *shg^j* embryos show broader peak width (D) at NC12. Scale Bar = 5 μm.

carboxyl terminal binding to β-catenin is truncated starting at 4954 bp, did not show a significant change in actin organization (Table 7.1). We, therefore, knocked down α-catenin and p120 using maternally driven RNAi (See Chapter 2 for details).

Maternal knockdown of α-catenin RNAi (*α-cat^d*) showed 100% embryo lethality (n=300) and loss of α-catenin antibody staining (Figure 7.5A-B). Maternal knockdown of p120 RNAi (*p120^d*) (See Chapter 2 for details) resulted in 65% embryo lethality (n=300) and significant reduction of p120 staining (Figure 7.5C-D). DE-cad levels, however, remained unaffected (Figure 7.5A'-D'). There was a small but significant decrease in furrow length in *α-cat^d* as observed by live imaging with tGPH. On the other hand, the furrow was significantly shorter in *p120^d* embryos in NC11-13

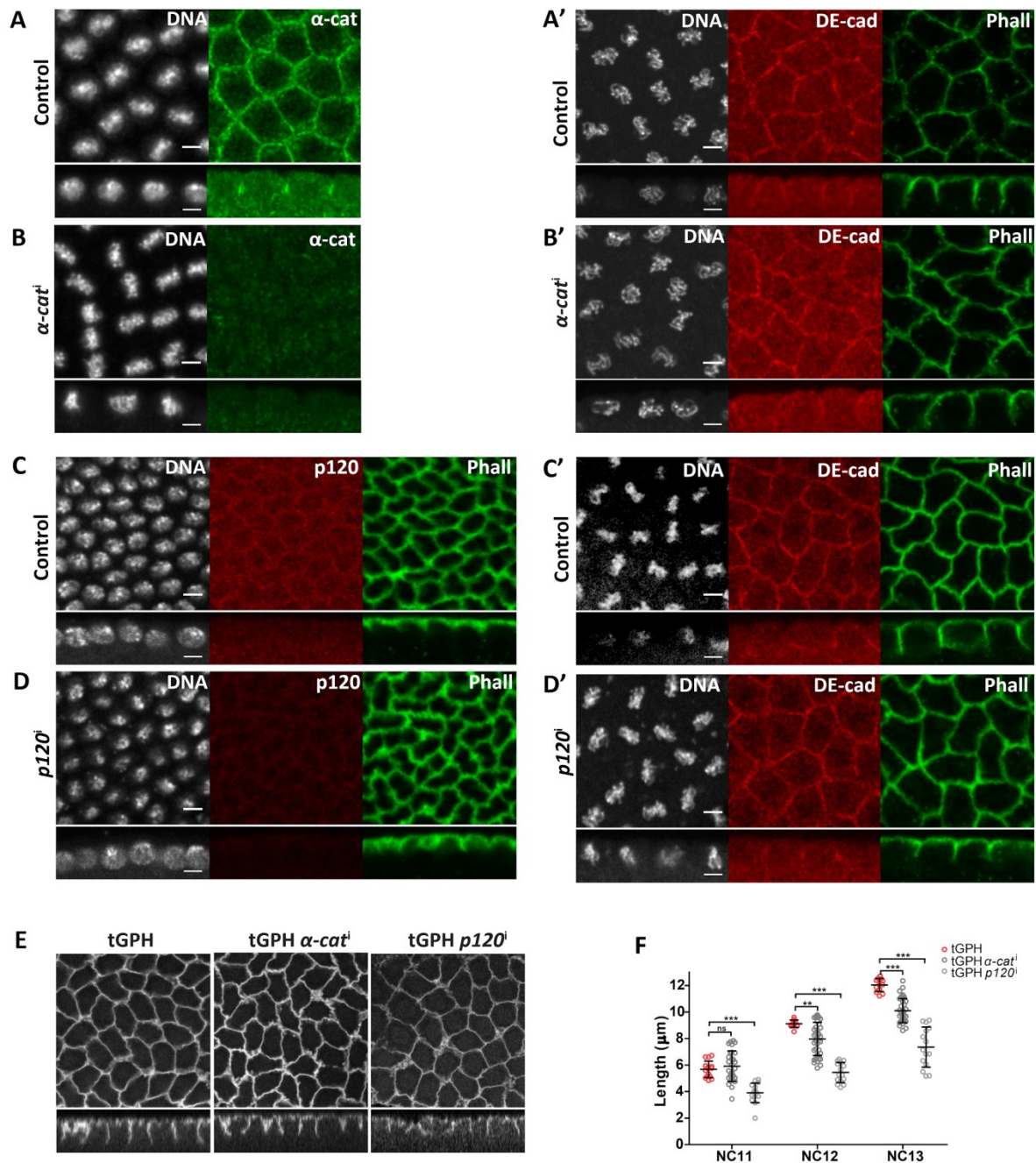


Figure 7.5 p120-catenin depletion results in short furrows delay in hexagon-dominance

(A-B') DE-cad levels are not affected in α -catⁱ embryos. *mat-Gal4*^{+/+} (n=18) (A) and α -catⁱ (B) are stained with α -cat (green); DE-cad (red) and phalloidin (green) (A'-B'). α -catⁱ embryos show reduced α -cat (green, 100%, n=14) (A-B) and no defect in DE-cad (A'-B'). (C-D') DE-cad levels are not affected in $p120^i$ embryos. Wild-type (n=18) (C) and $p120^i$ (D) embryos show reduced p120 (red, 100%, n=14) (C-D) and no defect in DE-cad levels or localization (red, 100%, n=17) (C'-D'). (E-F) α -catⁱ and $p120^i$ embryos show decreased furrow length. tGPH grazing sections in control, α -catⁱ and $p120^i$ embryos in NC12 (E). Quantification of metaphase furrow lengths in tGPH^{+/+}, α -catⁱ and $p120^i$ embryos (n=16, 4 furrows/embryo; 4 embryos) (F). Data is represented as Mean \pm SD, *p<0.05, **p<0.01, and ***p<0.001, unpaired Student's t test. Scale bar: 5 μ m.

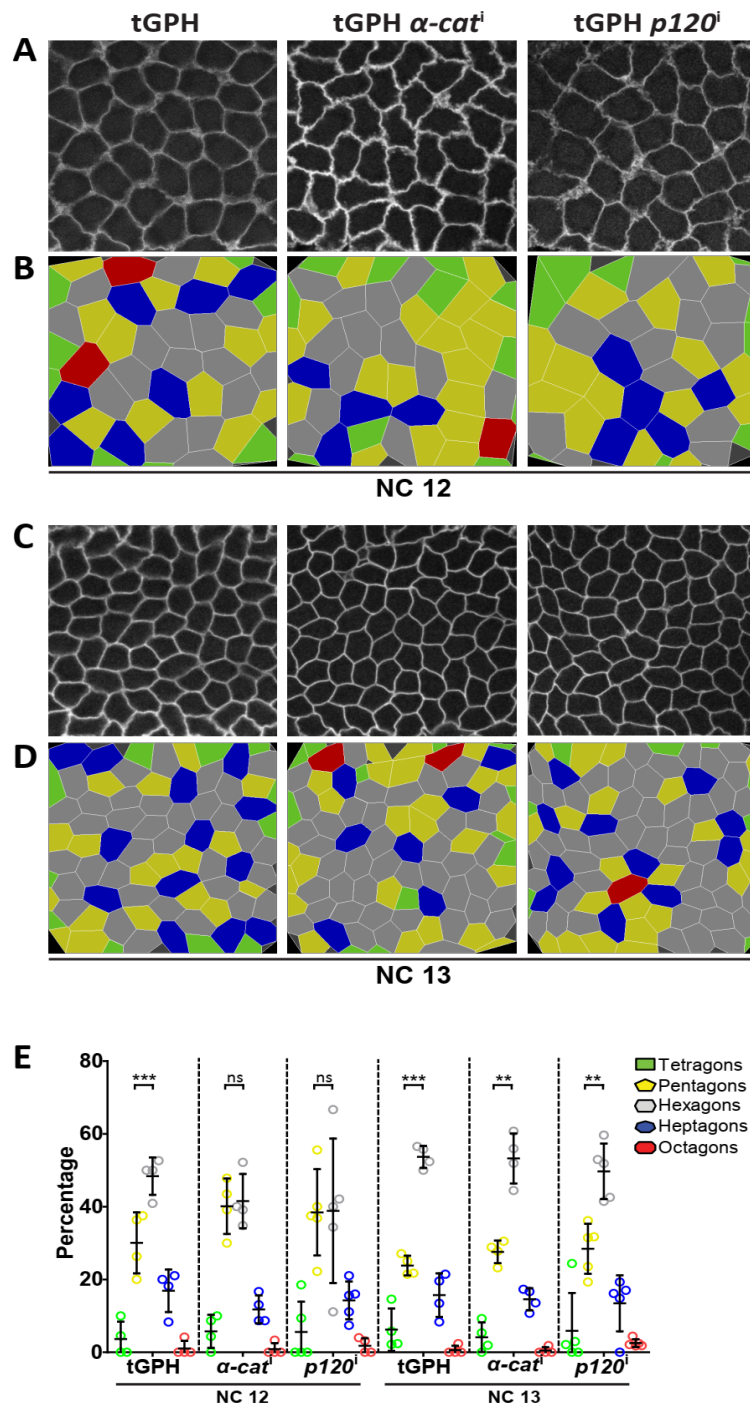


Figure 7.6 $\alpha\text{-cat}$ and $p120\text{-cat}$ knockdowns show delayed onset of hexagon dominance.

Grazing sections of tGPH/+, tGPH $\alpha\text{-cat}^i$ and tGPH $p120^j$ embryos (**A, C**) along with the respective colour-coded polygon renderings (**B, D**) in NC12 (**A-B**) and NC13(**C-D**). Graph showing quantification of polygonal distribution in $\alpha\text{-cat}^i$ and $p120^j$ embryos in NC12-13 (**E**). The hexagon dominance of $\alpha\text{-cat}^i$ and $p120^j$ embryos recovers at NC13. Pentagons and hexagons are compared in each cycle using the Unpaired Student's t test. (n=approx. 120 syncytial cells, 20-30 cells/embryo; 4 embryos). Data is represented as Mean \pm SD, *p<0.05, **p<0.01, and ***p<0.001.

as compared to α -catⁱ (Figure 7.5E-F, Movie 7.3). Thus, p120 is more important for plasma membrane organization in the syncytial embryos as compared to the other catenins. However, unlike the loose plasma membrane in *shg*ⁱ, the tGPH signal in *p120*ⁱ embryos was sharp (Figure 7.5E, Figure 7.4C).

Quantification of polygonal distribution in both α -catⁱ and *p120*ⁱ embryos showed an increase in pentagons at NC12, which recovered to hexagon-dominance at NC13 (Figure 7.6A-C, compared to 7.3C-D, G-H, J). Therefore, although p120 seems more important for furrow stabilization than other catenins, none of the catenins show as strong an effect on polygonal distribution as *shg*ⁱ embryos.

7.3.5 Loss of contractility in the plasma membrane also results in delay in the onset of hexagon dominance

Myosin is an important component of AJs in mammalian epithelial cells as well as the *Drosophila* epidermis. Rho-dependent activation of MyoII often drives the formation and stabilization of AJs (Ivanov et al., 2007; Sen et al., 2013; Shewan et al., 2005; Yamada and Nelson, 2007). Abrogation of MyoII activation in mammalian epithelial cells is known to cause a decrease in the percentage of hexagons (Kalaji et al., 2012). Hence, we decided to quantify polygon distribution in MyoII activity loss of function embryos. We used live movies from tGPH expressing *rhoGEF2*ⁱ and *rok*ⁱ embryos to this end (Refer to Chapter 6, section 6.3.5). Although the frequency of pentagons and hexagons were similar at NC12 in both, *rhoGEF2*ⁱ and *rok*ⁱ embryos, the frequency of hexagons increased as compared to pentagons at NC13, similar to controls (Figure 7.7A-E). Thus, both *rhoGEF2*ⁱ and *rok*ⁱ embryos showed a delay in the onset of hexagon dominance. In conclusion, most components of AJs, except the core component DE-cad, mostly cause a delay in onset of hexagon dominance. DE-cad, therefore, seems to be the most important molecule of the AJ complex in regulating the polygon distribution.

7.3.6 Overexpression of DE-cad with juxtamembrane domain deletion shows severe disruption of F-actin, furrow length and polygonality as compared to DE-cad depletion (Done in collaboration with Tirthasree Das)

p120 binds to the cytoplasmic domain of DE-cad adjacent to the

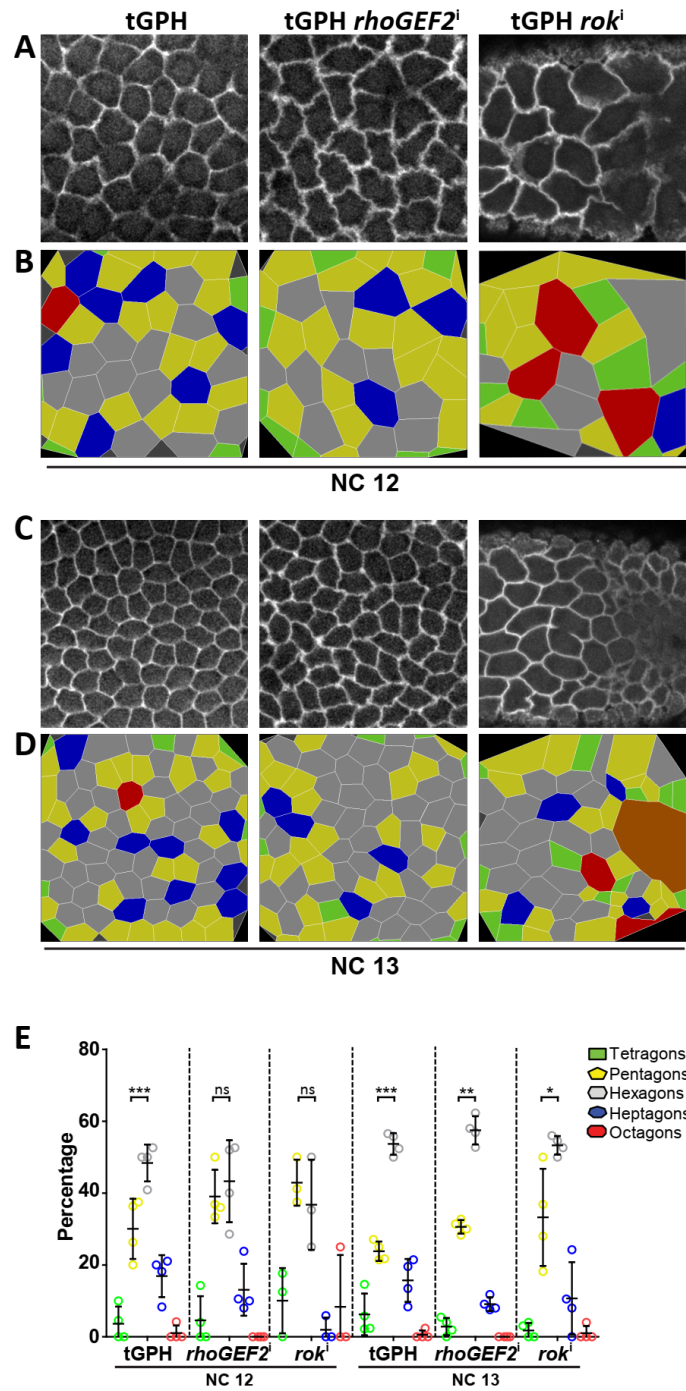


Figure 7.7 RhoGEF2 and Rok knockdowns show delayed onset of hexagon dominance.

Grazing sections of tGPH/+ , tGPH *rhoGEF2ⁱ* and tGPH *rokⁱ* embryos (**A, C**) along with the respective colour-coded polygon renderings (**B, D**) in NC12 (**A-B**) and NC13 (**C-D**). Graph showing quantification of polygonal distribution in *rhoGEF2ⁱ* and *rokⁱ* embryos in NC12-13 (**E**). The hexagon dominance of *rhoGEF2ⁱ* and *rokⁱ* embryos recovers at NC13. Pentagons and hexagons are compared in each cycle using the Unpaired Student's t test. (n=approx. 120 syncytial cells, 20-30 cells/embryo; 4 embryos). Data is represented as Mean \pm SD, * $p < 0.05$, ** $p < 0.01$, and *** $p < 0.001$.

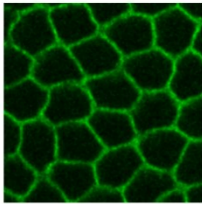
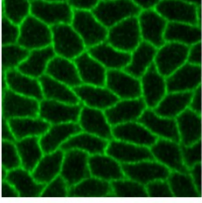
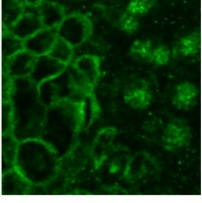
Genotype	Actin staining	Lethality
Shg Δ p120 x mat-Gal4 29°C, n=11		64% 24hrs 64% 48hrs n=176
Shg Δ β cat x mat-Gal4 29°C, n=10		52% 24hrs 48% 48hrs n=200
Shg Δ JM x mat-Gal4 25°C, n=20		80% 48hrs n=300

Table 7.2 List of DE-cad truncation mutants overexpressed in the syncytial embryo. The phalloidin stainings are compared to the controls in Figure 7.7A. Note that Shg Δ p120 is a pUAS τ construct which does not function well in the female germline (Rørth, 1998), while the other two truncation mutants are pUAS ρ constructs. It is possible that the differences in phenotype are due to the expression levels of the truncated proteins.

transmembrane domain, called the juxta-membrane(JM) domain (Anastasiadis and Reynolds, 2000). We overexpressed DE-cad/Shg transgenes with mutations in the JM region. Over- expression of Shg Δ JM, containing a truncation of 1355–1392 bp (JM domain) and Shg Δ p120 containing three glycine to alanine mutations (aa1376–1378) in the p120-binding region of JM domain, were used to test the DE-cad-p120 interaction (Pacquelet and Rørth, 2005; Pacquelet et al., 2003). Shg Δ JM gave even stronger phenotypes as compared (Figure 7.8A-B') to *shg^j* (Figure 7.4) and *p120^j* (Figure 7.5). Shg Δ JM overexpression caused 80% embryo lethality (n=300). Most of the embryos over-expressing Shg Δ JM did not develop post-fertilization (75%, n=331). Shg Δ JM overexpression embryos that developed showed diffused p120 localization and no change in α -catenin (Figure 7.5C, 7.7E-G). The F-actin architecture was severely defective in Shg Δ JM expressing embryos along with a decrease in Baz and Pnut (Figure 7.8 A-B', C-D). Shg Δ p120, however, did not give

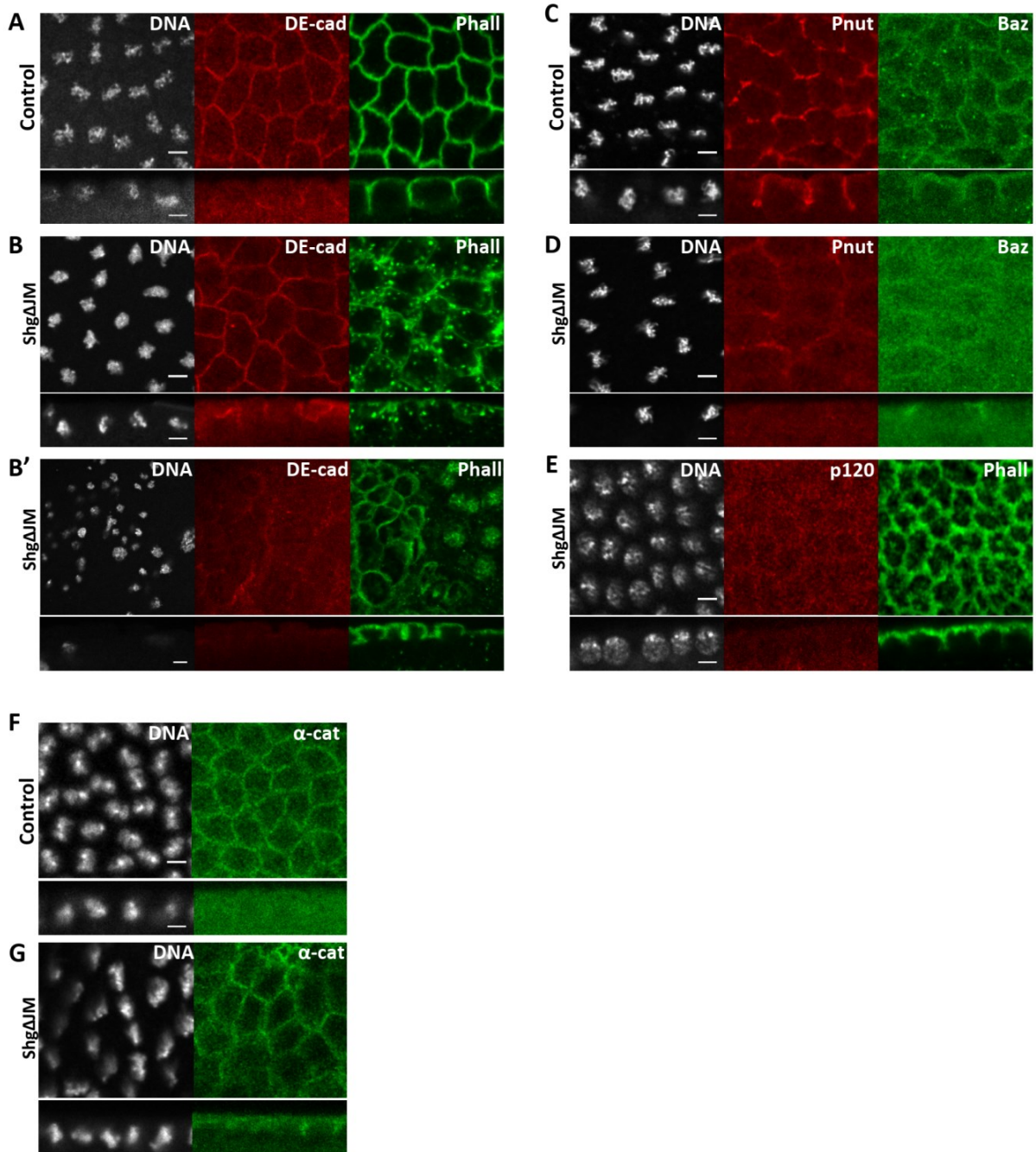


Figure 7.8 Overexpression of Shg Δ JM domain results in severely short furrows, F-actin, Baz and Pnut disorganization and loss of polygonal architecture. Shg Δ JM (B) expression shows lowered Baz (green), Pnut (red) (73%, n=11) (C-D) and disorganized phalloidin (green) as compared to *nanos-Gal4/+* (n=10) (A-B'). DE-cad (red) is on the membrane even though actin is disorganized (69%, n=16) (A-B). When the polygon architecture is completely disrupted, DE-cad is not observed (B'). (E-G) α -Catenin is unaffected while p120 localization is diffused in Shg Δ JM expressing embryos. Control and Shg Δ JM embryos stained with p120 (red) (E) and α -Cat (green) (F-G). Scale bar: 5 μ m.

significant phenotypes in actin organization, presumably because overexpression of the point mutation in a wild-type background did not cause dominant negative effects

(Table 7.2).

Live imaging of Shg Δ JM embryos with tGPH gave phenotypes categorised into 2 types: 57% embryos had either circular cells or were mosaic for circular and polygonal patches and 43% had some polygonal organization (Figure 7.9A-C). All embryos showed a severely depleted furrow length (Figure 7.9B). Most embryos completely lacked furrow extension and progressed through the NCs with a circular plasma membrane without transforming into polygons (Figure 7.9A-C, Movie 7.4). To quantify this, we performed a correlation between metaphase furrow length and circularity for different embryos in NC12-13. All embryos with metaphase furrow lengths below the threshold gave high circularity as compared to longer lengths and control embryos (Figure 7.9 E-F). This was especially apparent in mosaic embryos expressing Shg Δ JM, where part of the embryo had furrow length greater than the threshold and showed polygonal organization, whereas when the furrow length was below the threshold, the polygonal organization was not achieved (Figure 7.9D). It was not possible to carry out the polygon analysis for Shg Δ JM expressing embryos since the polygonal patches were not sufficiently large in number. Thus, the DE-cad JM domain plays an important role in the onset of polygonal architecture in syncytial PM and in organizing the underlying actin cytoskeleton.

7.3.7 Arp2/3 and Dia are additionally lost on overexpression of DE-cad with juxtamembrane domain deletion as compared to DE-cad and p120 loss of function

The DE-cad-catenin interactions regulate the actin cytoskeleton remodelling (Harris and Tepass, 2010). The severe defects observed in the Shg Δ JM embryos as compared to *shg*ⁱ embryos indicated the increased dependence of membrane extension on the DE-cad association with p120. However, loss of p120 alone did not result in such a severe phenotype, suggesting that the JM domain might have additional roles in organizing the cytoskeleton independent of p120. The JM domain deletion also causes morphogenetic defects more severe than p120 loss alone in other systems such as myotome cell rearrangement in chick embryos and tracheal cell fusion in *Drosophila* embryos. Here, JM domain loss blocks cytoskeletal rearrangements necessary for these developmental processes to occur (Horikawa and Takeichi, 2001; Lee et al., 2003). We, therefore, analyzed the distribution of

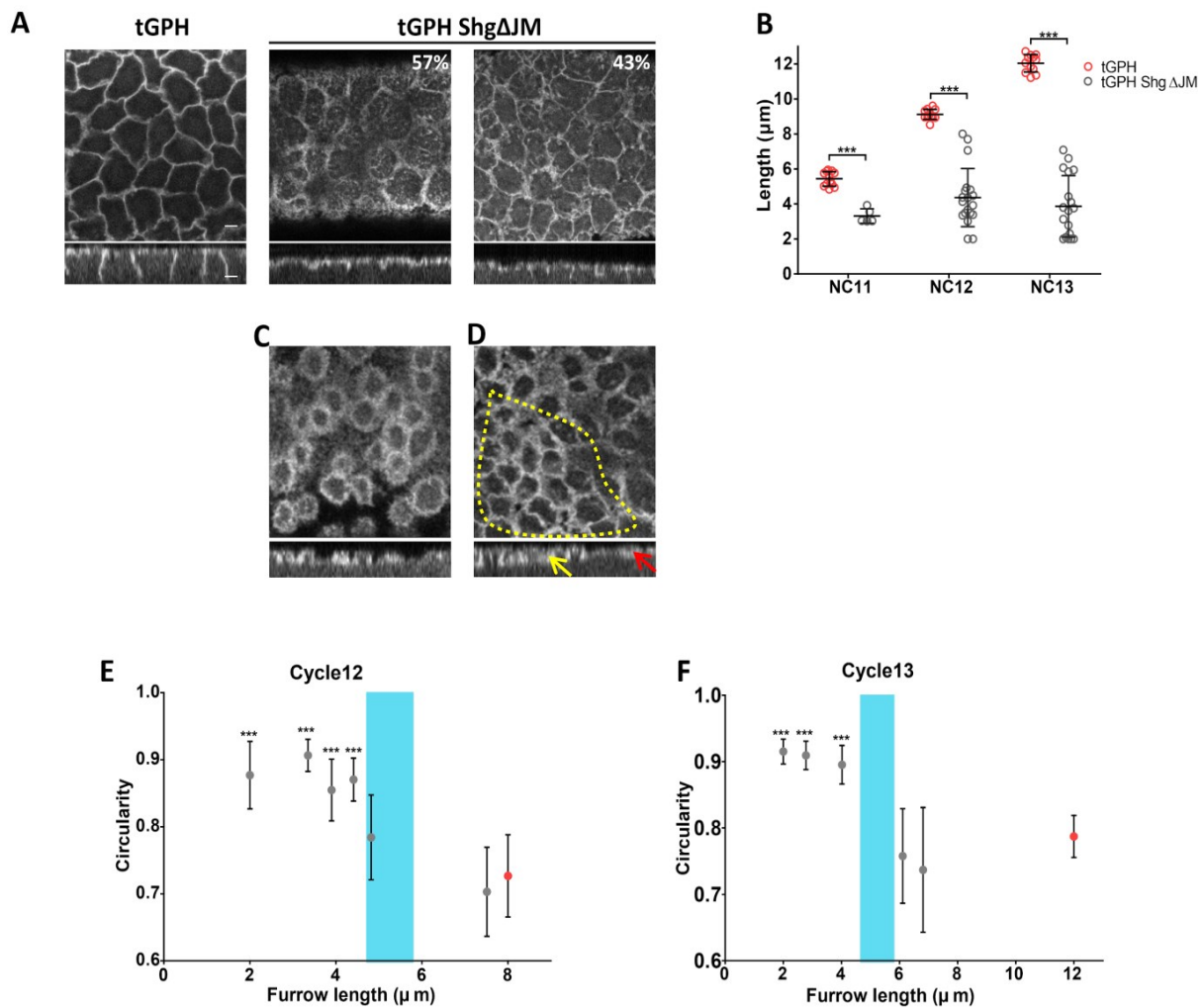


Figure 7.9 Shg Δ JM embryos show decreased furrow extension and increased circularity.

Grazing sections of tGPH in control and Shg Δ JM, Shg Δ JM embryos show 2 phenotypic categories: loss of furrow extension with abrogation of polygonal architecture (57%, n=14 embryos) and short furrows with polygonal architecture (43%, n=14 embryos) (A) at NC12. Quantification of metaphase furrow lengths of Shg Δ JM (n=19 furrows, 4 embryos) at each cycle compared to tGPH/+ (n=12 furrows, 4 embryos) (B). Data is represented as mean \pm SD, *p<0.05, **p<0.01, and ***p<0.001, Student's t test with Welch's correction. (C) Grazing sections at NC13 of tGPH expressing Shg Δ JM with loss of furrow extension and abrogation of polygonal architecture (57%, n=14 embryos). (D) Shg Δ JM embryos showing a mosaic phenotype where parts of the embryo show furrow ingression beyond the threshold (yellow arrows) while other parts do not show furrow ingression (red arrows). (E-F) Shg Δ JM syncytial cells with furrow extension less than the threshold are circular. Graphs show circularity in Shg Δ JM embryos at the indicated furrow length in NC12 (E) and NC13 (the control metaphase furrow length is same as Figure 6.F) (F). Each point shows circularity from one (or more embryos) at the indicated furrow length. Data is represented as mean \pm SD, *p<0.05, **p<0.01, and ***p<0.001, One way ANOVA with Dunnett's Multiple Comparison Test. Each point of the mutant compared to the control (red). Scale bar: 5 μ m.

actin remodelling proteins such as forming the Arp2/3 complex and have decreased furrow extension (Stevenson et al., 2002) and Dia mutant embryos also form short furrows (Afshar et al., 2000). Shg Δ JM expressing embryos showed a severe loss of

Arp2/3 and Dia (Figure 7.10 A-B). *p120ⁱ* and Arp2/3 complex and Dia in these embryos. *arp^{C1}* mutant embryos are deficient in *shgⁱ* expressing embryos, on the other hand, had slightly lowered Arp2/3 complex on the plasma membrane while Dia was unaffected (Figure 7.10 A-A', C-D'). DE-cad JM domain is, therefore, not only responsible for recruitment of p120 but also for stabilization of key actin remodelling proteins such as Arp2/3 complex and Dia on the syncytial plasma membrane.

7.4 Conclusions and Discussion

As shown previously (Chapter 3, 4, 6), ingression of furrows above a threshold lateral length range changed the plasma membrane shape from circular to polygonal. This threshold is reached for the first time in NC11 but the polygon distribution achieved had equal frequencies of pentagons and hexagons. Hexagon dominance was achieved at NC12 metaphase for the first time and consistently achieved in the subsequent cycles, hereafter. Although the threshold length is presumably determined by the concentration of active MyoII relative to DE-cad on the lateral membrane (Chapter 6), hexagon dominance is possibly regulated by optimal concentration and asymmetric distribution of various polarity protein complexes along the lateral membrane. Polarity proteins may not be essential for achieving this threshold length but have a supportive role in lateral membrane stabilization for the formation of an energy minimized network (Figure 7.11). Hexagon dominance can also be interpreted as the optimal number of contacts formed between neighbouring syncytial cells. Loss of hexagon dominance may, therefore, indicate reduced number of contacts between neighbouring cells, which might be as a result of either increased or decreased stability of adhesion (Classen et al., 2005; Hayashi and Carthew, 2004). This is corroborated by our finding that while depletion of Baz, Pnut and catenins delayed the onset of hexagon dominance, DE-cad depletion showed loss of hexagon dominance. Thus, Baz, Pnut and catenins may only play supportive roles in stability of adhesion between the lateral membranes in the syncytial embryo, while DE-cad assumes a central role in mediating adhesion. Both, Baz and DE-cad, play significant roles in initiating the polarity program in different tissues. Baz initiates polarity and facilitates spot adherens junction

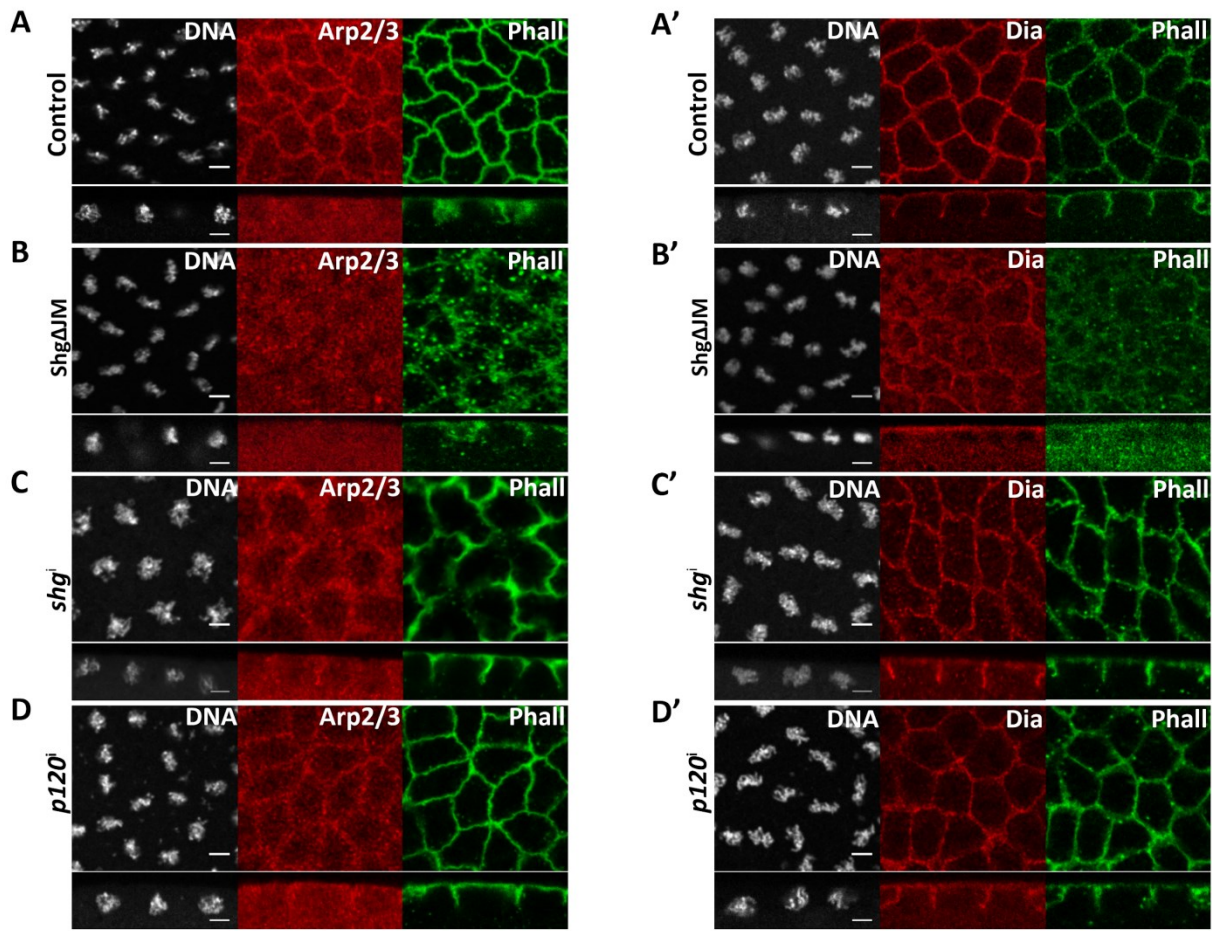


Figure 7.10 Actin regulatory proteins are affected in DE-cad mutant embryos. Wild-type (**A-A'**), *Shg* Δ JM (**B,B'**), *shg*¹ (**C,C'**) and *p120*¹ (**D,D'**) embryos co-stained with Arp2 (red) and phalloidin (green) (**A-D**); Dia (red) and phalloidin (green) (**A'-D'**). Arp2 is mislocalized in *Shg* Δ JM embryos (100%, n=14) and Dia is reduced (80%, n=10) (**B,B'**). Arp2 is lowered in *shg*¹ (38%, n=13) and in *p120*¹ (47%, n=21) (**C-D**) and Dia is unaffected in *shg*¹ (100%, n=10) and in *p120*¹ (100%, n=10) (**C'-D'**). Scale bar: 5 μ m

formation in *Drosophila* cellularization and gastrulation (Muller, 1996; Harris and Peifer, 2004) but is dispensable in follicle epithelial cells (Shahab et al., 2015). Conversely, in apically constricting cells during mesoderm invagination, apical migration of DE-cad precedes that of Baz, and thus, is independent of Baz (Shahab et al., 2015; Weng and Wieschaus, 2017). This is similar to mammalian cells where E-cad is recruited to contact points before Baz (Coopman and Djiane, 2016). This suggests that depending on the tissue type or developmental stage, the relative importance of Baz and E-cad in initiating polarity may change. We show that DE-cad is more important than Baz for syncytial polarity, lateral membrane extension and hexagon-dominated polygonal architecture. Syncytial *Drosophila* embryos lack most other transmembrane junctional proteins such as Crumbs and Neurexin and in such

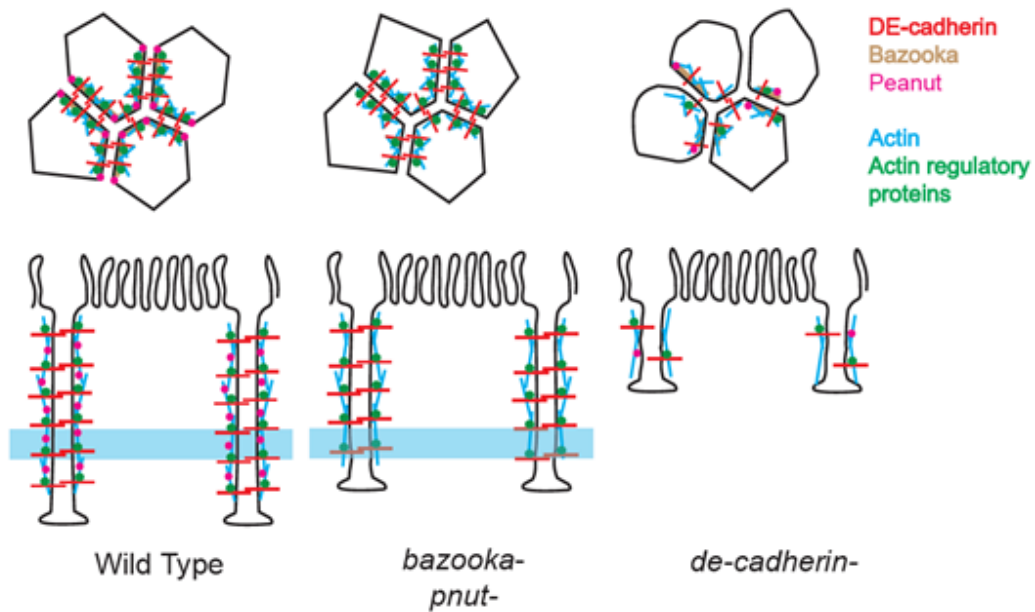


Figure 7.11 Schematic showing the importance of DE-cad in lateral membrane formation and hexagonal packing. Schematic model shows the organization of DE-cad, Baz, Pnut and actin on edges of polygons for furrow extension and summarises the phenotypes obtained on their loss in polygon architecture and furrow length. *baz* and *pnut* mutants result in loss of Pnut, slight decrease in furrow length and delay in hexagon dominance. Embryos mutant for DE-cad show loss of Baz, Pnut and actin organization, significant decrease in furrow length and disruption of onset of polygonal architecture.

a scenario DE-cad is likely to assume a significant role in lateral membrane formation. However, Echinoid is a cell adhesion molecule whose transcripts are present in a 0-4 hour old embryos (Graveley, 2010; Graveley et al., 2011), The modENCODE Consortium, 2010). It may be possible to further intensify the phenotype seen with depletion of DE-cad by depleting Echinoid in this background.

Actin polymerization has a key role in furrow extension and loss of actin regulators like Rhogef2, Diaphanous, Arp2/3 and SCAR decreases furrow lengths (Padash Barmchi et al., 2005a; Sherlekar and Rikhy, 2016; Stevenson et al., 2002; Zallen et al., 2002). Thus, the force for furrow extension is, most likely, generated from actin polymerization. In addition, our data suggests that fine tuning active MyoII levels relative to DE-cad also contributes to furrow extension as hyperactivity of MyoII and loss of DE-cad, both result in loss of furrow extension (Chapter 6). We think that, hyperactivity of MyoII or loss of DE-cad mediated adhesion, possibly, results in excessive membrane contractility rendering the force generated through actin polymerization insufficient to drive furrow extension. Thus, actin polymerization

along with appropriate levels of MyoII activity relative to DE-cad regulate mechanics of furrow extension.

E-cad mediated adhesion also regulates actin dynamics at the point of contact in order to strengthen newly formed junctions. Conversely, Formin mediated actin nucleation and Arp2/3 activity are, both, necessary for E-cad based contact expansion and stabilization (Kovacs et al., 2002; Carramusa et al., 2007). Thus, both E-cad mediated adhesion and actin dynamics influence each other. We observed a severe loss of Arp2/3 from the plasma membrane in *Shg Δ JM*, *shg^j* and *p120ⁱ* embryos. These embryos also showed defects in actin architecture, while *baz^j* and *pnut^d* embryos did not. Taken together, it implies that the cytosolic domain of DE-cad, and more specifically the JM domain, organises actin nucleators, in addition, to binding to p120. Absence of DE-cad, therefore, results in profound disorganization of the syncytial membrane through perturbation in the SCAR-Arp2/3 actin remodelling pathway. Thus, defective furrow extension in DE-cad and p120-cat perturbations is, possibly, due to a combination of problems in adhesion and in actin polymerization. Interestingly, there were examples among *shg^j* and *p120ⁱ* embryos which showed furrow extension beyond the threshold length range and formed polygons, but had loose plasma membrane organization. This was also true for *rhoGEF2ⁱ* embryos. This implies that while the residual actin polymerization could drive furrow extension in these embryos, lack of adhesion or contractility prevented the membranes from sticking together or stretching appropriately. In other words, these examples provided an opportunity to study the effects of adhesion and contractility, de-coupled from the force of actin polymerization in furrow extension.

The distribution of polygonal cell shapes in epithelia can also be described by a parameter called jamming, which refers to a state where cells are relatively frozen in place, resembling a solid phase. Conversely, unjamming refers to a more fluid-like phase where cells are free to rearrange and flow. In an unjammed state, group of cells appear more irregular in shape compared to regular shapes in a jammed state. Decreased adhesion and cell density or increased motility of cells are some factors that are known to favour unjamming which, in a way, corresponds to a soft network (Park et al., 2015; Sadati et al., 2013). Decreased number of edges in the polygonal array is also a favorable state for cell neighbor exchanges and gives rise to a soft network (Farhadifar et al., 2007). Based on this, the increase in pentagons in *Baz*, *Pnut* and catenin knockdowns indicate a similar transition to a soft network due to

fine modulations in adhesion even though the levels of DE-cad appear to be unchanged in these embryos. Thus, future analysis of change in lateral membrane tension in various genetic backgrounds along with mathematical modelling will be necessary to reveal the mechanisms that drive shape morphogenesis in syncytial blastoderm embryo. In conclusion, asymmetric distribution of proteins in the syncytial plasma membrane supports hexagon-dominated polygonal packing.

Chapter 8

Thesis summary and future perspectives

This section summarizes the results from this study along with discussing future perspectives based on some key conclusions. The key findings of the study can be summarized into the following three points:

8.1 Circular to polygonal shape transition of epithelial cells correlates with a threshold lateral membrane ingression.

Although a vast body of literature exists for characterizing the conserved hexagon-dominated polygonal architecture of epithelia across metazoans, little is known about the essential factors sufficient to initiate such an architecture (Aegerter-Wilmsen et al., 2010; Classen et al., 2005b; Farhadifar et al., 2007; Gibson et al., 2006; Sánchez-Gutiérrez et al., 2013). In our study, we use the syncytial *Drosophila* embryo to study such factors. We show that irrespective of cell size, crowding and cell cycle phase, the circular to polygonal shape transition of syncytial cells occurs after a minimum extent of lateral membrane ingression (Chapter 3, Figure 8.1A). This threshold length is possibly determined by fine tuning the activity of MyoII relative to DE-cad in the lateral membrane (Chapter 6, Figure 8.1E). This is supported by the observation that tipping the balance off to either excessive or reduced MyoII activity with respect to adhesion, impacts the achievement of threshold. Increasing MyoII activity prohibits the threshold length from being achieved altogether and gives rise to circular cells (Figure 6.6). On the other hand, decreasing MyoII activity allows adhesion to take over earlier, which facilitates contact formation even before the threshold length is being achieved. In other words, by reducing contractility, the threshold for circular to polygonal transition is shifted to a lower length (Figure 6.5). Thus, the threshold is not a fixed point but a dynamic point which reflects appropriate balancing of MyoII activity with adhesion and is subject to change based on the requirement of the system. The fact that we see the onset of polygonal shape in the absence of a basal domain also highlights the fact

that the lateral membrane height and stability are sufficient to induce this shape transition. The syncytial system, thus, provides a minimalistic system to test the role of lateral membranes in imparting epithelial-like characteristics to a cell in the absence of a basal domain.

A finer temporal handle over MyoII activity modulation can be made possible by optogenetic tools (Izquierdo et al., 2018). Locally increasing MyoII activity at a point when the lateral membrane length reaches above the threshold can provide us with the opportunity to see if the circular to polygonal transition can be reversed in real time with unbalanced MyoII hyperactivity. In addition, optogenetic tools allow ectopic activation of MyoII to study the functional relevance of the absence of MyoII or contractility at certain stages of development (Krueger et al., 2019). For example, MyoII can be ectopically activated at a stage like metaphase, where it is known to be inactive and absent from the cortex. Such experiments may provide insights into the need for MyoII to be inactive at certain stages of development.

Our model also predicts that if adhesion is weakened, contractility will take over and phenocopy the increased MyoII activity scenario. However, we see the loss of ingression and formation of circular cells in only a small percentage of DE-cad knockdown embryos (Figure 6.4). This implies either incomplete abrogation of adhesion or the presence of other adhesion molecules in the syncytial system. It would be beneficial to screen for other adhesion molecules of either AJs or SJs in the syncytium to supplement this model. As mentioned earlier, Echinoid is one such candidate that can be tested for, since it expresses at moderately high levels in the 0-4hr old embryos (Graveley, 2010; Graveley et al., 2011; The modENCODE Consortium, 2010).

On the other hand, over-expression of a DE-cad allele lacking the JM domain shows complete loss of furrow extension and abrogation of polygonality similar to MyoII hyperactivity (Figure 7.8). In addition to regulating the recruitment of actin regulators like Arp2/3 (Figure 7.9), this suggests that JM domain may be important in controlling active MyoII levels. However, since this experiment was done in a wildtype background we were unable to clearly assign this function to the DE-cad JM domain. Despite this, it is interesting to note that DE-cad truncated for the JM domain is reported to act dominant-negatively. In addition, both overexpression in a wildtype or in a DE-cad mutant background are reported to have similar phenotypes (Lee et al., 2003). To verify the role of JM domain in the syncytial system, it will be

necessary to carry out a systematic domain deletion analysis in a DE-cad null background to fit DE-cad better in this model.

Different types of epithelial cells, like squamous, cuboidal and columnar, have different levels of adhesive and contractile proteins on the lateral membrane (Kondo and Hayashi, 2015). Therefore, it is possible that each of these cell types may have different lateral length thresholds that can be determined. At the same time, this lateral membrane length based model is particularly relevant for studying the reverse transition of polygonal to circular, cells as seen in epithelial to mesenchymal transitions in development and diseases. Different epithelial cell types, therefore, may also require different extents of changes in adhesion and contractility to get extracted from the epithelium. This could also reflect the susceptibility of various epithelial tissues to cancers.

8.2 The syncytial *Drosophila* plasma membrane is polarized in both XZ and XY planes before cellularization.

Although epithelial polarity was known to be initiated during cellularization when the epithelial cells are first formed during development, few recent studies report the presence of asymmetries in the syncytial embryo as well (Mavrakis et al., 2009; Schmidt and Grosshans, 2018). Here, we provide details of finer asymmetries along the lateral membrane in a quantitative manner using live imaging (Chapter 5, Figure 8.1C). We find Dlg, Baz and Pnut to be more basolateral as compared to DE-cad which is spread along the entire lateral membrane. In addition, we also see the emergence of asymmetries between edges and vertices of a syncytial cell, with DE-cad, Dlg and Baz being enriched on the edges and Pnut-Sep1-Sep2 on the vertices (Figure 5.1 and 5.2). This may be thought of as a simplistic version of PCP. The syncytial plasma membrane, thus, appears to be a preparatory stage towards further polarization in later stages.

The polarity protein knockdown and mutant data also allow us to allude to the functions of these asymmetries in the syncytial embryo. In summary, DE-cad appears to be primarily responsible for the formation and stability of the lateral domain as well as the hexagon dominant polygonal plasma membrane architecture (Figure 7.3 and 7.4). Baz and Pnut, on the other hand, play a supportive role in regulating hexagon dominance. This is demonstrated by the data that hexagon

dominance is only delayed in the knockdowns of Baz and Pnut, unlike DE-cad knockdowns, where hexagon dominance is completely lost (Figure 7.1, 7.3 and 8.1D).

Since we assign an important role to lateral membrane length for the onset of polygonality, it will be interesting to test the role of a polarity complex enriched in the basolateral domain, like the Scrib complex, in this system. Studying the role of this complex in the syncytial stage may provide further insights to the role of these asymmetries in the early embryo.

8.3 The conserved hexagon dominated polygonal distribution depends on the length as well as polarity protein composition of the lateral membrane

As the lateral membrane length increases to reach the threshold length for polygon formation, edges are formed first by the expansion of contacts between the syncytial cells, followed by formation of vertices. Although polygonality is initiated at NC11, hexagon dominance is achieved only in NC12 for the first time (Figure 8.1B). This may be influenced by the number of neighbouring cells, in other words, crowding. It is possible that a minimum extent of crowding is required to increase the sidedness of each cell. However, when we looked at the polygon distribution at a lower length than metaphase, that is, at a point just above the threshold (furrow length $\cong 6.5\mu\text{m}$), we saw the onset of hexagon dominance later, in NC13 (Figure 4.1 and 8.1B). This indicates that both crowding and lateral membrane length could contribute to the onset of hexagon dominance. However, unlike a fixed threshold length for the onset of polygonality, we did not find a threshold length for the onset of hexagon dominance. At a fixed lateral membrane length, the only variable across NCs is the cell number and cell size. It is possible that a combination of cell crowding, cell size and lateral membrane length contribute to hexagon dominance. Therefore, onset of hexagon-dominance is, possibly, a multifactorial process.

Smaller lateral membrane lengths are known to influence polygonal distribution (Kalaji et al., 2012). Similarly, we observe a correlation between decrease in lateral membrane length and delay in the onset of hexagon dominance with knockdowns of polarity proteins. One possible explanation for this is that the length may correspond to a minimum amount of protein complexes required for appropriate tension and stability of the lateral membrane. It is interesting to note that

the extent of decrease in lateral membrane length in the knockdowns also correlates with the spread of the polarity proteins on the furrow. While basolaterally enriched Baz and Pnut knockdowns show a marginal decrease in furrow length, knockdown of DE-cad, which is spread throughout the lateral membrane, results in much shorter furrow lengths.

Polarity protein distributions are different across the syncytial cycles. While DE-cad increased three fold by NC13, Baz and Pnut only increased two fold till NC12 on the syncytial membrane. This may be the reason why the polygon distribution is more sensitive to the loss of DE-cad than Baz or Pnut. It is possible that the relative levels and distribution of polarity complexes change during NCs as per the requirement to form an energy minimized network. This is further corroborated by the data that at NC13, rescue of hexagon dominance in Baz and Pnut knockdown embryos correlates with an increase in the level of DE-cad.

At the same time, DE-cad levels also increase within an NC from interphase to metaphase, which correlates with the initiation of polygonal architecture. While in the case of initiation of polygonality, the role of increasing DE-cad is to counter-balance MyoII based contractility to achieve the threshold, in the case of onset of hexagon dominance the mechanism is still unclear. Even then, both events rely on appropriate levels of specific protein complexes on the plasma membrane to facilitate the process.

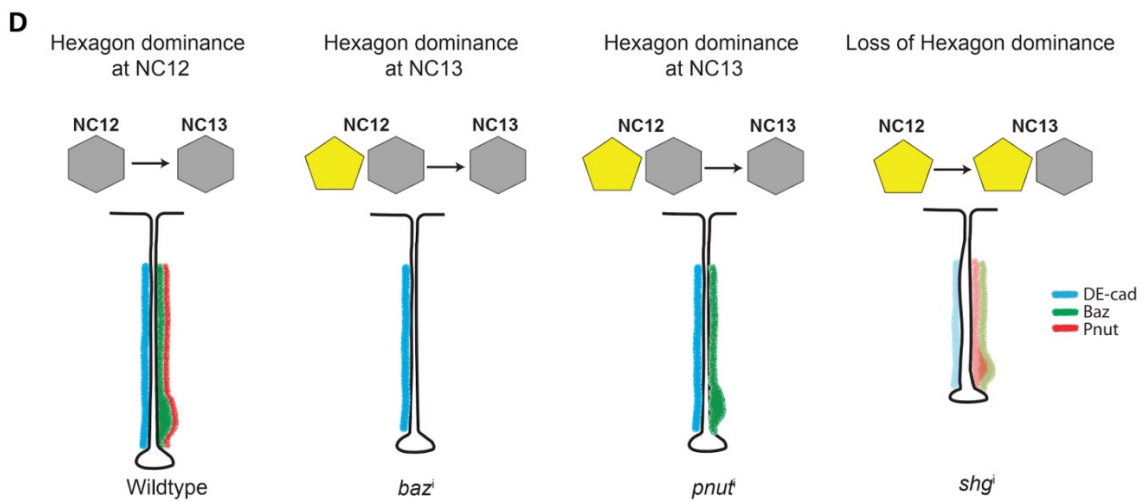
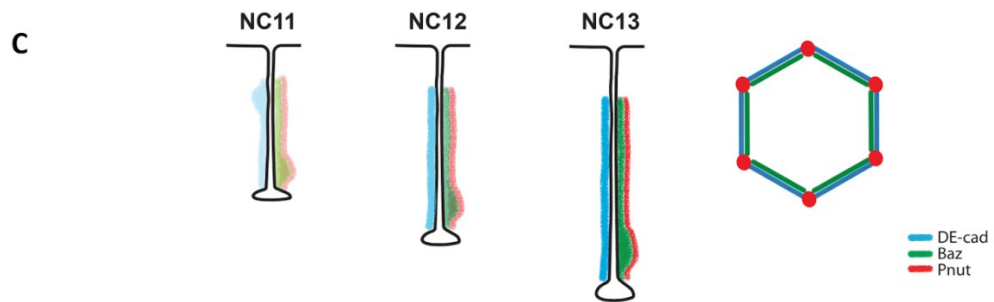
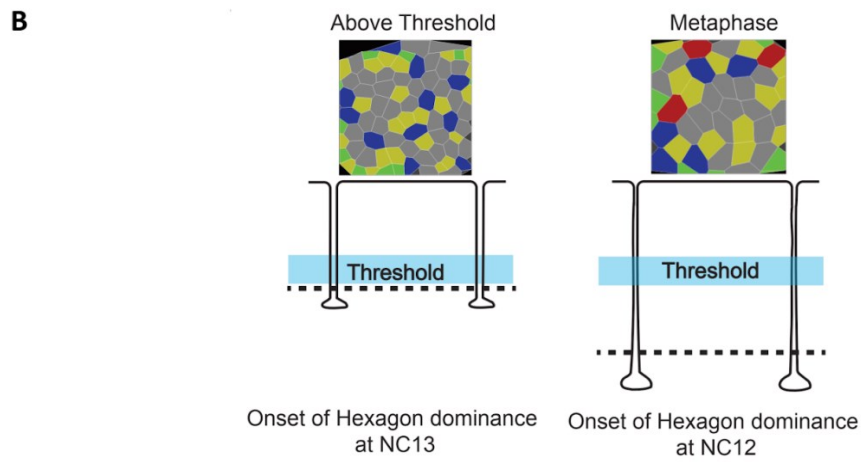
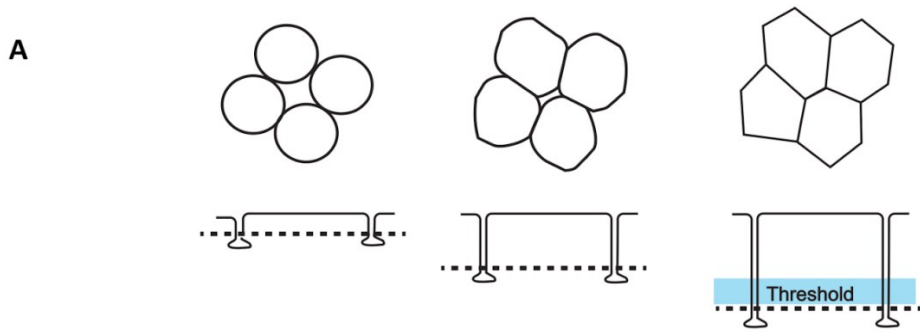
Squamous, cuboidal and columnar epithelial cells show manifold differences in lateral membrane length with respect to width. In addition, each of these epithelial cell types has different levels of adhesion and contractile molecules on the lateral membrane (Kondo and Hayashi, 2015). It will be of interest to observe how the polygon distribution varies between these cell types with similar levels of crowding. This will enable us to dissect out the contributions of crowding versus lateral membrane length or cell sizes.

Baz is required to maintain the mobile pool of DE-cad in the plasma membrane in stage 15 *Drosophila* embryos (Bulgakova et al., 2013). Therefore, it is possible that the mobility of DE-cad in the syncytium is altered in Baz knockdowns. Decreased mobility of DE-cad usually corresponds to more stable adhesion and over stabilization of DE-cad on the membrane is known to reduce the percentage of hexagons in the wing disc (Classen et al., 2005; Iyer et al., 2018). It is possible that the delay in hexagon-dominance in Baz knockdowns is via this mechanism.

Comparing DE-cad mobilities in metaphase of all the polarity mutants that show delay in the onset of hexagon-dominance may provide further insights into this.

Changing levels or mobility and, hence, stability of adhesion might also affect tension in the membrane. Since we also observe an increase in DE-cad levels across the NCs (Figure 5.2), it will be interesting to study the differences in tension in the membrane from NC11-NC14 in a wildtype scenario. In addition, comparing tension at NC12, where loss of hexagon dominance is usually observed, across the mutants as compared to the controls can help deduce the mechanical impacts of perturbations in polarity proteins. Experimentally this can be done via gross laser ablations and comparison of recoil velocities between the different cycles (Krueger et al., 2019). But laser ablations are difficult to perform and getting high n values is a problem, therefore, another high throughput approach could be to theoretically determine tension from still images using a Bayesian statistics based method (Ishihara and Sugimura, 2012; Krueger et al., 2019).

Taken together, we find that the syncytial plasma membrane shows epithelial-like characteristics, both in terms of polarity and polygonal packing, even before complete cell formation in cellularization. To the best of our knowledge, our study is the first to identify a limiting geometric factor i.e. a threshold lateral membrane length for the onset of polygonality and highlights the role of the known molecular forces in regulating it. Since the syncytial system lacks a basal domain, it is a powerful system to demonstrate that the lateral domain is sufficient to induce this shape change.



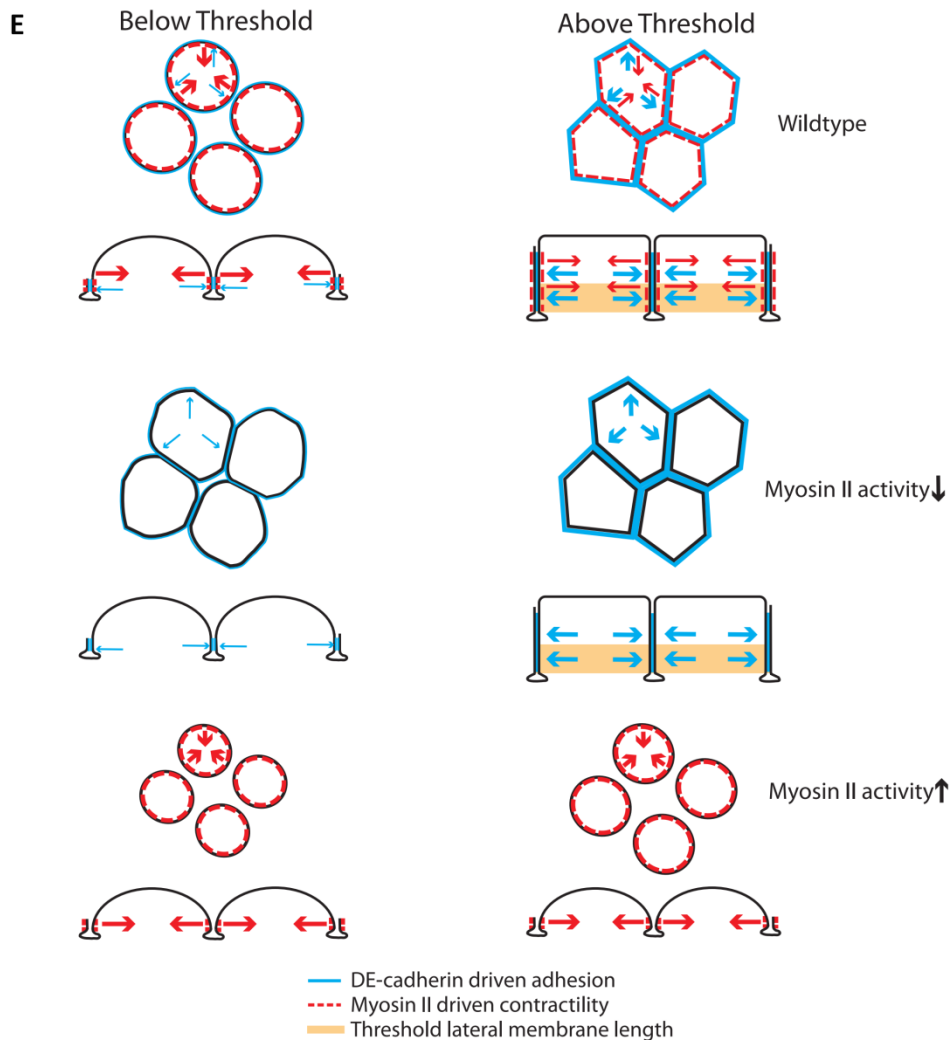


Figure 8.1 Summary models. Circular to polygonal plasma membrane transition occurs after a threshold lateral membrane length ingression (A). The blue region corresponds to the threshold while the black dashed line corresponds to the plane through which the XY views on top are shown. Onset of hexagon dominance occurs at NC12 metaphase in the syncytial *Drosophila* embryo (B). The black dashed line corresponds to the plane through which the XY views of polygon renderings are shown on top. At a shorter lateral length just above threshold (approximately 6.5 μ m), hexagon dominance occurs at NC13. The syncytial plasma membrane is polarized along XY and XZ planes (C). DE-cad is spread all along the lateral membrane while Baz and Pnut are enriched at the basolateral end. DE-cad and Baz are enriched on the edge while Pnut (and other Septins) is enriched on the vertices. Loss of Baz or Pnut results in a delay in the onset of hexagon-dominance while loss of DE-cad results in loss of hexagon dominance (D). Note the difference in the protein complex composition of the various mutants. *baz*¹ shows loss of Pnut in addition to loss of Baz, while *pnut*¹ shows loss of Pnut only. DE-cad is unperturbed in both these cases. *shg*¹, on the other hand, shows lowering of all three proteins. Adhesion and contractility balance to achieve a threshold lateral length for circular to polygon formation (E). Decreasing MyoII activity allows adhesion to take over and form polygons at lower threshold length while increasing MyoII activity, removes adhesion completely and prevents reaching the threshold, thereby forming circular cells.

Bibliography

- Aegerter-Wilmsen, T., Smith, A.C., Christen, A.J., Aegerter, C.M., Hafen, E., and Basler, K. (2010). Exploring the effects of mechanical feedback on epithelial topology. *Development* 137, 499–506.
- Afshar, K., Stuart, B., and Wasserman, S.A. (2000). Functional analysis of the *Drosophila* diaphanous FH protein in early embryonic development. *Development* 127, 1887–1897.
- Alford, L.M., Ng, M.M., and Burgess, D.R. (2009). Cell polarity emerges at first cleavage in sea urchin embryos. *Dev. Biol.* 330, 12–20.
- Alt, S., Ganguly, P., and Salbreux, G. (2017). Vertex models: from cell mechanics to tissue morphogenesis. *Philos. Trans. R. Soc. Lond. B Biol. Sci.* 372.
- Anastasiadis, P.Z., and Reynolds, A.B. (2000). The p120 catenin family: complex roles in adhesion, signaling and cancer. *J. Cell Sci.* 113 (Pt 8), 1319–1334.
- Anderson, D.C., Gill, J.S., Cinalli, R.M., and Nance, J. (2008). Polarization of the *C. elegans* Embryo by RhoGAP-Mediated Exclusion of PAR-6 from Cell Contacts. *Science* 320, 1771–1774.
- Benton, R., and St Johnston, D. (2003). A conserved oligomerization domain in *drosophila* Bazooka/PAR-3 is important for apical localization and epithelial polarity. *Curr. Biol.* 13, 1330–1334.
- Bertet, C., Sulak, L., and Lecuit, T. (2004). Myosin-dependent junction remodelling controls planar cell intercalation and axis elongation. *Nature* 429, 667–671.
- Bilder, D., and Perrimon, N. (2000). Localization of apical epithelial determinants by the basolateral PDZ protein Scribble. *Nature* 403, 676–680.
- Bilder, D., Li, M., and Perrimon, N. (2000). Cooperative regulation of cell polarity and growth by *Drosophila* tumor suppressors. *Science* 289, 113–116.
- Bilder, D., Schober, M., and Perrimon, N. (2003). Integrated activity of PDZ protein complexes regulates epithelial polarity. *Nat. Cell Biol.* 5, 53–58.
- Blankenship, J.T., Backovic, S.T., Sanny, J.S.P., Weitz, O., and Zallen, J.A. (2006). Multicellular rosette formation links planar cell polarity to tissue morphogenesis. *Dev. Cell* 11, 459–470.
- Bloor, J.W., and Kiehart, D.P. (2002). *Drosophila* RhoA regulates the cytoskeleton and cell-cell adhesion in the developing epidermis. *Development* 129, 3173–3183.
- Borghi, N., Sorokina, M., Shcherbakova, O.G., Weis, W.I., Pruitt, B.L., Nelson, W.J., and Dunn, A.R. (2012a). E-cadherin is under constitutive actomyosin-generated tension that is increased at cell-cell contacts upon externally applied stretch. *Proc. Natl. Acad. Sci. U. S. A.* 109, 12568–12573.
- Borghi, N., Sorokina, M., Shcherbakova, O.G., Weis, W.I., Pruitt, B.L., Nelson, W.J., and Dunn, A.R. (2012b). E-cadherin is under constitutive actomyosin-generated tension that is

increased at cell-cell contacts upon externally applied stretch. *Proc. Natl. Acad. Sci. U. S. A.* **109**, 12568–12573.

Britton, J.S., Lockwood, W.K., Li, L., Cohen, S.M., and Edgar, B.A. (2002). *Drosophila's* insulin/PI3-kinase pathway coordinates cellular metabolism with nutritional conditions. *Dev. Cell* **2**, 239–249.

Bulgakova, N.A., Grigoriev, I., Yap, A.S., Akhmanova, A., and Brown, N.H. (2013). Dynamic microtubules produce an asymmetric E-cadherin–Bazooka complex to maintain segment boundaries. *The Journal of Cell Biology* **201**, 887–901.

Byri, S., Misra, T., Syed, Z.A., Bätz, T., Shah, J., Boril, L., Glashauser, J., Aegerter-Wilmsen, T., Matzat, T., Moussian, B., et al. (2015). The Triple-Repeat Protein Anakonda Controls Epithelial Tricellular Junction Formation in *Drosophila*. *Dev. Cell* **33**, 535–548.

Cao, J., Crest, J., Fasulo, B., and Sullivan, W. (2010). Cortical actin dynamics facilitate early-stage centrosome separation. *Curr. Biol.* **20**, 770–776.

Carramusa, L., Ballestrem, C., Zilberman, Y., and Bershadsky, A.D. (2007). Mammalian diaphanous-related formin Dia1 controls the organization of E-cadherin-mediated cell-cell junctions. *J. Cell Sci.* **120**, 3870–3882.

Chalmers, A.D., Pambos, M., Mason, J., Lang, S., Wylie, C., and Papalopulu, N. (2005). aPKC, Crumbs3 and Lgl2 control apicobasal polarity in early vertebrate development. *Development* **132**, 977–986.

Choi, W., Harris, N.J., Sumigray, K.D., and Peifer, M. (2013). Rap1 and Canoe/afadin are essential for establishment of apical-basal polarity in the *Drosophila* embryo. *Mol. Biol. Cell* **24**, 945–963.

Chougule, A.B., Hastert, M.C., and Thomas, J.H. (2016). Drak Is Required for Actomyosin Organization During *Drosophila* Cellularization. *G3* **6**, 819–828.

Classen, A.-K., Anderson, K.I., Marois, E., and Eaton, S. (2005). Hexagonal Packing of *Drosophila* Wing Epithelial Cells by the Planar Cell Polarity Pathway. *Developmental Cell* **9**, 805–817.

Coopman, P., and Djiane, A. (2016). Adherens Junction and E-Cadherin complex regulation by epithelial polarity. *Cell. Mol. Life Sci.* **73**, 3535–3553.

Cox, R.T., Kirkpatrick, C., and Peifer, M. (1996). Armadillo is required for adherens junction assembly, cell polarity, and morphogenesis during *Drosophila* embryogenesis. *J. Cell Biol.* **134**, 133–148.

Crest, J., Concha-Moore, K., and Sullivan, W. (2012). RhoGEF and positioning of rappaport-like furrows in the early *Drosophila* embryo. *Curr. Biol.* **22**, 2037–2041.

Drubin, D.G., and Nelson, W.J. (1996). Origins of cell polarity. *Cell* **84**, 335–344.

Farhadifar, R., Röper, J.-C., Aigouy, B., Eaton, S., and Jülicher, F. (2007). The Influence of Cell Mechanics, Cell-Cell Interactions, and Proliferation on Epithelial Packing. *Current Biology* **17**, 2095–2104.

Field, C.M., al-Awar, O., Rosenblatt, J., Wong, M.L., Alberts, B., and Mitchison, T.J. (1996). A purified *Drosophila* septin complex forms filaments and exhibits GTPase activity. *J. Cell Biol.* **133**, 605–616.

- Figard, L., Xu, H., Garcia, H.G., Golding, I., and Sokac, A.M. (2013). The Plasma Membrane Flattens Out to Fuel Cell-Surface Growth during *Drosophila* Cellularization. *Developmental Cell* **27**, 648–655.
- Figard, L., Wang, M., Zheng, L., Golding, I., and Sokac, A.M. (2016). Membrane Supply and Demand Regulates F-Actin in a Cell Surface Reservoir. *Developmental Cell* **37**, 267–278.
- Foe, V.E., and Alberts, B.M. (1983). Studies of nuclear and cytoplasmic behaviour during the five mitotic cycles that precede gastrulation in *Drosophila* embryogenesis. *J. Cell Sci.* **61**, 31–70.
- Foe, V.E., Field, C.M., and Odell, G.M. (2000). Microtubules and mitotic cycle phase modulate spatiotemporal distributions of F-actin and myosin II in *Drosophila* syncytial blastoderm embryos. *Development* **127**, 1767–1787.
- Fox, D.T., Homem, C.C.F., Myster, S.H., Wang, F., Bain, E.E., and Peifer, M. (2005). Rho1 regulates *Drosophila* adherens junctions independently of p120ctn. *Development* **132**, 4819–4831.
- Frescas, D., Mavrikakis, M., Lorenz, H., Delotto, R., and Lippincott-Schwartz, J. (2006). The secretory membrane system in the *Drosophila* syncytial blastoderm embryo exists as functionally compartmentalized units around individual nuclei. *J. Cell Biol.* **173**, 219–230.
- Gibson, M.C., Patel, A.B., Nagpal, R., and Perrimon, N. (2006). The emergence of geometric order in proliferating metazoan epithelia. *Nature* **442**, 1038–1041.
- Gomez, J.M., Wang, Y., and Riechmann, V. (2012). Tao controls epithelial morphogenesis by promoting Fasciclin 2 endocytosis. *J. Cell Biol.* **199**, 1131–1143.
- Gómez-Gálvez, P., Vicente-Munuera, P., Tagua, A., Forja, C., Castro, A.M., Letrán, M., Valencia-Expósito, A., Grima, C., Bermúdez-Gallardo, M., Serrano-Pérez-Higuera, Ó., et al. (2018). Author Correction: Scutoids are a geometrical solution to three-dimensional packing of epithelia. *Nat. Commun.* **9**, 4210.
- Graveley, B. (2010). The developmental transcriptome of *Drosophila melanogaster*. *Genome Biology* **11**, 111.
- Graveley, B.R., Brooks, A.N., Carlson, J.W., Duff, M.O., Landolin, J.M., Yang, L., Artieri, C.G., van Baren, M.J., Boley, N., Booth, B.W., et al. (2011). The developmental transcriptome of *Drosophila melanogaster*. *Nature* **471**, 473–479.
- Guillot, C., and Lecuit, T. (2013). Mechanics of epithelial tissue homeostasis and morphogenesis. *Science* **340**, 1185–1189.
- Hannezo, E., Prost, J., and Joanny, J.-F. (2014). Theory of epithelial sheet morphology in three dimensions. *Proc. Natl. Acad. Sci. U. S. A.* **111**, 27–32.
- Harris, T.J.C., and Peifer, M. (2004). Adherens junction-dependent and -independent steps in the establishment of epithelial cell polarity in *Drosophila*. *J. Cell Biol.* **167**, 135–147.
- Harris, T.J.C., and Tepass, U. (2010). Adherens junctions: from molecules to morphogenesis. *Nature Reviews Molecular Cell Biology* **11**, 502–514.
- Hayashi, T., and Carthew, R.W. (2004). Surface mechanics mediate pattern formation in the developing retina. *Nature* **431**, 647–652.
- Heisenberg, C.-P., and Bellaïche, Y. (2013). Forces in Tissue Morphogenesis and

Patterning. *Cell* 153, 948–962.

Herzberg, F., Wildermuth, V., and Wedlich, D. (1991). Expression of XBCad, a novel cadherin, during oogenesis and early development of *Xenopus*. *Mech. Dev.* 35, 33–42.

Higashi, T., and Miller, A.L. (2017). Tricellular junctions: how to build junctions at the TRICKiest points of epithelial cells. *Mol. Biol. Cell* 28, 2023–2034.

Higashi, T., Tokuda, S., Kitajiri, S.-I., Masuda, S., Nakamura, H., Oda, Y., and Furuse, M. (2013). Analysis of the “angulin” proteins LSR, ILDR1 and ILDR2--tricellulin recruitment, epithelial barrier function and implication in deafness pathogenesis. *J. Cell Sci.* 126, 966–977.

Holly, R.M., Mavor, L.M., Zuo, Z., and Blankenship, J.T. (2015). A rapid, membrane-dependent pathway directs furrow formation through RalA in the early *Drosophila* embryo. *Development* 142, 2316–2328.

Horikawa, K., and Takeichi, M. (2001). Requirement of the juxtamembrane domain of the cadherin cytoplasmic tail for morphogenetic cell rearrangement during myotome development. *J. Cell Biol.* 155, 1297–1306.

Huang, J., Zhou, W., Dong, W., Watson, A.M., and Hong, Y. (2009). From the Cover: Directed, efficient, and versatile modifications of the *Drosophila* genome by genomic engineering. *Proc. Natl. Acad. Sci. U. S. A.* 106, 8284–8289.

Ikenouchi, J., Furuse, M., Furuse, K., Sasaki, H., Tsukita, S., and Tsukita, S. (2005). Tricellulin constitutes a novel barrier at tricellular contacts of epithelial cells. *The Journal of Cell Biology* 171, 939–945.

Ishihara, S., and Sugimura, K. (2012). Bayesian inference of force dynamics during morphogenesis. *J. Theor. Biol.* 313, 201–211.

Ivanov, A.I., Bachar, M., Babbin, B.A., Adelstein, R.S., Nusrat, A., and Parkos, C.A. (2007). A unique role for nonmuscle myosin heavy chain IIA in regulation of epithelial apical junctions. *PLoS One* 2, e658.

Iyer, K.V., Venkatesan Iyer, K., Piscitello-Gómez, R., Jülicher, F., and Eaton, S. (2018). Mechanosensitive binding of p120-Catenin at cell junctions regulates E-Cadherin turnover and epithelial viscoelasticity.

Izquierdo, E., Quinkler, T., and De Renzis, S. (2018). Guided morphogenesis through optogenetic activation of Rho signalling during early *Drosophila* embryogenesis. *Nat. Commun.* 9, 2366.

Kalaji, R., Wheeler, A.P., Erasmus, J.C., Lee, S.Y., Endres, R.G., Cramer, L.P., and Braga, V.M.M. (2012). ROCK1 and ROCK2 regulate epithelial polarisation and geometric cell shape. *Biol. Cell* 104, 435–451.

Kinoshita, M. (2006). Diversity of septin scaffolds. *Curr. Opin. Cell Biol.* 18, 54–60.

Knox, A.L., and Brown, N.H. (2002). Rap1 GTPase regulation of adherens junction positioning and cell adhesion. *Science* 295, 1285–1288.

Kondo, T., and Hayashi, S. (2015). Mechanisms of cell height changes that mediate epithelial invagination. *Dev. Growth Differ.* 57, 313–323.

Kong, D., Wolf, F., and Großhans, J. (2017). Forces directing germ-band extension in

Drosophila embryos. *Mech. Dev.* **144**, 11–22.

Kovacs, E.M., Goodwin, M., Ali, R.G., Paterson, A.D., and Yap, A.S. (2002). Cadherin-directed actin assembly: E-cadherin physically associates with the Arp2/3 complex to direct actin assembly in nascent adhesive contacts. *Curr. Biol.* **12**, 379–382.

Krahn, M.P., Klopfenstein, D.R., Fischer, N., and Wodarz, A. (2010). Membrane targeting of Bazooka/PAR-3 is mediated by direct binding to phosphoinositide lipids. *Curr. Biol.* **20**, 636–642.

Krueger, D., Tardivo, P., Nguyen, C., and De Renzis, S. (2018). Downregulation of basal myosin-II is required for cell shape changes and tissue invagination. *EMBO J.* **37**.

Krueger, D., Quinkler, T., Mortensen, S.A., Sachse, C., and De Renzis, S. (2019). Cross-linker-mediated regulation of actin network organization controls tissue morphogenesis. *The Journal of Cell Biology* jcb.201811127.

Lamouille, S., Xu, J., and Derynck, R. (2014). Molecular mechanisms of epithelial–mesenchymal transition. *Nat. Rev. Mol. Cell Biol.* **15**, 178–196.

Laprise, P., and Tepass, U. (2011). Novel insights into epithelial polarity proteins in *Drosophila*. *Trends Cell Biol.* **21**, 401–408.

Lecuit, T., and Lenne, P.-F. (2007). Cell surface mechanics and the control of cell shape, tissue patterns and morphogenesis. *Nat. Rev. Mol. Cell Biol.* **8**, 633–644.

Lecuit, T., and Yap, A.S. (2015). E-cadherin junctions as active mechanical integrators in tissue dynamics. *Nat. Cell Biol.* **17**, 533–539.

Lee, M., Lee, S., Zadeh, A.D., and Kolodziej, P.A. (2003). Distinct sites in E-cadherin regulate different steps in *Drosophila* tracheal tube fusion. *Development* **130**, 5989–5999.

Letizia, A., Ricardo, S., Moussian, B., Martín, N., and Llimargas, M. (2013). A functional role of the extracellular domain of Crumbs in cell architecture and apicobasal polarity. *J. Cell Sci.* **126**, 2157–2163.

Liang, X., Michael, M., and Gomez, G.A. (2016). Measurement of Mechanical Tension at Cell-cell Junctions Using Two-photon Laser Ablation. *Bio Protoc* **6**.

Luedeke, C., Frei, S.B., Sbalzarini, I., Schwarz, H., Spang, A., and Barral, Y. (2005). Septin-dependent compartmentalization of the endoplasmic reticulum during yeast polarized growth. *J. Cell Biol.* **169**, 897–908.

Lye, C.M., Naylor, H.W., and Sanson, B. (2014). Subcellular localisations of the CPTI collection of YFP-tagged proteins in *Drosophila* embryos. *Development* **141**, 4006–4017.

Macara, I.G. (2004). Parsing the polarity code. *Nat. Rev. Mol. Cell Biol.* **5**, 220–231.

Magie, C.R., Pinto-Santini, D., and Parkhurst, S.M. (2002). Rho1 interacts with p120ctn and alpha-catenin, and regulates cadherin-based adherens junction components in *Drosophila*. *Development* **129**, 3771–3782.

Maître, J.-L., and Heisenberg, C.-P. (2013). Three functions of cadherins in cell adhesion. *Curr. Biol.* **23**, R626–R633.

Martin, A.C., Kaschube, M., and Wieschaus, E.F. (2009). Pulsed contractions of an actin-myosin network drive apical constriction. *Nature* **457**, 495–499.

- Mason, F.M., Xie, S., Vasquez, C.G., Tworoger, M., and Martin, A.C. (2016). RhoA GTPase inhibition organizes contraction during epithelial morphogenesis. *J. Cell Biol.* *214*, 603–617.
- Masuda, S., Oda, Y., Sasaki, H., Ikenouchi, J., Higashi, T., Akashi, M., Nishi, E., and Furuse, M. (2011). LSR defines cell corners for tricellular tight junction formation in epithelial cells. *J. Cell Sci.* *124*, 548–555.
- Mavrakakis, M., Rikhy, R., Lilly, M., and Lippincott-Schwartz, J. (2008). Fluorescence imaging techniques for studying *Drosophila* embryo development. *Curr. Protoc. Cell Biol.* *Chapter 4*, Unit 4.18.
- Mavrakakis, M., Rikhy, R., and Lippincott-Schwartz, J. (2009). Plasma Membrane Polarity and Compartmentalization Are Established before Cellularization in the Fly Embryo. *Dev. Cell* *16*, 93–104.
- Mavrakakis, M., Azou-Gros, Y., Tsai, F.-C., Alvarado, J., Bertin, A., Iv, F., Kress, A., Basselet, S., Koenderink, G.H., and Lecuit, T. (2014). Septins promote F-actin ring formation by crosslinking actin filaments into curved bundles. *Nature Cell Biology* *16*, 322–334.
- Mays, R.W., Beck, K.A., and Nelson, W.J. (1994). Organization and function of the cytoskeleton in polarized epithelial cells: a component of the protein sorting machinery. *Curr. Opin. Cell Biol.* *6*, 16–24.
- McCartney, B.M., McEwen, D.G., Grevengoed, E., Maddox, P., Bejsovec, A., and Peifer, M. (2001a). *Drosophila* APC2 and Armadillo participate in tethering mitotic spindles to cortical actin. *Nat. Cell Biol.* *3*, 933–938.
- McCartney, B.M., McEwen, D.G., Grevengoed, E., Maddox, P., Bejsovec, A., and Peifer, M. (2001b). *Drosophila* APC2 and Armadillo participate in tethering mitotic spindles to cortical actin. *Nat. Cell Biol.* *3*, 933–938.
- McDonald, J.A., Khodyakova, A., Aranjuez, G., Dudley, C., and Montell, D.J. (2008). PAR-1 Kinase Regulates Epithelial Detachment and Directional Protrusion of Migrating Border Cells. *Curr. Biol.* *18*, 1659–1667.
- Melani, M., Simpson, K.J., Brugge, J.S., and Montell, D. (2008). Regulation of Cell Adhesion and Collective Cell Migration by Hindsight and Its Human Homolog RREB1. *Current Biology* *18*, 532–537.
- Miles, C.M., Lott, S.E., Hendriks, C.L.L., Ludwig, M.Z., Manu, Williams, C.L., and Kreitman, M. (2011). Artificial selection on egg size perturbs early pattern formation in *Drosophila melanogaster*. *Evolution* *65*, 33–42.
- Miller, J.R., and McClay, D.R. (1997). Changes in the pattern of adherens junction-associated beta-catenin accompany morphogenesis in the sea urchin embryo. *Dev. Biol.* *192*, 310–322.
- Mizuno, T., Amano, M., Kaibuchi, K., and Nishida, Y. (1999). Identification and characterization of *Drosophila* homolog of Rho-kinase. *Gene* *238*, 437–444.
- Mizuno, T., Tsutsui, K., and Nishida, Y. (2002). *Drosophila* myosin phosphatase and its role in dorsal closure. *Development* *129*, 1215–1223.
- Mostowy, S., and Cossart, P. (2012). Septins: the fourth component of the cytoskeleton. *Nat. Rev. Mol. Cell Biol.* *13*, 183–194.
- Muller, H.A. (1996). armadillo, bazooka, and stardust are critical for early stages in formation

- of the zonula adherens and maintenance of the polarized blastoderm epithelium in *Drosophila*. *The Journal of Cell Biology* *134*, 149–163.
- Müller, H.A., and Hausen, P. (1995). Epithelial cell polarity in early *Xenopus* development. *Dev. Dyn.* *202*, 405–420.
- Munjal, A., Philippe, J.-M., Munro, E., and Lecuit, T. (2015). A self-organized biomechanical network drives shape changes during tissue morphogenesis. *Nature* *524*, 351–355.
- Nance, J. (2014). Getting to know your neighbor: cell polarization in early embryos. *J. Cell Biol.* *206*, 823–832.
- Nance, J., and Priess, J.R. (2002). Cell polarity and gastrulation in *C. elegans*. *Development* *129*, 387–397.
- Nance, J., Munro, E.M., and Priess, J.R. (2003). *C. elegans* PAR-3 and PAR-6 are required for apicobasal asymmetries associated with cell adhesion and gastrulation. *Development* *130*, 5339–5350.
- Nelson, W.J., and James Nelson, W. (1991). Generation of plasma membrane domains in polarized epithelial cells: role of cell-cell contacts and assembly of the membrane cytoskeleton. *Biochemical Society Transactions* *19*, 1055–1059.
- Neufeld, T.P., and Rubin, G.M. (1994). The *Drosophila* peanut gene is required for cytokinesis and encodes a protein similar to yeast putative bud neck filament proteins. *Cell* *77*, 371–379.
- Ohsugi, M., Larue, L., Schwarz, H., and Kemler, R. (1997). Cell-junctional and cytoskeletal organization in mouse blastocysts lacking E-cadherin. *Dev. Biol.* *185*, 261–271.
- O’Keefe, D.D., Gonzalez-Niño, E., Edgar, B.A., and Curtiss, J. (2012). Discontinuities in Rap1 activity determine epithelial cell morphology within the developing wing of *Drosophila*. *Dev. Biol.* *369*, 223–234.
- Okuda, S., Inoue, Y., and Adachi, T. (2015). Three-dimensional vertex model for simulating multicellular morphogenesis. *Biophys Physicobiol* *12*, 13–20.
- Pacquelet, A., and Rørth, P. (2005). Regulatory mechanisms required for DE-cadherin function in cell migration and other types of adhesion. *J. Cell Biol.* *170*, 803–812.
- Pacquelet, A., Lin, L., and Rørth, P. (2003). Binding site for p120/ δ -catenin is not required for *Drosophila* E-cadherin function in vivo. *The Journal of Cell Biology* *160*, 313–319.
- Padash Barmchi, M., Rogers, S., and Häcker, U. (2005). DRhoGEF2 regulates actin organization and contractility in the *Drosophila* blastoderm embryo. *J. Cell Biol.* *168*, 575–585.
- Park, J.-A., Kim, J.H., Bi, D., Mitchel, J.A., Qazvini, N.T., Tantisira, K., Park, C.Y., McGill, M., Kim, S.-H., Gweon, B., et al. (2015). Unjamming and cell shape in the asthmatic airway epithelium. *Nat. Mater.* *14*, 1040–1048.
- Pesacreta, T.C., Byers, T.J., Dubreuil, R., Kiehart, D.P., and Branton, D. (1989). *Drosophila* spectrin: the membrane skeleton during embryogenesis. *J. Cell Biol.* *108*, 1697–1709.
- Pinheiro, E.M., and Montell, D.J. (2004). Requirement for Par-6 and Bazooka in *Drosophila* border cell migration. *Development* *131*, 5243–5251.

- Quiros, M., and Nusrat, A. (2014). RhoGTPases, actomyosin signaling and regulation of the epithelial Apical Junctional Complex. *Semin. Cell Dev. Biol.* **36**, 194–203.
- Rauzi, M., Lenne, P.-F., and Lecuit, T. (2010). Planar polarized actomyosin contractile flows control epithelial junction remodelling. *Nature* **468**, 1110–1114.
- Rodriguez-Boulan, E., and Macara, I.G. (2014). Organization and execution of the epithelial polarity programme. *Nat. Rev. Mol. Cell Biol.* **15**, 225–242.
- Roh-Johnson, M., Shemer, G., Higgins, C.D., McClellan, J.H., Werts, A.D., Tulu, U.S., Gao, L., Betzig, E., Kiehart, D.P., and Goldstein, B. (2012). Triggering a cell shape change by exploiting preexisting actomyosin contractions. *Science* **335**, 1232–1235.
- Rørth, P. (1998). Gal4 in the *Drosophila* female germline. *Mech. Dev.* **78**, 113–118.
- Rothwell, W.F., and Sullivan, W. (2007). Fixation of *Drosophila* embryos. *CSH Protoc.* **2007**, db.prot4827.
- Royou, A., Sullivan, W., and Karess, R. (2002). Cortical recruitment of nonmuscle myosin II in early syncytial *Drosophila* embryos: its role in nuclear axial expansion and its regulation by Cdc2 activity. *J. Cell Biol.* **158**, 127–137.
- Rupprecht, J.-F., Ong, K.H., Yin, J., Huang, A., Dinh, H.-H.-Q., Singh, A.P., Zhang, S., Yu, W., and Saunders, T.E. (2017). Geometric constraints alter cell arrangements within curved epithelial tissues. *Mol. Biol. Cell* **28**, 3582–3594.
- Sadati, M., Taheri Qazvini, N., Krishnan, R., Park, C.Y., and Fredberg, J.J. (2013). Collective migration and cell jamming. *Differentiation* **86**, 121–125.
- Sánchez-Gutiérrez, D., Sáez, A., Pascual, A., and Escudero, L.M. (2013). Topological progression in proliferating epithelia is driven by a unique variation in polygon distribution. *PLoS One* **8**, e79227.
- Schejter, E.D., and Wieschaus, E. (1993). Functional elements of the cytoskeleton in the early *Drosophila* embryo. *Annu. Rev. Cell Biol.* **9**, 67–99.
- Schmidt, A., and Grosshans, J. (2018). Dynamics of cortical domains in early development. *J. Cell Sci.* **131**.
- Schmidt, A., Lv, Z., and Großhans, J. (2018). ELMO and Sponge specify subapical restriction of Canoe and formation of the subapical domain in early *Drosophila* embryos. *Development* **145**, dev157909.
- Schulte, J., Tepass, U., and Auld, V.J. (2003). Gliotactin, a novel marker of tricellular junctions, is necessary for septate junction development in *Drosophila*. *J. Cell Biol.* **161**, 991–1000.
- Sen, A., Nagy-Zsvér-Vadas, Z., and Krahn, M.P. (2013). *Drosophila*PATJ supports adherens junction stability by modulating Myosin light chain activity. *The Journal of Cell Biology* **200**, 853–853.
- Shahab, J., Tiwari, M.D., Honemann-Capito, M., Krahn, M.P., and Wodarz, A. (2015). Bazooka/PAR3 is dispensable for polarity in *Drosophila* follicular epithelial cells. *Biol. Open* **4**, 528–541.
- Sherlekar, A., and Rikhy, R. (2016). Syndapin promotes pseudocleavage furrow formation

- by actin organization in the syncytial *Drosophila* embryo. *Mol. Biol. Cell* 27, 2064–2079.
- Shewan, A.M., Maddugoda, M., Kraemer, A., Stehens, S.J., Verma, S., Kovacs, E.M., and Yap, A.S. (2005). Myosin 2 is a key Rho kinase target necessary for the local concentration of E-cadherin at cell-cell contacts. *Mol. Biol. Cell* 16, 4531–4542.
- Silverman-Gavrila, R.V., Hales, K.G., and Wilde, A. (2008). Anillin-mediated targeting of peanut to pseudocleavage furrows is regulated by the GTPase Ran. *Mol. Biol. Cell* 19, 3735–3744.
- Simões, S., Oh, Y., Wang, M.F.Z., Fernandez-Gonzalez, R., and Tepass, U. (2017). Myosin II promotes the anisotropic loss of the apical domain during *Drosophila* neuroblast ingression. *J. Cell Biol.* 216, 1387–1404.
- Stevenson, V., Hudson, A., Cooley, L., and Theurkauf, W.E. (2002). Arp2/3-dependent pseudocleavage [correction of pseudocleavage] furrow assembly in syncytial *Drosophila* embryos. *Curr. Biol.* 12, 705–711.
- Sugimura, K., and Ishihara, S. (2013). The mechanical anisotropy in a tissue promotes ordering in hexagonal cell packing. *Development* 140, 4091–4101.
- Sullivan, W., and Theurkauf, W.E. (1995). The cytoskeleton and morphogenesis of the early *Drosophila* embryo. *Curr. Opin. Cell Biol.* 7, 18–22.
- Swedlow, J. (2011a). Immunolabeling of *Drosophila* Embryos and Tissues. Cold Spring Harb. Protoc. 2011, db.prot5657 – pdb.prot5657.
- Swedlow, J. (2011b). Fixation of *Drosophila* tissues for immunofluorescence. Cold Spring Harb. Protoc. 2011, 931–934.
- Tabler, J.M., Yamanaka, H., and Green, J.B.A. (2010). PAR-1 promotes primary neurogenesis and asymmetric cell divisions via control of spindle orientation. *Development* 137, 2501–2505.
- Takizawa, P.A., DeRisi, J.L., Wilhelm, J.E., and Vale, R.D. (2000). Plasma membrane compartmentalization in yeast by messenger RNA transport and a septin diffusion barrier. *Science* 290, 341–344.
- Tan, C., Stronach, B., and Perrimon, N. (2003). Roles of myosin phosphatase during *Drosophila* development. *Development* 130, 671–681.
- Tanentzapf, G., Smith, C., McGlade, J., and Tepass, U. (2000). Apical, lateral, and basal polarization cues contribute to the development of the follicular epithelium during *Drosophila* oogenesis. *J. Cell Biol.* 151, 891–904.
- Thomas, G.H., and Williams, J.A. (1999). Dynamic rearrangement of the spectrin membrane skeleton during the generation of epithelial polarity in *Drosophila*. *J. Cell Sci.* 112 (Pt 17), 2843–2852.
- Turner, F.R., and Mahowald, A.P. (1976). Scanning electron microscopy of *Drosophila* embryogenesis. 1. The structure of the egg envelopes and the formation of the cellular blastoderm. *Dev. Biol.* 50, 95–108.
- Tyler, S. (2003). Epithelium—the primary building block for metazoan complexity. *Integr. Comp. Biol.* 43, 55–63.
- Vega-Salas, D.E. (1987). Formation of the apical pole of epithelial (Madin-Darby canine

kidney) cells: polarity of an apical protein is independent of tight junctions while segregation of a basolateral marker requires cell-cell interactions. *The Journal of Cell Biology* 104, 905–916.

Vestweber, D., Gossler, A., Boller, K., and Kemler, R. (1987). Expression and distribution of cell adhesion molecule uvomorulin in mouse preimplantation embryos. *Dev. Biol.* 124, 451–456.

Vinot, S., Le, T., Ohno, S., Pawson, T., Maro, B., and Louvet-Vallée, S. (2005). Asymmetric distribution of PAR proteins in the mouse embryo begins at the 8-cell stage during compaction. *Dev. Biol.* 282, 307–319.

Wang, A.Z., Ojakian, G.K., and Nelson, W.J. (1990a). Steps in the morphogenesis of a polarized epithelium. I. Uncoupling the roles of cell-cell and cell-substratum contact in establishing plasma membrane polarity in multicellular epithelial (MDCK) cysts. *J. Cell Sci.* 95 (Pt 1), 137–151.

Wang, A.Z., Ojakian, G.K., and Nelson, W.J. (1990b). Steps in the morphogenesis of a polarized epithelium. II. Disassembly and assembly of plasma membrane domains during reversal of epithelial cell polarity in *J. Cell Sci.*

Wang, F., Dumstrei, K., Haag, T., and Hartenstein, V. (2004). The role of DE-cadherin during cellularization, germ layer formation and early neurogenesis in the *Drosophila* embryo. *Dev. Biol.* 270, 350–363.

Wei, S.-Y., Escudero, L.M., Yu, F., Chang, L.-H., Chen, L.-Y., Ho, Y.-H., Lin, C.-M., Chou, C.-S., Chia, W., Modolell, J., et al. (2005). Echinoid is a component of adherens junctions that cooperates with DE-Cadherin to mediate cell adhesion. *Dev. Cell* 8, 493–504.

Weng, M., and Wieschaus, E. (2017). Polarity protein Par3/Bazooka follows myosin-dependent junction repositioning. *Dev. Biol.* 422, 125–134.

Widmann, T.J., and Dahmann, C. (2009). Dpp signaling promotes the cuboidal-to-columnar shape transition of *Drosophila* wing disc epithelia by regulating Rho1. *J. Cell Sci.* 122, 1362–1373.

Wodarz, A., Ramrath, A., Kuchinke, U., and Knust, E. (1999). Bazooka provides an apical cue for Inscuteable localization in *Drosophila* neuroblasts. *Nature* 402, 544–547.

Xie, Y., and Blankenship, J.T. (2018). Differentially-dimensioned furrow formation by zygotic gene expression and the MBT. *PLoS Genet.* 14, e1007174.

Xue, Z., and Sokac, A.M. (2016). -Back-to-back mechanisms drive actomyosin ring closure during *Drosophila* embryo cleavage. *The Journal of Cell Biology* 215, 335–344.

Yamada, S., and Nelson, W.J. (2007). Localized zones of Rho and Rac activities drive initiation and expansion of epithelial cell-cell adhesion. *J. Cell Biol.* 178, 517–527

Yonemura, S., Wada, Y., Watanabe, T., Nagafuchi, A., and Shibata, M. (2010). alpha-Catenin as a tension transducer that induces adherens junction development. *Nat. Cell Biol.* 12, 533–542.

Yu, H.H., Dohn, M.R., Markham, N.O., Coffey, R.J., and Reynolds, A.B. (2016). p120-catenin controls contractility along the vertical axis of epithelial lateral membranes. *J. Cell Sci.* 129, 80–94.

Zallen, J.A., Cohen, Y., Hudson, A.M., Cooley, L., Wieschaus, E., and Schejter, E.D. (2002).

SCAR is a primary regulator of Arp2/3-dependent morphological events in *Drosophila*. *J. Cell Biol.* *156*, 689–701.

Zhang, C.X., Lee, M.P., Chen, A.D., Brown, S.D., and Hsieh, T. (1996). Isolation and characterization of a *Drosophila* gene essential for early embryonic development and formation of cortical cleavage furrows. *J. Cell Biol.* *134*, 923–934.

Zhang, Y., Yu, J.C., Jiang, T., Fernandez-Gonzalez, R., and Harris, T.J.C. (2018). Collision of Expanding Actin Caps with Actomyosin Borders for Cortical Bending and Mitotic Rounding in a Syncytium. *Dev. Cell* *45*, 551–564.e4.